Using cosmogenic ^{36}Cl to determine periods of enhanced seismicity in western Anatolia, Turkey

Inauguraldissertation
der Philosophisch-naturwissenschaftlichen Fakultät
der Universität Bern

vorgelegt von
Nasim Mozafari Amiri
Aus Iran

Leiter der Arbeit:
PD Dr. Naki Akçar
Institut für Geologie, Universität Bern

Co-Leiterin der Arbeit:
PD Dr. Susan Ivy-Ochs
Institut für Teilchenphysik, ETH Zürich

Using cosmogenic ^{36}Cl to determine periods of enhanced seismicity in western Anatolia, Turkey

Inauguraldissertation
Der Philosophisch-naturwissenschaftlichen Fakultät
der Universität Bern

vorgelegt von
Nasim Mozafari Amiri
Aus Iran

Leiter der Arbeit:
PD Dr. Naki Akçar
Institut für Geologie, Universität Bern

Co-Leiterin der Arbeit:
PD Dr. Susan Ivy-Ochs
Institut für Teilchenphysik, ETH Zürich

Von der Philosophisch-naturwissenschaftlichen Fakultät angenommen
Bern, den 28 August 2017

Der Dekan:
Prof. Dr. Gilberto Colangelo

Abstract

Reconstruction of paleoearthquakes is an essential step in order to widen our understanding of future seismic behavior on specific faults and in a larger extent in a regional tectonic framework. Fault scarp dating using cosmogenic ^{36}Cl is a powerful technique to explore the rupture history of faults that provide valuable information to be contributed in seismic hazard assessment. Western Anatolia is a roughly N-S rapidly extensional region since early Miocene. Deformation pattern of this intensively active region is strongly dominated by normal faults, locally built in carbonates, within the large-scale horst-graben systems. Carbonate bedrock fault scarps are the most direct indication of past earthquakes in order to explore seismic behavior of faults using cosmogenic ^{36}Cl. The oldest recorded earthquake in the Eastern Mediterranean and Middle East dates back to 2100 B.C, whereas the instrumental earthquakes were recorded only during the last century. However, to assess the seismic activity of faults, a more complete seismic database within and prior to the existing seismic archives is required.

In this study, in order to model a long-term seismic history of western Anatolia, we applied fault scarp dating on several fault scarps within Büyük Menderes Graben, Gediz Graben, and Gökova half-graben by analysing 584 samples. We could recover at least 12 large seismic events, mostly occurred as clustered earthquakes with magnitude of 5.4 to 7.1 during the past 15 ka. The correlation of timing of paleoearthquakes at ca. 2.0, 3.5, 6.0 and 8.0 ka lead us to assert that western Anatolia experienced at least four periods of high seismic activity during Holocene, in addition to the recent time with the high record of major earthquakes. The regional recurrence interval of approximately 2000 years is concordant with the return period of earthquakes of several faults in the extensional tectonic setting of Aegean region. The vertical slip rates of faults are estimated to be in a range of 0.1 to 1.9 mm/yr, which generally increase through time. This indicates that the largest amount of strain during the whole Holocene time is transmitting to western Anatolia in recent time.

Contents

Acknowledgment

This work and the completion of my PhD studies would have not been possible without the encouragement and support of many people. I would like to say thank to everybody who made this effort possible and helped me along the way.

First, I would like to express my sincere gratitude to my supervisor Naki Akçar for giving me the opportunity to start this amazing project that was highly relevant to my interests. I thank his guidance, motivation, enthusiasm, patience and immense knowledge through these years. He always welcomed me to assist and discuss the problems, in spite of his busy schedule.

I am deeply grateful to my co-supervisor Susan Ivy-Ochs for her supports and encouragements during my PhD and especially the positive energy she always transferred by her laughter.

A special thanks to Dmitry Tikhomirov for his time and patience while teaching me how to deal with his robust Matlab code developed for fault scarp dating.

I wish to thank the team at the Laboratory of Ion Beam Physics, ETH Zurich for their supports with the AMS measurements of a large number of samples, especially Christof Vockenhuber and Hans-Arno Synal.

Thanks are also extended to all my colleagues in the Geology Institute, who kindly welcomed me in their group, especially Fritz Schlunegger for his supports, Julia Krbanjevic for her assistance and guidance during lab works and Regina Reber for all her cares and kindness. I am very thankful to Serdar Yesilyurt that without his help during the lab works and specially crushing, my project would be continued forever! I also acknowledge Cihan Bayrakdar, from Istanbul University for helping me of crushing part of my samples.

I want also thank Christian Schlüchter for his encouragements, kindness and the pleasant times we had especially during conferences.

And a big thank to all my Turkish colleagues, from Dokuz Eylül and Afyon Kocatepe Universities, whom I have had the pleasure to work during this project. First, I send my sincere appreciation to Hasan Sözbilir, the big Tectonic scientist of Turkey for accepting to be in my dissertation committee and also for his assistance and support in the field. I also acknowledge Ökmen Sümer, Çağlar Özkaymak, Bora Uzel and Tayfun Guler, without whom certainly the collection of that large number of samples would have been difficult. I always benefited from their valuable comments and ideas. Thanks for all the good memories you made during the tough field campaign in wonderful Turkey.

Finally, I wish to express my deepest feeling to my family back home for their endless love and unconditional support they have given me throughout the years. Pedar and Maman, without you I would never have enjoyed so many opportunities. For this and much more, I am forever in your debt and proud of you both in every second of my life.

Chapter 1

Introduction

Introduction

The idea of production of radioactive nuclides as a result of interaction of cosmic rays with Earth's surface elements was first introduced by Grosse (1934). The principle of cosmogenic nuclide dating lies in spallation process, which is defined as the collision of high-energy cosmic rays with nuclei in the atmosphere and breakage of the nuclei into particles followed by new nuclides creation. The accumulation of nuclides at or near the Earth surface material reveals the specific time that the surface material has been exposed to cosmic rays, when the production rate is known. Radiocarbon was the first nuclide used to date the organic materials in the late 1940s (Libby 1946; Libby et al. 1949). Davis and Schaeffer (1955) developed the surface exposure dating methodology and proposed the plausibility of dating using cosmogenic ^{36}Cl. A decade later, Lal and Peters (1967) proposed a fundamental theory for cosmogenic nuclide dating. Until mid-1980s the method developed slowly, due to the absence of sufficient instrumentation to measure the low concentrations of terrestrial in-situ produced cosmogenic nuclides (TCN). Through years TCN applications increased with development of analytical methods to calculate production and erosion rates (Lal, 1991; Stone, 2000; Dunai, 2000) as well as instrumental progress in AMS (Accelerator Mass Spectrometry) (e.g., Klein et al., 1982; Elmore and Phillips, 1987). Most used cosmogenic nuclides are ^{3}He, ^{10}Be, ^{26}Al, ^{36}Cl, ^{21}Ne and ^{14}C with a wide range of applications in different geomorphological features such as reconstruction of ice volume fluctuations, dating of landslides, shorelines, fault scarps, volcanic landforms, determination of uplift timing, quantifying mass erosion events, determination of fluvial sediment storage and transfer time and many others (Gosse and Philips, 2001 and references therein).

Bedrock fault scarps can provide direct evidence of paleoearthquakes in order to date their occurrence time and determine the related slip values, if the periods of activity and quiescence are analyzed along fault scarps with cosmogenic nuclides. Fault scarp dating is based on the analysis of the accumulation of cosmogenic nuclides in a few outermost centimeters of the fault scarp surface. Mainly cosmogenic ^{36}Cl is used for fault scarp dating, but also ^{10}Be, ^{26}Al and ^{14}C have been tested (Kong et al., 2010;

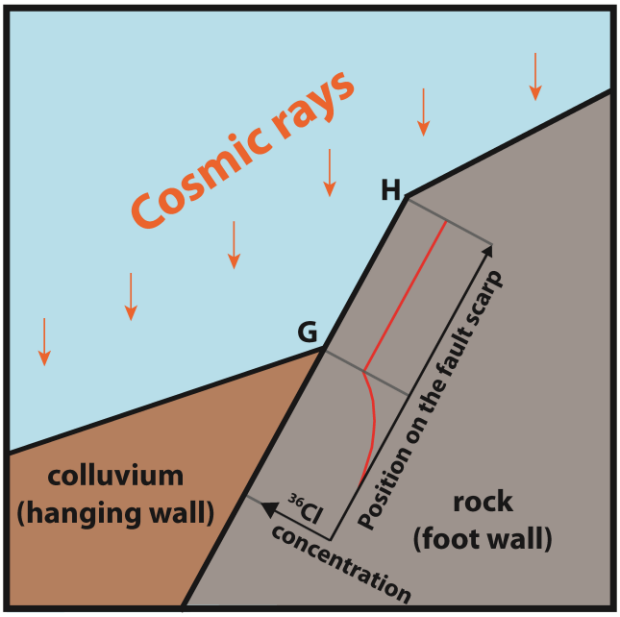

Fig. 1. Schematic distribution of cosmogenic ^{36}Cl concentration along the outermost couples of centimeters of an exposed fault scarp and covered surface by colluvium.

Harrington et al., 2000). ^{36}Cl is considered as the most common cosmogenic nuclide, which is regularly applied for dating of non-quartz-bearing lithology such as carbonates. Episodic history of the activity and quiescence of a given normal fault leads to creation of cosmogenic ^{36}Cl profile (Fig. 1). By processing the cosmogenic ^{36}Cl along the fault scarp height we are able: (1) to date the past seismic events and in case of regularity of the return interval, approximate the time of future event (2) to determine the vertical component of slips and the magnitude of the earthquakes in charge of displacements; and (3) to estimate the slip rates both cumulative and short-term, which all are fundamental elements in earthquake risk reduction (e.g., Cluff & Cluff, 1984). Generally, before the fault activation, shielding of colluvium causes the creation of exponential profile of ^{36}Cl concentration in the footwall and the outermost fault scarp surface, once the fault is completely covered by colluvium at time t_0 (Fig. 2). At the time of t_1, when the first rupture (EQ_1) occurs, a previously covered part of the fault scarp exposes to the cosmic rays with slip amount of S_1 and the colluvium level shifts from the position G_0 to G_1 (Fig. 2). Such event is reflected in a uniform concentration of cosmogenic ^{36}Cl resulted by acceleration of production of cosmogenic ^{36}Cl during the subsequent period of dormancy of the fault (time period of t_1 to t_2, where t_2 is timing of the second earthquake). At the time of t_2, the second rupture (EQ_2) occurs and the ground level moves from the position G_1 to G_2 with respective slip of S_2. This cycle recurs for the third and fourth ruptures, which finally the ground level shifts to G (the recent ground level) (Fig. 2). In the profile of ^{36}Cl concentrations during these four rupture events, discontinuities represent the timing of ruptures, while the convex shape of profile defines periods of inactivity (Fig. 2).

The vertical components of slips are defined by the vertical separations between two adjacent discontinuities (Fig. 2).

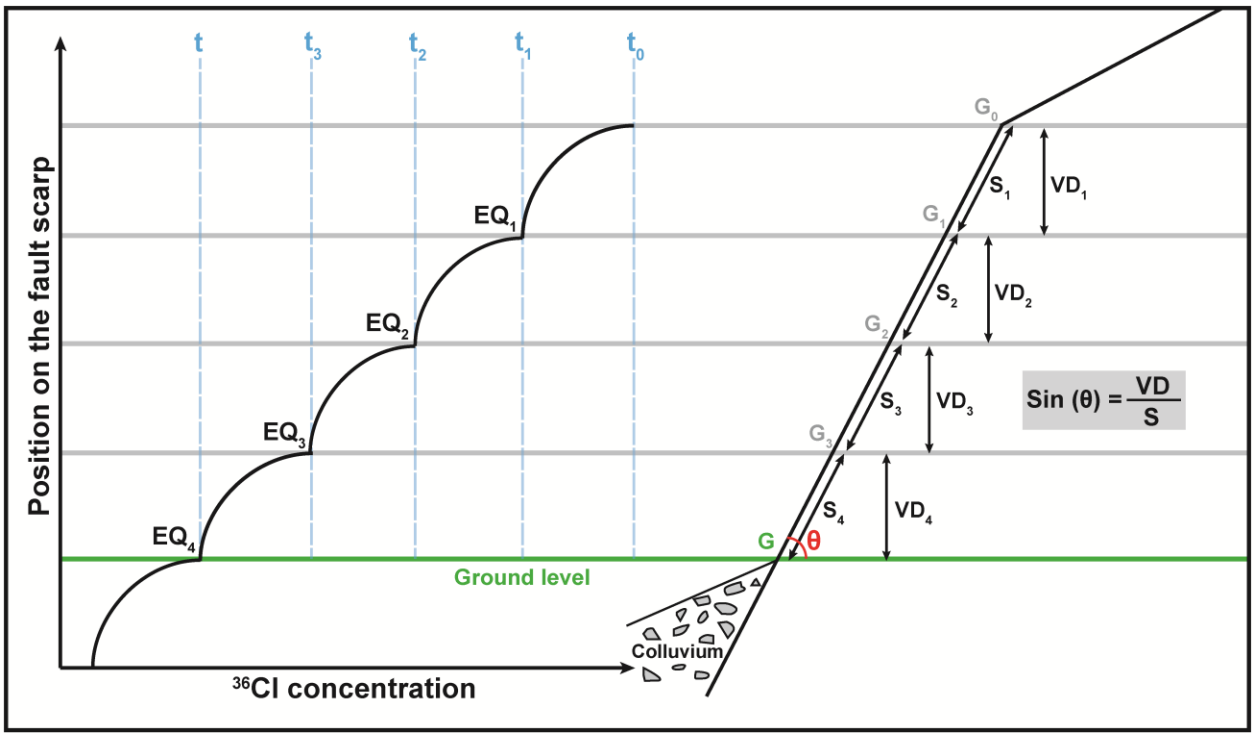

Fig. 2. Sketch of cosmogenic ^{36}Cl concentration profile as a function of height along fault scarp through exposure history of four episodic earthquakes (modified after Akçar et al., 2012). G_0 and t_0 represent the ground level and time before the first earthquake, when the fault was covered by colluvium; G_1 and S_1 show the ground level and the slip value after the first earthquake at the time of t_1; t is the time of the fourth and most recent earthquake, when ground level shifted from G_3 to its current level (G); S_4 represents slip amount of the last earthquake. The differences between adjacent times of t_0 to t indicate inactivity times of the fault; VD_1 to VD_4 are vertical displacement caused by earthquakes 1 to 4.

For the first time, the fault scarp dating with cosmogenic ^{36}Cl was used by Zreda and Noller (1998), in the Hebgen Lake fault scarp, Montana, USA with dating of six paleoseismic activities. A computer code was developed by Mitchell et al. (2001) to model the past earthquakes. They reconstructed three phases of paleoseismic activity on the Nahef East Fault scarp, Israel. Benedetti et al. (2002) recovered six rupture events the Sparta Normal Fault scarp (Greece) including the 464 B.C Sparta earthquake. In addition, Benedetti et al. (2003) reconstructed three seismic events on the Kaparelli Fault, Greece. Palumbo et al. (2004) explored five to seven seismic activities on the Mangola Fault, Italy. Schlagenhauf et al. (2010) developed a new Matlab® code and reanalysed the cosmogenic ^{36}Cl data set from the Mangola Fault

(Palumbo et al., 2004). They modeled the same number of ruptures but with younger ages in comparison to the results of Palumbo et al. (2004). Schlagenhauf et al. (2011) reconstructed paleoseismic history of at least nine significant ruptures through the last 15 ka. This has been done with sampling four more fault surfaces on Velino-Magnola Fault in addition to one site of Palumbo et al. (2004). Akçar et al. (2012) applied the Matlab® code of Schlagenhauf et al. (2011) and modeled two seismic scenarios on the Mugırtepe Fault in the Manisa Fault Zone, Turkey (Fig. 3). Benedetti et al. (2013) reconstructed at least 30 major seismic events since 12 ka ago on the Fucino Fault System, Italy from 11 locations, including one site from Palumbo et al. (2004) and four sites from Schlagenhauf et al. (2011). Tikhomirov (2014) developed a new Matlab® code and re-processed the data set from the Mugırtepe Fault (Akçar et al., 2012) as well as the Manastır Fault in the Manisa Fault Zone (Fig. 3). His modeling resulted in one seismic event for each fault. Mouslopoulou et al. (2014) used the code developed by Schlagenhauf et al. (2011) on the Spili Fault (Crete) and yielded five destructive events over the last 16.5 ka. Cowie et al. (2017) reconstructed the seismic history of Italian Apennines over the last 18 ka by linking cosmogenic ^{36}Cl dating to LiDAR (Light Detection and Ranging) and GPR (Ground Penetrating Radar) methods and discovered the episodic activity of the Fiamignano Fault.

In this study, we used fault scarp dating using cosmogenic ^{36}Cl in order to model seismically active periods in western Anatolia, one of the most active regions in the world, which formed as a result of a roughly N-S extensional tectonic regime since early Miocene. The complex deformation pattern of this region is dominated by major horst-graben systems namely Büyük Menderes Graben, Küçük Menderes Graben, Gediz Graben and Gökova half-graben characterized by normal faults built in carbonates (Fig. 3). This region is subject to high seismicity, where the major earthquakes are recorded historically and instrumentally (e.g., Ambraseys, 2009; Ergin et al. 1967; Soysal et al. 1981). The population density in the western Anatolia is up to 500 person per km^2 (European Environment Agency, 2010), which highlights the necessity of earthquake risk reduction studies, in order to minimize the probable damages of potential earthquakes. Basically, the return period of major earthquakes produced by faults is

several hundred years (Molnar, 1979; Scholz, 2002). But the oldest known historical earthquake in the Eastern Mediterranean and Middle East dates back to 2100 B.C.

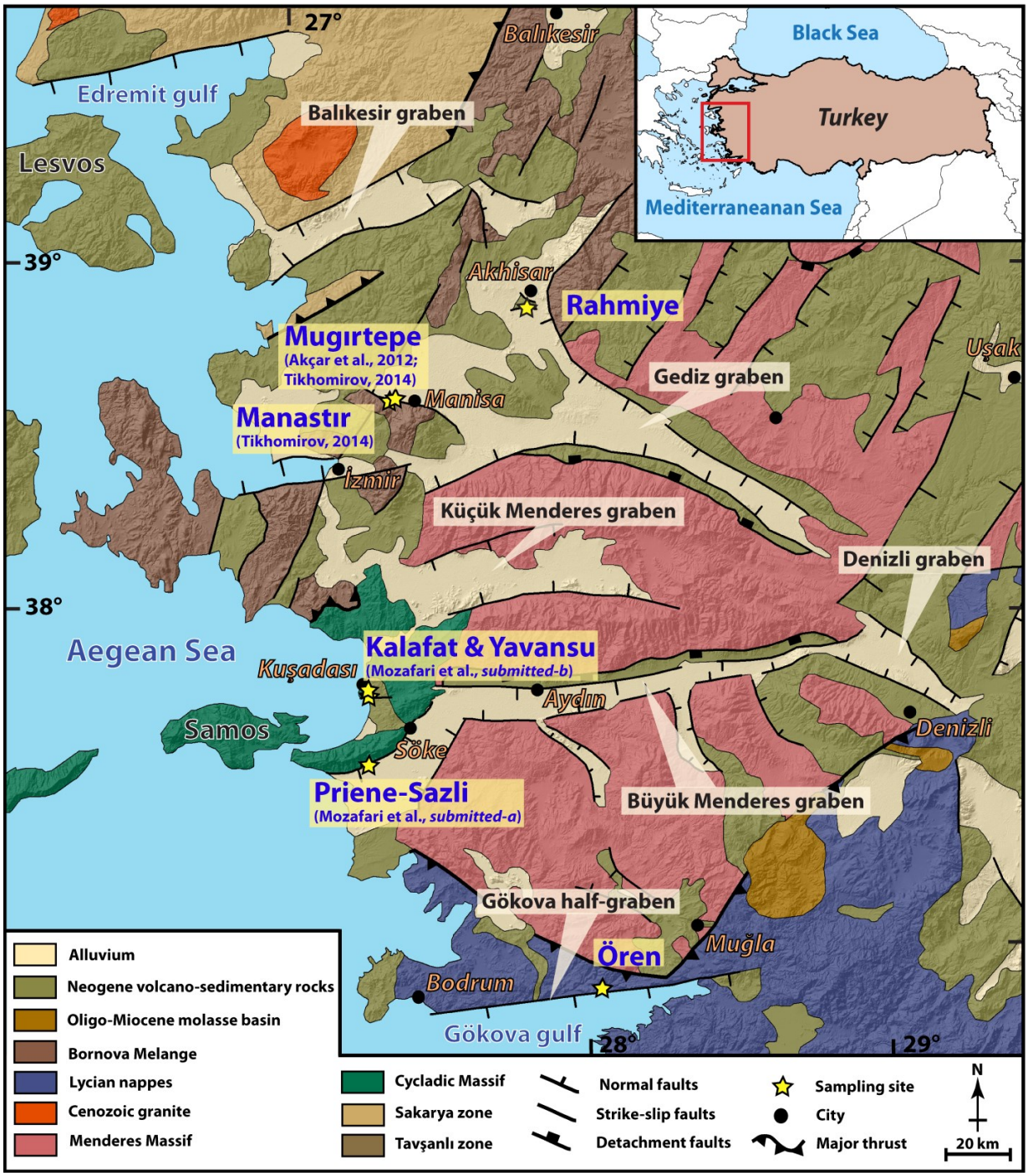

Fig. 3. Simplified geological map of western Anatolia (modified after Akçar et al., 2012; Sümer et al., 2013; Hancock and Barka, 1987). The yellow stars show the locations of the sampling sites of this study in Priene-Sazlı, Yavansu and Kalafat faults within Büyük Menderes Graben, Ören Fault in Gökova half-graben, Mugırtepe Fault (Akçar et al., 2012), Manastır Fault (Tikhomirov, 2014) and Rahmiye Fault (this study) within Gediz Graben.

(Shebalin et al., 1974; Soysal et al., 1981; Ambraseys, 2009), and the instrumental earthquakes have been recorded only since 1900. However, in order to assess a long-term seismic behavior of faults and evaluation of probability of the occurrence of destructive future earthquakes, more complete data over larger time-scale is required. The main objectives of this thesis were dating of paleoseismic events to assess the return periods of major earthquakes and forecast timing of future ones; modeling amount of vertical component of slips and evaluating magnitude of reconstructed ruptures; and quantifying short-term and long-term slip rates, which all provide important data for earthquake risk reduction. To fulfil our aims, we collected a total of 453 samples from well-preserved fault scarps within Gediz Graben (Rahmiye Fault), Büyük Menderes Graben (Kalafat, Yavansu and Priene-Sazlı faults), and Gökova half-graben (Ören Fault). After sample processing, a Matlab® code (Tikhomirov, 2014) was used to model the seismic history of the faults. The results of our fault scarp modeling were compared with the existing results of Manastır and Mugırtepe faults (Akçar et al., 2012; Tikhomirov, 2014) in Gediz Graben. Correlation of ages of paleoearthquakes of these faults indicates that western Anatolia experienced at least four periods of high seismic activity at ca. 2.0, 3.5, 6.0 and 8.0 ka with a return period of approximately 2000 years during Holocene.

References

- Akçar, N., Tikhomirov, D., Özkaymak, Ç., Ivy-Ochs, S., Alfimov, V., Sözbilir, H., Uzel, B., Schlüchter, Ch., 2012. ^{36}Cl Exposure Dating of Paleoearthquakes in the Eastern Mediterranean: First Results from Western Anatolian Extensional Province, Turkey. GSA Bulletin 124, no. 11/12, 1724-1735.
- Ambraseys, N., 2009. Earthquakes in the Mediterranean and Middle East: a multidisciplinary study of seismicity up to 1900. Cambridge University Press, 947 p.
- Benedetti, L., Finkel, R., King, G., Armijo, R., Papanastassiou, D., Ryerson, F.J., Flerit, F., Farber, D., Stavrakakis, G., 2003. Motion on the Kaparelli fault (Greece) prior to the 1981 earthquake sequence determined from Cl-36 cosmogenic dating: Terra Nova, v. 15, no. 2, p. 118-124.
- Benedetti, L., Finkel, R., Papanastassiou, D., King, G., Armijo, R., Ryerson, F., Farber, D., Flerit, F., 2002. Post-glacial slip history of the Sparta fault (Greece) determined by Cl-36 cosmogenic dating: Evidence for non-periodic earthquakes, Geophysical Research Letters, 29, no. 8, 1246, doi:10.1029/2001GL014510.
- Benedetti, L., Manighetti, I., Gaudemer, Y., Finkel, R., Malavieille, Y., Pou, Kh., Arnold, M., Aumaître, G., Bourlès, D., Keddadouche, K., 2013. Earthquake synchrony and clustering on Fucino faults (Central Italy) as revealed from in situ ^{36}Cl exposure dating. Journal of Geophysical Reasearch, Solid Earth 118, 4948-4974.

- Cluff, L.S., Cluff, J.L., 1984. Importance of assessing degrees of fault activity for engineering decisions, Proceeding 8th World Conference on Earthquake Engineering, vol. 2, 629-636.
- Cowie, P.A., Phillips, R.J., Roberts, G.P., McCaffrey, K., Zijerveld, L.J.J., Gregory, L.C., Faure Walker, J., Wedmore, L.N.J., Dunai, T.J., Binnie, S.A., Freeman, S.P.H.T. , Wilcken, K., Shanks, R.P., Huismans, R.S., Papanikolaou, I., Michetti, A.M., Wilkinson, M., 2017. Orogen-scale uplift in the central Italian Apennines drives episodic behaviour of earthquake faults, Scientific Reports 7, Article number 44858.
- Davis, P.T., Schaeffer, O.A., 1955. Chlorine-36 in nature, Annals of the Ney York Academy of Sciences 62, 105-121.
- Dunai, T., 2000. Scaling factors for production rates of in situ produced cosmogenic nuclides: a critical reevaluation. Earth Planet. Sci. Lett. 176, 157-169.
- Elmore, D., Phillips, F.M., 1987. Accelerator mass spectrometry for measurement of long-lived radioisotopes. Science 236, 543-550.
- Ergin, K., Güçlü, U., Uz, Z., 1967. A Catalogue of Earthquakes for Turkey and Surrounding Area (11 A.D.–1964). Technical University of İstanbul, Publications, no. 24 (in Turkish).
- Gosse, J. C., Phillips, F. M., 2001. Terrestrial in situ cosmogenic nuclides: theory and application, Quater. Sci. Rev., 20, 1475-1560.
- Grosse, A., 1934. An unknown radioactivity, J. Am. Chem. Soc. 56, 1922-1924.
- Hancock, P.L., Barka, A.A., 1987. Kinematic indicators on active faults in western Turkey, Journal of Structural Geology 9, No. 5/6, 573-584.
- Harrington, Ch.D., Whitney, J.W., Jull, A.J.T., Phillips, W., 2000. Cosmogenic Dating and Analysis of Scarps Along the Solitario Canyon and Windy Wash Faults, Yucca Mountain, Nevada, *In* Geologic and Geophysical Characterization Studies of Yucca Mountain, Nevada, A Potential High-Level Radioactive-Waste Repository. By Whitney, J.W. and Keefer, W.R., Scientific Editors, U.S. Geological Survey Digital Data Series 058.
- Klein, J., Middleton, R., Tang, H.Q., 1982. Modifications of an FN Tandem for Quantitative Measurements of ^{10}Be. Nuclear Instruments and Methods 193, 601-616.
- Kong, P., Fink, D., Chunguang, Na., Xiao, W., 2010. Dip-slip rate determined by cosmogenic surface dating on a Holocene scarp of the Daju fault, Yunnan, China, Tectonophysics, 493, 106-112.
- Lal, D., Peters, B., 1967. Cosmic ray produced radioactivity on the earth. In: Sitte, K. (Ed.), Handbuch der Physik. Springer, Berlin, 551-612.
- Libby, W., 1946. Atmospheric helium three and radiocarbon from cosmic radiation, Physical Review. 69, 671-672.
- Libby, W., Anderson E.C., Arnold J.R., 1949. Age determination by radiocarbon content: worldwide essay of natural radiocarbon, Science 109, 227-228.
- Mitchell, S.G., Matmon, A., Bierman, P.R., Enzel, Y., Caffee, M., Rizzo, D., 2001. Displacement history of a limtesone normal fault scarp, northern Israel, from cosmogenic ^{36}Cl, J. geophys. Res., 106(B3), 4247-4264.
- Molnar, P., 1979. Earthquake recurrence intervals and plate tectonics, Bull. seism. Soc. Am., 69(1), 115-133.
- Mouslopoulou, V., Moraetis, D., Benedetti, L., Guillou, V., Bellier, O., Hristopulos, D., 2014. Normal faulting in the forearc of the Hellenic subduction margin: Paleoearthquake history and kinematics of the Spili Fault, Crete, Greece. - Journal of Structural Geology 66, 298-308.
- Palumbo, L., Benedetti, L., Bourles, D., Cinque, A., Finkel, R., 2004. Slip history of the Magnola fault (Apennines, Central Italy) from ^{36}Cl surface exposure dating: evidence for strong earthquake over the Holocene, Earth planet. Sci. Lett., 225, 163-176.
- Schlagenhauf, A., Manighetti, I., Benedetti, L., Gaudemer, Y., Finkel, R., Malavieille, J., Pou, K., 2011. Earthquake supercycles in Central Italy, inferred from ^{36}Cl exposure dating. Earth and Planetary Science Letters, 307(3-4), 487-500.
- Schlagenhauf, A., Gaudemer, Y., Benedetti, L., Manighetti,I., Palumbo, L., Schimmelpfennig, I., Finkel, R., Pou, K., 2010. Using in situ chlorine-36 cosmonuclide to recover past earthquake histories on limestone normal fault scarps: A reappraisal of methodology and interpretations, Geophysical Journal International, v. 182, no. 1, p. 36-72.

- Scholz Ch. H., 2002. The Mechanics of Earthquakes and Faulting. Second Edition, Cambridge University Press, 464 p.
- Shebalin, N.V., Karnik, V., Hadzievski, D. (eds.), 1974. Catalogue of earthquakes of the Balkan region. I, UNDP- UNESCO Survey of the seismicity of the Balkan region. Skopje, 600 p.
- Soysal, H., Sipahioğlu, S., Kolçak, D., Altınok, Y., 1981. Historical earthquake catalogue of Turkey and surrounding area (2100 B.C.-1900 A.D.). Technical Report, TUBİTAK, No: TBAG-341.
- Sümer, Ö., İnci U., Sözbilir, H., 2013. Tectonic evolution of the Söke Basin: Extension-dominated transtensional basin formation in western part of the Büyük Menderes Graben, Western Anatolia, Turkey. Journal of Geodynamics 65, 148-175.
- Tikhomirov, D., 2014. PhD thesis, University of Bern, An advanced model for fault scarp dating and paleoearthquake reconstruction, with a case study of the Gediz Graben formation (Turkey).
- Zreda, M., Noller, J., 1998. Ages of prehistoric earthquakes revealed by cosmogenic chlorine-36 in a bedrock fault scarp at Hebgen Lake. Science, 282, 1097-1099.

Chapter 2

Holocene seismic activity of the Priene-Sazlı Fault revealed by cosmogenic ^{36}Cl, western Anatolia,Turkey

Nasim Mozafari Amiri[1], Ökmen Sümer[2], Dmitry Tikhomirov[1], Susan Ivy-Ochs[3], Vasily Alfimov[3], Christof Vockenhuber[3], Uğur İnci[2], Hasan Sözbilir[2] and Naki Akçar[1]

[1]Institute of Geological Sciences, University of Bern, 3012 Bern, Switzerland
[2]Dokuz Eylül University, Geological Engineering Department, 35160 İzmir, Turkey
[3]Institute for Particle Physics, ETH Hönggerberg, 8093 Zürich, Switzerland

Submitted to Journal of Tectonophysics

Holocene seismic activity of the Priene-Sazlı Fault revealed by cosmogenic ^{36}Cl, western Anatolia, Turkey

Abstract

Bedrock fault scarps built in carbonates are the most direct evidence of paleoearthquakes to reconstruct seismic history using cosmogenic ^{36}Cl. Western Anatolia is a seismically active region, whose deformation pattern is mainly governed by major horst-graben systems initiated by a roughly N-S extensional tectonic regime since early Miocene. The Priene-Sazlı Fault is a major structure in the westernmost part of the Büyük Menderes Graben, one of these essential graben systems. The oldest known earthquake in the Eastern Mediterranean and Middle East dates back to 2100 B.C. However, to evaluate the earthquake behavior, a complete seismic data sequence through a large time-scale is needed.

In this study, we measured cosmogenic ^{36}Cl concentrations in 117 samples along the Priene-Sazlı Fault scarp to reconstruct the age of paleoearthquakes along with their slip amounts, beyond the available historical and instrumental archives. Our results indicate four high seismic phases in the Priene-Sazlı Fault since early Holocene at 8.1 ± 2.0 ka, 6.0 ± 1.5 ka, 3.7 ± 0.9 ka and 2.2 ± 0.5 ka, with slip mounts of 3.4 ± 0.5 m, 1.5 ± 0.2 m, 1.4 ± 0.2 m and 1.5 ± 0.2 m, respectively. These ruptures mostly occurred as clusters of earthquakes with magnitudes of 6.7 – 7.0 in a short period of time. Estimated slip rates of the fault are greater than 0.3, 0.7, 0.6 and 1.0 mm/yr from the oldest to the youngest modeled earthquake. In addition, the long-term slip rate is 0.7 mm/yr. Based on the rupture length and capacity to produce earthquakes with magnitudes of average 6.9, the Priene-Sazlı Fault is considered a seismogenic fault.

Keywords: fault scarp; dating; Eastern Mediterranean; neotectonic; horst-graben

1. Introduction

Displacement history of the faults, along with the size of their responsible destructive earthquakes, provides essential data to assess the frequency of the recurrence interval of earthquakes, and to estimate the likelihood of their occurrence in the future (e.g. McCalpin, 2009). Generally, major earthquakes produced by faults have return periods of several hundred years (e.g., Molnar, 1979; Scholz, 2002). This has been shown by the historical and instrumental seismic records around the world: e.g., Turkey (Ambraseys, 1971), Greece (Pantosti et al., 1996; Pavlides, 1996; Caputo et al., 1998) and northeast China (Lee et al., 1976). The oldest known historical earthquakes in the world are the eastern Crete and the Sodom earthquake, Judaea (around the current Dead Sea). The first earthquake occurred in 2100 B.C. and the second one struck around 2100-1700 B.C. (Shebalin et al., 1974; Soysal et al., 1981; Ambraseys, 2009) in the Eastern Mediterranean and Middle East. These regions were highly suitable places to record the paleoseismic activity evidence due to their geographic capacity for the emergence of the oldest civilizations on Earth. Instrumental recording of destructive earthquakes was, however, started only after the 19th century. Nevertheless, in order to evaluate the long-term seismic behavior of the faults and the analysis of probability of future earthquakes, more seismic data over a longer time span is required. Paleoseismic trenching is the most common method to determine displacement amounts and the return period of earthquakes (e.g., McCalpin, 2009). Displacement amount is derived from the offset of clear soil horizons and the return period of the earthquakes is determined by ^{14}C and/or OSL dating depending on the type of suitable materials found. These, however, provide not very precise timing of paleoearthquakes, whereas bedrock fault scarps are the most direct evidence of past earthquakes resulting in precise dating, where the episodes of dormancy and activity can be analyzed along the bedrock fault scarp using cosmogenic ^{36}Cl dating.

The cosmogenic ^{36}Cl dating technique has been successfully applied during the last two decades on carbonate fault scarps in the USA, Israel, Greece, Italy and Turkey (Zreda and Noller, 1998; Mitchell et al., 2001; Benedetti et al., 2002; 2003; 2013; Palumbo et al., 2004; Schlagenhauf et al., 2010; 2011; Akçar et al., 2012;

Tikhomirov, 2014; Mouslopoulou et al., 2014; Cowie et al., 2017). Fault scarp dating analyzes the profile of cosmogenic ^{36}Cl concentration in the uppermost fault scarp surface along the scarp height. This profile is created by successive earthquakes and episodes of quiescence (Fig. 1) (Gosse and Phillips, 2001 and references therein). The analysis of cosmogenic ^{36}Cl along the fault scarp height enables: (1) dating of the past ruptures and estimation of the recurrence period of the earthquakes, and thus approximate timing of future ruptures; (2) determination of the vertical component of slip and the size of the responsible earthquakes; and (3) estimation of the long-term and short-term slip rates, which are essential parameters for earthquake hazard analysis (e.g. Cluff and Cluff, 1984). Basically, during the dormancy period prior to a rupture, shielding of colluvium defines exponential shape of ^{36}Cl concentration in the uppermost few centimeters of the footwall surface (Fig. 1a). The time when the fault was totally covered by colluvium is shown as t_0 (Fig. 1b). Once rupture occurs (at the time of t_1), the faulting exposes a previously buried

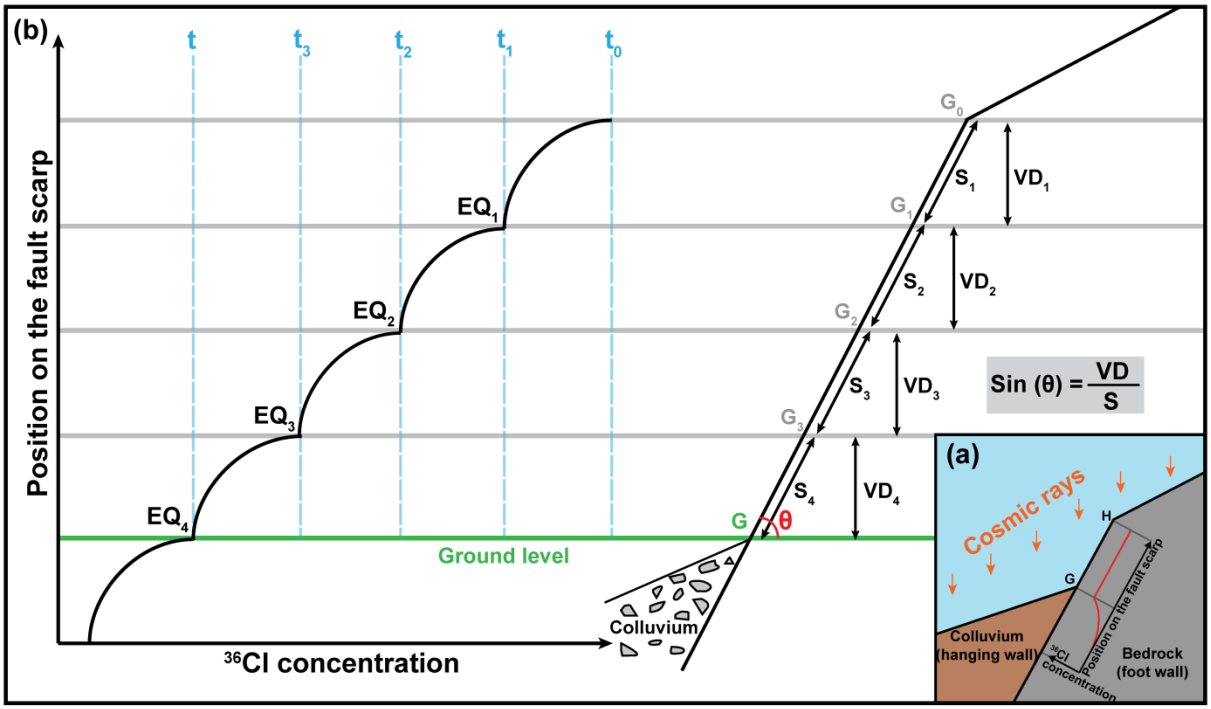

Fig. 1. (a) Schematic distribution of cosmogenic ^{36}Cl concentration along an exposed fault scarp and covered surface by colluvium; (b) sketch of cosmogenic ^{36}Cl concentration profile as a function of height along fault scarp through exposure history of four episodic earthquakes (modified after Akçar et al., 2012). G_0 and t_0 represent the ground level and time before the first earthquake, when the fault was covered by colluvium; G_1 and S_1 show the ground level and the slip value after the first earthquake at the time of t_1; t is the time of the fourth and most recent earthquake, when ground level shifted from G_3 to its current level (G); S_4 represents slip amount of the last earthquake. The differences between adjacent times of t_0 to t indicate inactivity times of the fault; VD_1 to VD_4 are vertical displacement caused by earthquakes 1 to 4.

segment of the scarp at the slip amount of S_1 and the colluvium position shifts from the position G_0 to G_1 (Fig. 1b, EQ_1); this leads to a uniform accumulation of cosmogenic ^{36}Cl over the segment at a higher rate through the consequent periods of quiescence (time span of t_1 to t_2, where t_2 is timing of the second earthquake). Then the second earthquake (EQ_2) occurs at the time of t_2 with slip of S_2 and ground level moves from the position G_1 to G_2. This cycle repeats for the third and fourth earthquakes, after which the ground level shifts to G, which is the recent ground level (Fig. 1b). Hence, each discontinuity in the profile of ^{36}Cl concentrations accumulated during these four earthquakes marks the timing of one rupture. The convex intervals of the ^{36}Cl profile along the fault scarp indicate phases of inactivity (Fig. 1b). The vertical separation between two successive discontinuities equates to the respective slip of the rupture (Fig. 1b).

The complex deformation framework of the Mediterranean region has resulted from the collision of the African and Eurasian plates in the Alpine-Himalayan belt (e.g. Dewey and Şengör, 1979). This framework contains one of the most seismically active regions in the world, namely the 300 km wide Western Anatolian Extensional Province (Dewey and Şengör, 1979; Şengör et al., 1985). In addition, major normal faults there mainly occur in carbonates (Fig. 2). Therefore, western Anatolia is an ideal natural laboratory to investigate periods of seismic activities using exposure dating with cosmogenic ^{36}Cl. Since the region is subject to intensive seismic activity and has records of many destructive earthquakes in history (Fig. 3), modeling of the future seismic events provides a remarkable potential regarding earthquake risk reduction. The extensional tectonic regime in western Anatolia since early Miocene caused the formation of roughly E-W trending main graben systems of Büyük Menderes, Küçük Menderes and Gediz (Fig. 2). These graben systems are basically characterized by well-exposed limestone normal fault scarps against Quaternary sedimentary basins. The Priene-Sazlı Fault is geomorphologically the most prominent fault system of the Büyük Menderes Graben because of its length and height (Figs. 2 and 4) (e.g. Gürer et al., 2001; Sümer et al., 2013). There are two known significant seismic events that have occurred on the Priene-Sazlı Fault. The first destructive earthquake occurred in 68 AD with an epicenter at the NE-end of the fault segment, south of Söke, and with an intensity of VII according to the historical

records (Ergin et al., 1967) (Fig. 4). The second, the Söke-Balat earthquake occurred on July 16, 1955 (M = 6.8) (Öcal, 1958; Şengör 1987). Its epicenter was close to the ancient city of Priene. In this disaster, 23 people were killed and more than 470 buildings were damaged, mostly in the cities of Söke and Balat (ancient Miletus), 15 km south of ancient Priene (Fig. 4).

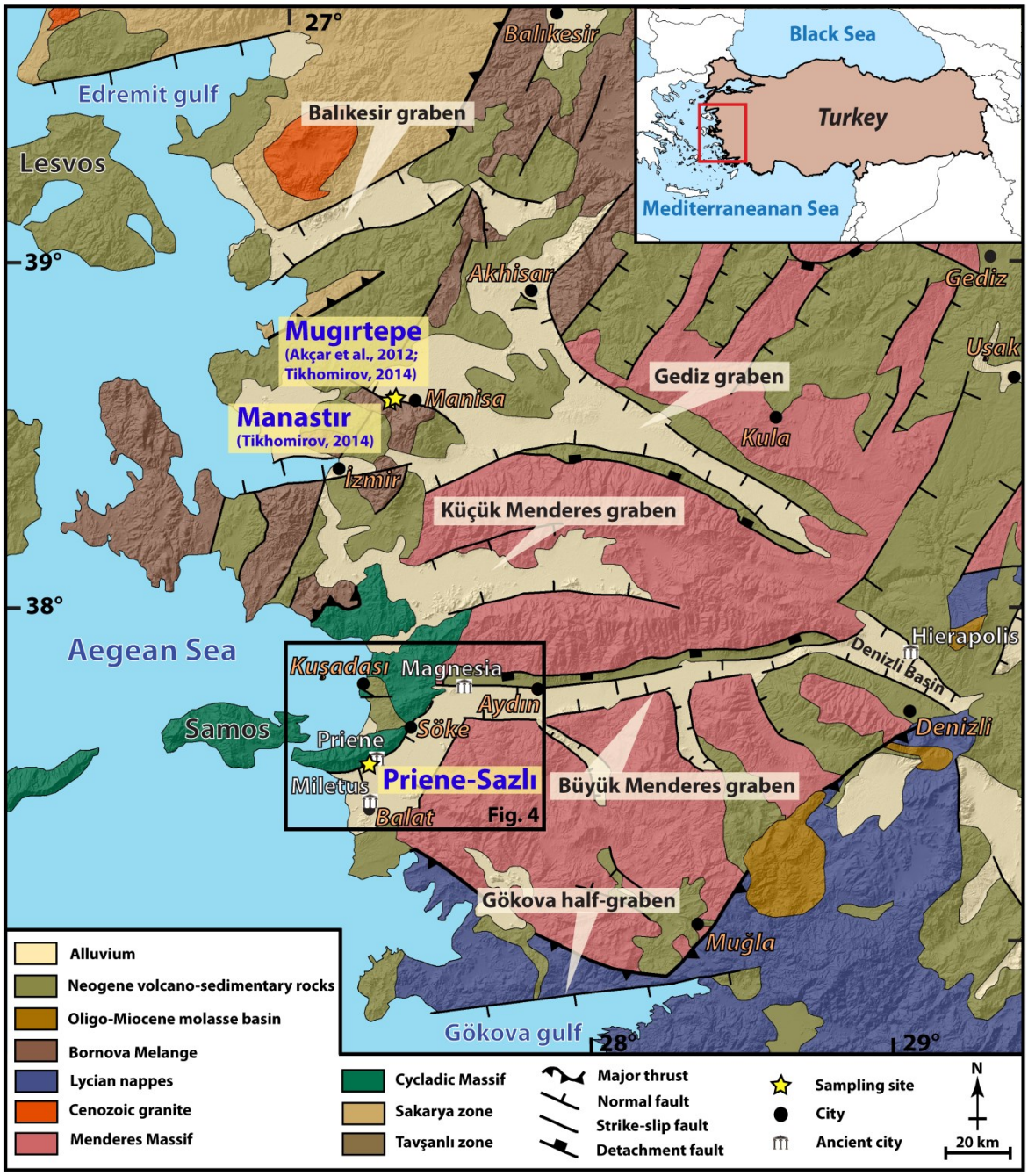

Fig. 2. Simplified geological map of western Anatolia (modified after Hancock and Barka, 1987; Akçar et al., 2012; Sümer et al., 2013). The yellow stars show the locations of the sampling sites of this study in Priene-Sazlı Fault, Mugırtepe Fault in Manisa fault zone (Akçar et al., 2012) and Manastır Fault within Manisa Fault Zone (Tikhomirov, 2014). The black box gives location of Fig 4.

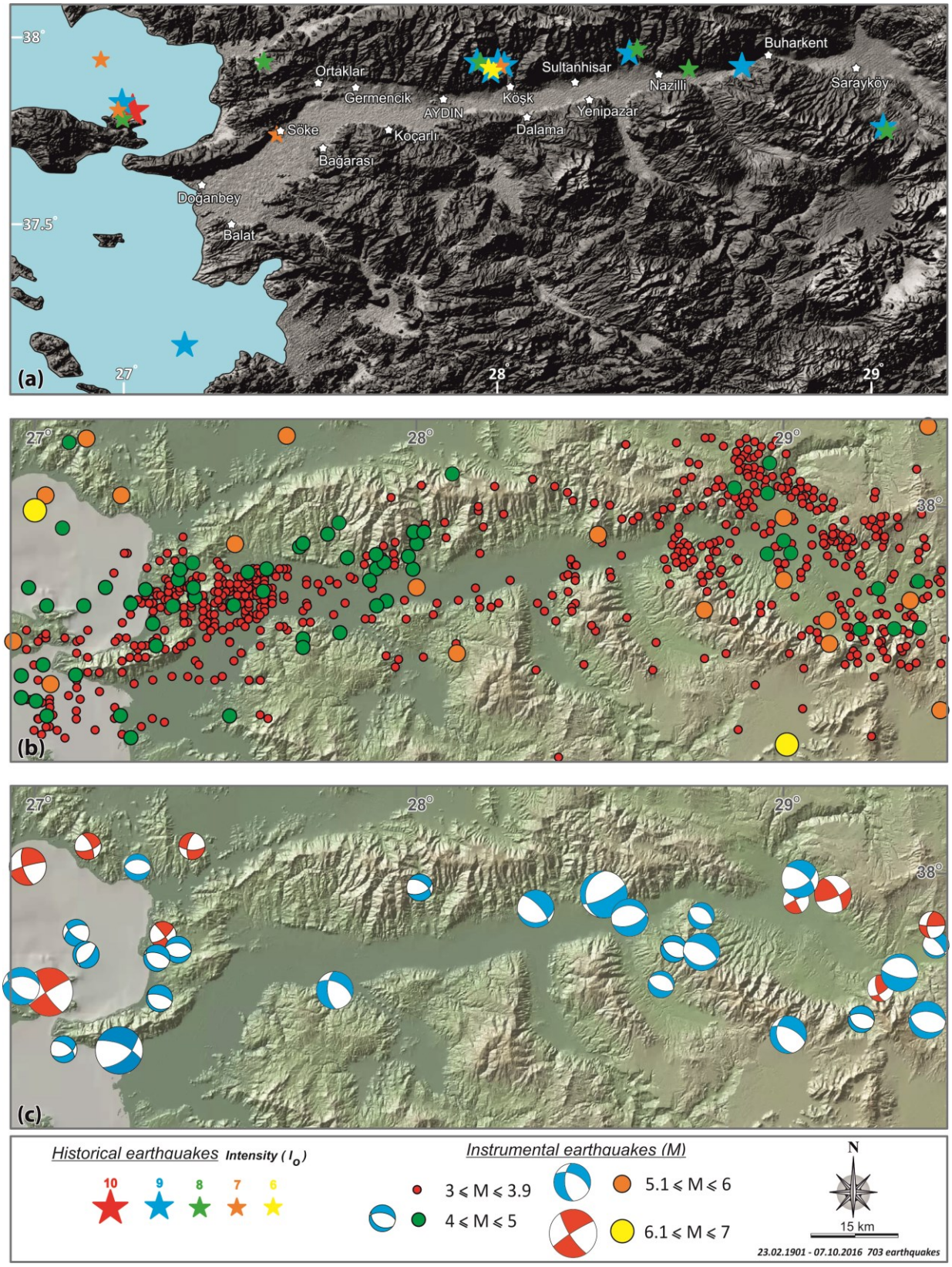
38°
37.5°
27°
28°
29°
(a)
Ortaklar
Germencik
AYDIN
Köşk
Sultanhisar
Nazilli
Buharkent
Sarayköy
Yenipazar
Dalama
Söke
Koçarlı
Bağarası
Doğanbey
Balat
(b)
(c)
Historical earthquakes Intensity (I_o)
10
9
8
7
6
Instrumental earthquakes (M)
3 ⩽ M ⩽ 3.9
4 ⩽ M ⩽ 5
5.1 ⩽ M ⩽ 6
6.1 ⩽ M ⩽ 7
N
15 km
23.02.1901 - 07.10.2016 703 earthquakes

Fig. 3. Seismotectonic map of Büyük Menderes Graben and surrounding area showing locations of (a) historical earthquakes (Collection Academique. Tome VI de la Partie Entrange et Premier Tome de la Physique Experimentale Separee. 1766; Broughton, 1938, Calvi, 1941; Dikmen, 1952; Pınar & Lahn, 1952; Ergin et al., 1967; Öcal, 1968; Karnik, 1971; Shebalin et al., 1974; Ambraseys, 1975; Soysal et al., 1981; Guidoboni et al., 1994; Ambraseys, 2009; (b) Instrumental earthquakes; and (c) selected focal mechanism solution (FMS) of the instrumental earthquakes (McKenzie, 1972; Cannıtez & Üçer, 1967; Kalafat, 1998; Taymaz, 1993; Harvard Centroid -Moment Tensor Project CMT, Harvard University, MA, USA (1977–2015) (www.globalcmt.org/CMTsearch); Tan & Taymaz, 2001; 2003; Taymaz et al., 2004; Kalafat et al., 2009; National Observatory of Athens, Greece (bbnet.gein.noa.gr); Istituto Nazionale di Geofisica e Vulcanologia, Italy (http://istituto.ingv.it/); Boğaziçi University Kandilli Observatory and Earthquake Research Institute (koeri.boun.edu.tr/scripts/lst4.asp); Republic of Turkey Prime Ministry Disaster & Emergency Managment Presidensy-Earthquake Research Department (AFAD-ERD) (https://www.afad.gov.tr/en/); United States Geological Survey National Earthquake Information Center (earthquake.usgs.gov/contactus/golden/neic.php).

In this study, we revealed the paleoseismic history of the Priene-Sazlı Fault by focusing on historical archives and beyond it, to present seismic behavior of the fault. Therefore, our aims are to: (1) identify the past ruptures and reconstruct the chronology of the Priene-Sazlı Fault activity; (2) determine the average slip rates; (3) calculate the return period of the destructive earthquakes; and (4) approximate the magnitude of future earthquakes. To fulfill this, we selected a well-exposed surface of the Priene-Sazlı Fault at the lowermost level of successive scarp. This site is close to the epicenter of 1955 earthquake and the ancient city of Priene. A total of 117 samples along four strips were collected for cosmogenic ^{36}Cl analysis. We used Fault Scarp Dating Tool (FSDT) (Tikhomirov, 2014), a Matlab® code developed to analyze measured cosmogenic ^{36}Cl concentrations. According to our results and based on the modeled vertical components of slips, the Priene-Sazlı Fault experienced at least four major periods of earthquakes with average magnitude of 6.8 during the Holocene. Taking into account the length of the fault, an earthquake with magnitude of average 6.9 in future is expected.

2. Büyük Menderes Graben and Priene-Sazlı Fault

Büyük Menderes Graben is a roughly arc-shaped 140 km long and 2-14 km wide structure (Gürer et al., 2009). The graben system extends between Denizli Basin in the east (E-W trending) and the Aegean Sea in the west (NE-SW) (Fig. 2). The Menderes Massif borders the Büyük Menderes Graben to the north and south. Gentle topography of the southern part of the graben in comparison to the northern side gives rise to its asymmetric morphological feature (Gürer et al., 2009). The horst-graben structure of the Büyük Menderes is influenced by the Büyük Menderes

Fault Zone with faulting extending along the entire length of its northern edge. The fault zone is composed of six main segments with individual characteristics regarding morphological and geological properties that form an en-echelon structure (Altunel et al., 2009). Along the active Büyük Menderes Fault Zone, well-exposed archaeological sites (e.g., Priene) have been discovered, where destructive earthquakes caused damage during both the historical period and the 20th century (Fig. 4) (Altunel, 1998; Yönlü et al., 2010).

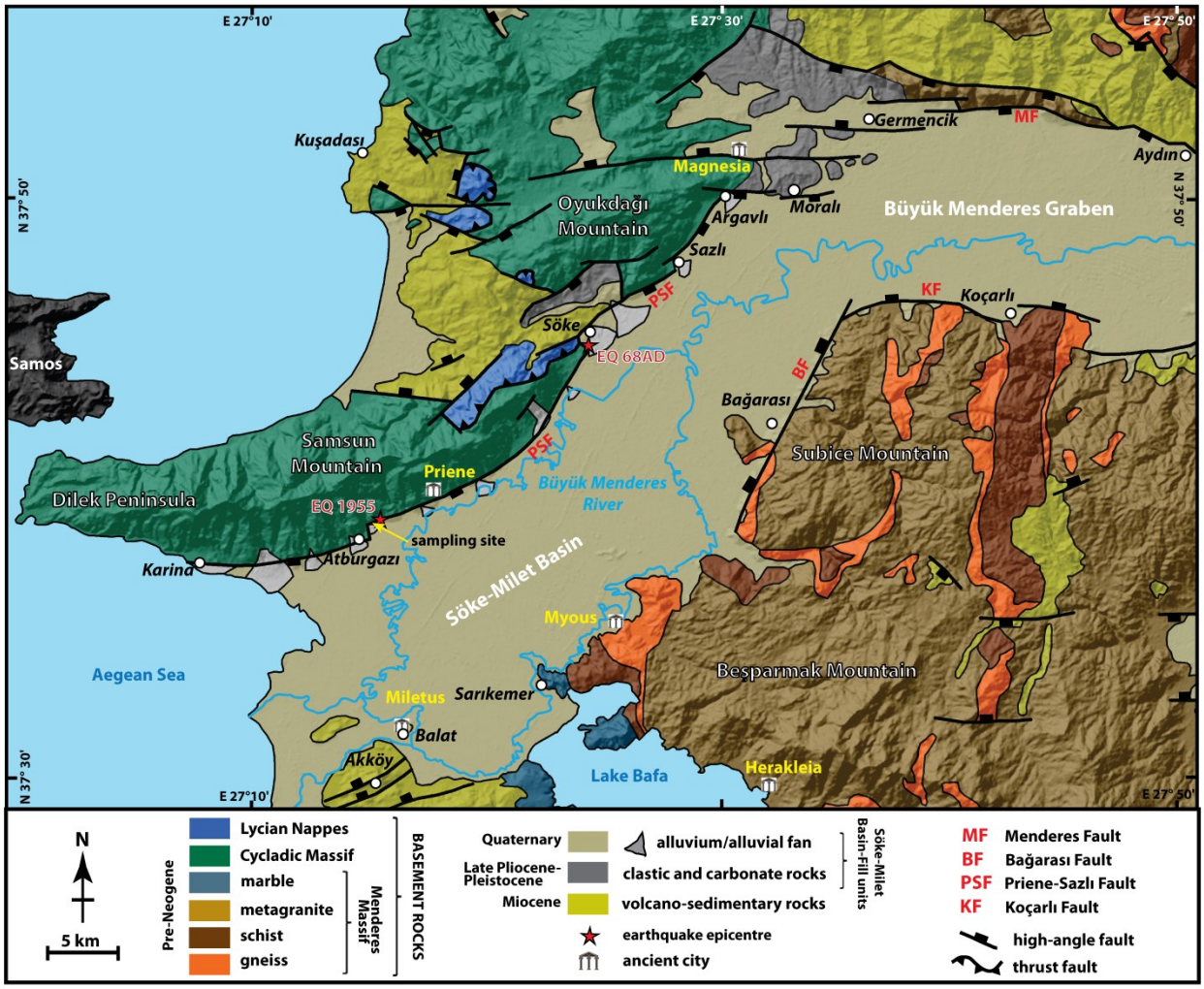

Fig. 4. Geological map of the western part of Büyük Menderes Graben, including location of earthquakes of 68 AD and 1955 and the sampling site (modified after Sümer et al., 2012).

The Priene-Sazlı Fault is located at the westernmost end of the Büyük Menderes Graben (Figs. 2 and 4). The fault has the longest length within the entire fault zone, and extends along the margin of Samsun Mountain (Fig. 4). Altunel et al. (2009) consider the Priene-Sazlı Fault to be 30 km long; whereas Sümer et al. (2013) assert that the total fault length is 37 km (including the 30 km Priene segment and a

section of the Sazlıköy segment; Altunel et al., 2009). According to Sümer et al. (2013), the Priene and Sazlıköy segments are probably connected around Söke, even though tracing is difficult due to overburden of alluvial fan deposits. The fault length is given as 38 km long in the active fault map of Turkey (Şaroğlu et al., 1992). However, the longest length suggested for the fault is 40 km in length (Duman et al., 2011; Emre et al., 2013).

In general, the northeastern segments of the Priene-Sazlı Fault are structurally characterized by strike-slip lineations representing dextral and sinistral movements, which are later overprinted by an oblique-slip normal component. The southwestern segment of the fault, however, is dominated by dip-slip lineations along with minor dextral movement. These oblique and dip slips are present along the entire length of the fault segments (Sümer et al., 2013). According to Sümer et al. (2013), the Priene-Sazlı Fault is a reactivated structure initiated in the Miocene as a dextral strike-slip fault, whose mechanism later changed to sinistral strike-slip. The fault was reactivated again during the Quaternary as an oblique to dip-slip normal fault. The activity of the fault during the Quaternary is, however, proven by development of the lateral alluvial fans near Atburgazı in the late Pleistocene, which were intersected and uplifted the new segment of the fault (Gürer et al., 2001 and references therein). Additionally, Sümer et al. (2012), assert that the fault cut and uplifted the Late Pliocene to Pleistocene aged sedimentary formation near Söke. The formation contains an ash layer with the youngest age is 950 Ka, which indicates that the fault has been active at least since the middle Pleistocene until today (Sümer et al., 2012).

The Söke-Milet Basin stratigraphically constitutes three main groups of rocks: (1) basement rocks, mainly Cycladic Massif; (2) Miocene Söke Basin-fill units; and (3) post-Miocene Söke-Milet Basin fill units (Sümer et al., 2012). The Quaternary Söke-Milet Basin constitutes the hanging-wall of the Priene-Sazlı Fault (Figs. 4 and 5). The Priene-Sazlı Fault generally juxtaposes the Quaternary sediments of the Söke-Milet Basin with the Cycladic Massif in the footwall, which is largely consists of marble and recrystallized limestone (Sümer et al., 2013) (Fig. 4).

Fig. 5. Field view of the Priene-Sazlı Fault, showing pre-Neogene basement rocks against Söke-Milet Quaternary Basin. Photo was taken from the sampling site.

3. Fault scarp dating

Fault scarp dating with cosmogenic ^{36}Cl was first introduced by Zreda and Noller (1998), with reconstruction of six pre-historic seismic activity ages in the Hebgen Lake fault scarp, Montana, USA. During the last two decades, the time-slip histories of limestone fault scarps have been modeled in several locations in the Eastern Mediterranean and the Middle East (Mitchell et al., 2001; Benedetti et al., 2002; 2003; 2013; Palumbo et al., 2004; Schlagenhauf et al., 2010; 2011; Akçar et al., 2012; Tikhomirov, 2014; Mouslopoulou, 2014).

Mitchell et al. (2001) provided a computer code and modeled three distinct periods of paleoseismic activity using cosmogenic ^{36}Cl surface fault scarp dating on the Nahef East Fault scarp, Israel. Benedetti et al. (2002) studied the Sparta Normal Fault scarp (Greece) and reconstructed six seismic events including the 464 B.C Sparta earthquake. Furthermore, Benedetti et al. (2003) recovered three rupture events on the Kaparelli Fault, Greece, aged between 10-20 ka. Palumbo et al. (2004) revealed five to seven seismic ruptures during the last 12 ka on the Mangola Fault, Italy, at one site. Schlagenhauf et al. (2010) developed a new Matlab® code and reprocessed the cosmogenic ^{36}Cl data from the Mangola Fault (Palumbo et al., 2004). They recovered the same number of events at ca. 7.2, 4.9, 4.0, 3.4 and 1.5 ka, but with younger ages compare to Palumbo et al. (2004), who determined events at ca. 12, 10.5, 7.4, 6.7 and 4.8 ka ago. Schlagenhauf et al. (2011) sampled four additional sites on Velino-Magnola Fault, and have reconstructed an age-slip history

of a minimum of nine major ruptures over the last 15 ka based on the results from the five sites (one from Palumbo et al., 2004). Akçar et al. (2012) applied the Matlab® code of Schlagenhauf et al. (2011) on the Mugırtepe Fault in the Manisa Fault Zone, Turkey to model measured cosmogenic ^{36}Cl (Fig. 2). They proposed two scenarios for the exposure of the fault, including one or two seismic event(s). Benedetti et al. (2013) recovered more than 30 major earthquakes over the last 12 ka on the Fucino Fault System, Italy, based on cosmogenic ^{36}Cl measurements from 11 sites, including one and four site(s) studied by Palumbo et al. (2004) and Schlagenhauf et al. (2011), respectively. Tikhomirov (2014) developed a new Matlab® code and re-analyzed the results from the Mugırtepe Fault (Akçar et al., 2012) and in addition the Manastır Fault in the Manisa Fault Zone (Fig. 2). The new modeling resulted in one rupture for each fault. Mouslopoulou et al. (2014) applied the code of Schlagenhauf et al. (2011) on the Spili Fault (Crete) and reconstructed five major rupture events over the last 16.5 ka. Cowie et al. (2017) combined cosmogenic ^{36}Cl dating with LiDAR and GRP methods to reconstruct slip history of Italian Apennines over the last 18 ka and found episodic activity of the Fiamignano Fault.

3a. Sampling

In normal faults, vertical displacement is not uniform along the entire fault strike (e.g. Walsh and Watterson, 1988; Marrett and Allmendinger, 1991). In general, normal fault has the highest vertical displacement in the center of its strike, whereas it decreases to zero towards the tips. The displacement pattern follows an approximate elliptical isoline with the short axis parallel to the displacement and the long axis parallel to the fault strike (Barnett et al., 1987; Walsh and Watterson, 1987; Walsh et al., 2003; Kim and Sanderson, 2005) (Fig. 6). Therefore, an appropriate sampling site for cosmogenic ^{36}Cl analysis is a neat surface around the fault scarp centre. In addition, the surface to be sampled should have minimum amount of weathering and erosion (e.g. Mitchell et al., 2001). In order to model at least one past rupture using FSDT code by Tikhomirov (2014), the length of the exposed fault scarp for sample collection should be a minimum of two meters from the ground level. Preferably, a continuous strip parallel to the vertical slip vector is sampled. However, a series of strips shifted laterally can be also sampled (e.g., Benedetti et al., 2002;

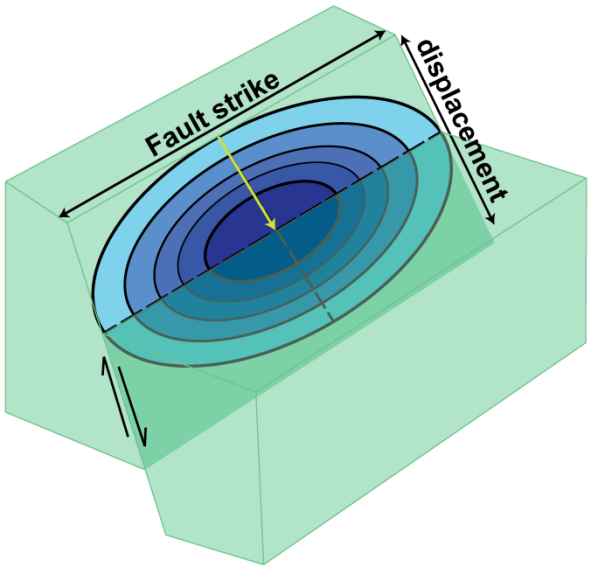

Fig. 6. Schematic cartoon of normal fault illustrating displacement distribution on elliptical fault pattern, which has a maxima in the center of the fault strike (modified after Kim and Sanderson, 2005). The short axis of elliptical isolines is parallel to displacement and the long axis is parallel to the fault strike.

Sclaugenhauf et al., 2011; Akçar et al., 2012), where there is clear evidence for weathering and erosion (Tikhomirov, 2014).

We sampled a well-exposed, N60E, 50°-55°, SE-dipping section of the scarp surface in the lowermost part of the Priene-Sazlı Normal Fault escarpment with minimum weathering and erosion along the centre of the fault strike close the maximum slip (Figs. 7 and 8). We marked four sampling strips, in total ca. 12 meters high, and parallel to the slip direction (Figs. 7b and 7c). A total of 117 slabs of 15 cm wide and 10 cm high were cut using a hand-held diamond saw. From the 7.3 m long strip A, 73 slabs were collected as the main strip (Fig. 7d), while the remaining 44 slabs were collected from strips B, C and D. Afterwards, the slabs were taken out using a chisel and hammer (Fig. 7d). The geometry of the fault scarp strongly determines the shape of the modeled concentration profile. Hence, field measurements of the scarp are important for precise dating of the fault scarp. The main parameters of the scarp geometry required to model the rupture history are: (1) scarp dip (the angle between the fault scarp surface and horizontal plane); (2) scarp height (height of the fault scarp surface from the ground level to the fault scarp top edge); (3) top surface dip (angle between upper part of the fault scarp and the horizontal plane); and (4) colluvium dip (angle between colluvium surface of about 15 m apart from the fault surface and horizontal plane) (e.g. Schlagenhauf et al., 2010; Tikhomirov, 2014) (Fig. 7e). During our fieldwork, the exact position of each sample was measured relative to the ground level. Topographic shielding was defined as obstacles around the scarp including mountains, ridges and upper scarps. In addition, the density of colluvium was measured with a bucket of known volume and a balance in the field.

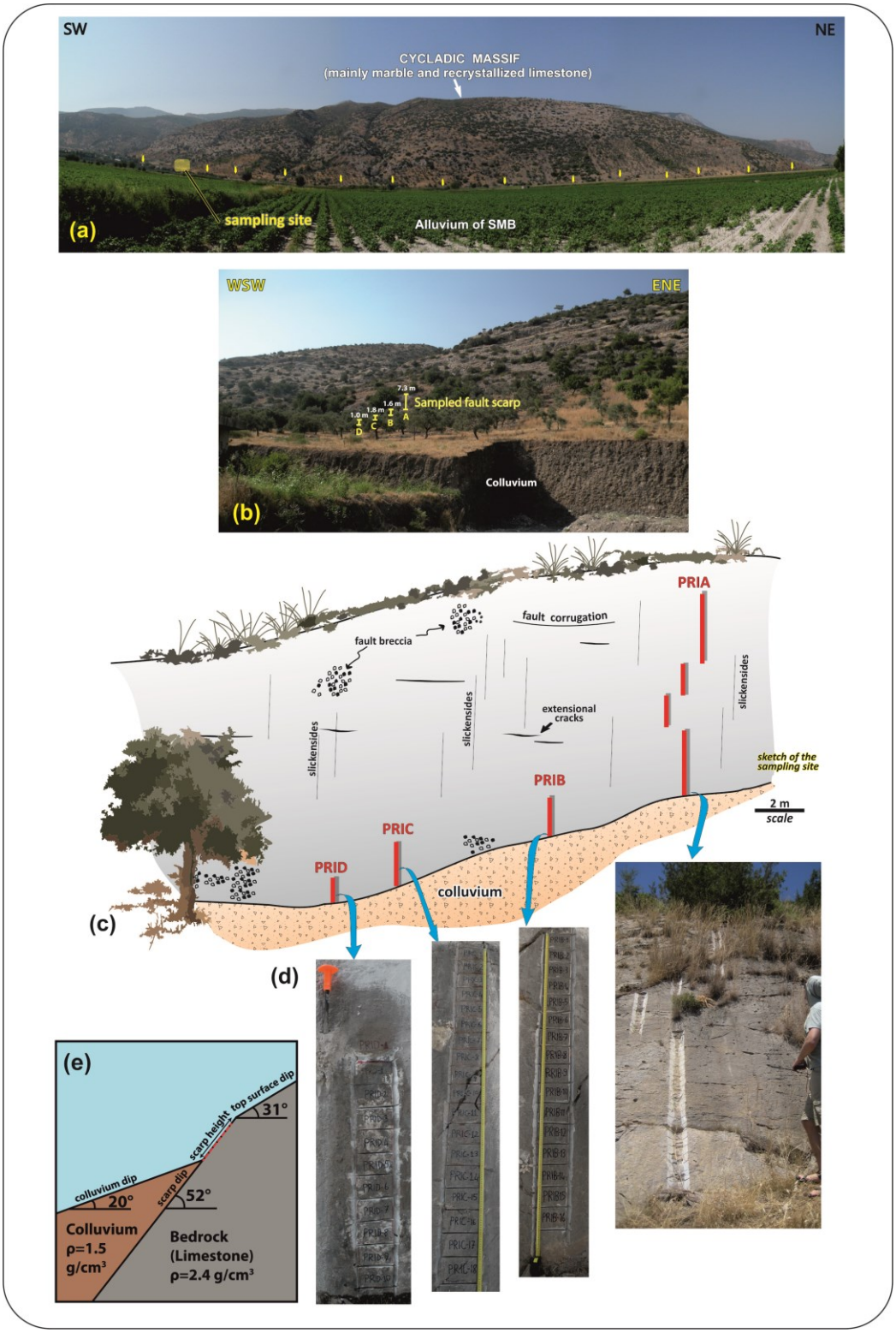

Fig. 7. (a) Field view of the Priene-Sazlı Fault scarp at the base of the escarpment. (b) More detailed view of fault scarp with positions of the continuous sampled strips A, B, C and D. The sampled surface is the lowest exposed surface of the successive scarp system. (c) Schematic sketch of fault scarp surface representing four sampled strips. (d) Fault scarp surface showing sampling slabs along strip A, B, C and D. (e) Schematic sketch showing important parameters of the fault scarp for modeling, including scarp height, scarp dip, colluvium dip, top surface dip and density of the bedrock and colluvium. Red dashed line shows the sampled surface.

Fig. 8. The sampled surface of the Priene-Sazlı Fault scarp.

3b. Cosmogenic ^{36}Cl analysis

The samples were prepared at the Surface Exposure Dating Laboratory of University of Bern, according to the procedure introduced by Stone et al. (1996) and Ivy-Ochs et al. (2004; 2009), and based on the isotope dilution technique (Elmore et al., 1997; Ivy-Ochs et al., 2004; Desilets et al., 2006). The collected slabs were cut parallel to the surface to a maximum thickness of 3 cm. The samples were then crushed and sieved into the 0.25-0.4 mm fraction. Thereafter, the metal-chips from the grinding material were removed by a hand magnet. In order to remove non-in situ Cl (Zreda et al., 1991), the crushed material was leached in 75 ml of 2M HNO_3 overnight and then rinsed four times with ultrapure water (18.2 MΩ.cm). Leaching was repeated for a second time. The samples were then dried on a hotplate at 60 °C. Aliquots of around 12 g from each of 10 samples as representative samples were analyzed for major and trace elements by ICP-MS at SGS Mineral Services, Toronto, Canada. In addition, the Ca content was determined for each sample individually.

Afterwards, batches of 15 samples along with one full process blank were processed. Samples were spiked with about 2.5 mg ultra-pure ^{35}Cl to determine the amount of total Cl concentration (^{35}Cl, ^{37}Cl) (Ivy-Ochs et al., 2004; 2009) and

dissolved with HNO_3. Determination of the total Cl concentration is required in order to calculate: (1) ^{36}Cl concentration in the sample from the AMS measured $^{36}Cl/Cl$ ratio; (2) ^{36}Cl production on ^{35}Cl by low-energy neutron capture; and (3) non-cosmogenic subsurface production of ^{36}Cl (Ivy-Ochs et al., 2004). The samples were centrifuged to separate impurities. In the dark, 10 ml of $AgNO_3$ was added to the supernatant at 200 °C to precipitate AgCl. Then, the precipitated AgCl was collected and dissolved with 2 ml of NH_4OH. The samples were centrifuged to eliminate cations. $BaSO_4$ was precipitated by addition of $Ba(NO_3)_2$ to the supernatant, in order to avoid interference of ^{36}S isobar with ^{36}Cl during Accelerator Mass Spectrometry (AMS) measurements. Finally, the AgCl decant was recovered as a solid, rinsed by ultrapure water and dried. AgCl samples were pressed into targets for AMS measurements.

The concentrations of total Cl and ^{36}Cl were measured from a single target at the ETH AMS facility following the isotope dilution technique (Synal et al., 1997; Ivy-Ochs et al., 2004), which results in increasing precision and sensitivity of the ^{36}Cl measurement (Ivy-Ochs et al., 2004; Desilets et al., 2006). The stable ratio of $^{37}Cl/^{35}Cl$ was normalized to the neutral ratio $^{37}Cl/^{35}Cl$ = 31.98 % of the K382/4N standard and the machine blank, whereas sample ratios of $^{36}Cl/^{35}Cl$ were normalized to the ETH internal standard K382/4N with a $^{36}Cl/Cl = 17.36 \times 10^{-12}$ (normalized to the Nishiizumi standard in 2009). The sulfur correction of measured $^{36}Cl/^{35}Cl$ ratios was negligible. In addition, $^{36}Cl/^{35}Cl$ ratios of the measured samples were corrected for a procedure blank of 6×10^{-15}, which amounted to a correction of less than 2.5 % for the samples.

3c. Data analysis software

We carried out an analysis of the Priene-Sazlı data set with the FSDT forward modeling Matlab® code -Fault Scarp Dating Tool- (Tikhomirov, 2014). The code applies the fault scarp shielding model (Tikhomirov et al., 2014) to calculate the ^{36}Cl accumulation, a two-step approximation to reconstruct a particular rupture history, and the Monte-Carlo method to search for the most realistic rupture history. Rupture histories are randomly generated in bounded solution space and evaluated with statistical tests to compare the measured and modeled ^{36}Cl profiles.

Reconstruction of an exposure history of a fault scarp is performed in two stages (Tikhomirov, 2014). At the first stage, distributions of particle fluxes are precisely calculated at the nodes of a 3D mesh, which covers all possible positions of the sample strip. The program automatically saves the results of the first stage, which is used as a database for the second stage of calculations. At the second stage, database fluxes are interpolated to represent a given exposure history of the fault scarp, and the concentration profile of accumulated cosmogenic ^{36}Cl is calculated. The modeled and measured ^{36}Cl profiles are compared using statistical tests of chi-square (X^2), weighted root mean square (RMSw) and Akaike information criterion (AICc), which are computed for each rupture history. Modeled rupture histories are automatically generated in a bounded solution space with the Monte-Carlo method. In the initial runs, a wide solution space in terms of various scenarios with different number of rupture events, ages and associated slips are applied. In later simulations, the solution space is narrowed around the most probable values. And finally, the scenario with the lowest X^2 and AICc value is accepted as the most probable solution.

The FSDT code accounts for all production pathways of cosmogenic ^{36}Cl, such as high energy neutrons, fast and negative muons, thermal and epithermal neutrons (Liu et al., 1994; Phillips et al.; 1996; 2001; Stone et al., 1996; 1998; Alfimov and Ivy-Ochs, 2009; Schimmelpfennig et al., 2009). We used the following production rates of ^{36}Cl by high-energy neutron spallation 48.8 ± 3.4 at.g^{-1} yr^{-1} on Ca (Stone et al., 1996), 170 ± 25 at.g^{-1} yr^{-1} on K (Evans et al., 1997), 13 ± 3 at.g^{-1} yr^{-1} on Ti (Fink et al., 2000) and 1.9 ± 0.2 at.g^{-1} yr^{-1} on Fe (Stone, 2005). The production rate of epithermal neutrons from fast neutrons in the atmosphere at the land/atmosphere interface of 760 ± 150 n/g^{-1} yr^{-1} was used (Alfimov and Ivy-Ochs, 2009). In order to scale to the local production rates, we applied the scaling factors of Stone (2000) for a constant geomagnetic field. Besides the production rates, an analysis with the FSDT code requires scarp geometry, topographic shielding, chemical composition of each sample and colluvium, as well as thickness and position of each sample.

4. Results

The position of the samples along the fault scarp, the sample thickness, the cosmogenic ^{36}Cl concentration and its uncertainty, the natural chlorine concentration, as well as calcium, oxygen and carbon concentrations are listed in Tables 1-4 for the sampling strips A, B, C and D, respectively. Major and trace elements concentrations of 14 representative samples of the fault scarp and averaged values used for modeling are given in Table 5. The fault scarp parameters are shown in Table 6. The density of colluvium was measured as 1.5 g/cm^3 in the field and the density of the scarp is considered as 2.4 g/cm^3.

Measured cosmogenic ^{36}Cl concentrations and their 1σ errors are plotted as a function of height within each strip (Fig. 9). The concentration of cosmogenic ^{36}Cl varies between 0.918 (± 0.052) x 10^5 at.g^{-1} to 3.558 (± 0.133) x 10^5 at.g^{-1} along the strips (Fig. 9). Cosmogenic ^{36}Cl concentrations along the fault scarp in strip A show a clear logarithmic increase with height (Fig. 9a), while they vary almost within 1σ in B, C and D strips (Figs. 9b, 9c and 9d).

The probability density function (PDF) of cosmogenic ^{36}Cl normalized to Ca concentrations for strips A, B, C and D are plotted in Figure 10. The PDF plot of strip A detects nonlinear ^{36}Cl distributions, in which vertical dashed lines mark maximum probability density indicating three notable peaks at the heights of around 1.0, 2.5 and 5.5 m along the fault scarp (Fig. 10a). In strips B, C and D concentrations of cosmogenic ^{36}Cl along the scarp height form only one peak in each PDF plot (Figs. 10b, 10c and 10d).

For the modeling of the paleoseismic history of the Priene-Sazlı Fault, we first run the code with various rupture scenarios in terms of constraining the number of earthquakes, age of the earthquakes, slip amounts and erosion rates. Then, we focused on three scenarios with the best statistics. The best fit solution for each scenario is summarized in Table 7. These are four earthquake scenario with the RMSw = 1.5851, X^2 = 2.9094 and AICc = 291.5423, five earthquake scenario with RMSw = 1.5889, X^2 = 3.0235 and AICc = 296.9936 and six earthquake scenario with RMSw = 1.5923, X^2 = 3.1286 and AICc = 301.6824. The known earthquakes of 68

AD and 1955 were given as independent input parameters for the five and six earthquake scenarios. However, the value of modeled slip for the youngest event fitted to the 1955 earthquake, was either zero or very negligible in all runs (Table 7). In all examined scenarios, the slip value of the oldest modeled earthquake was higher than the succeeding slips.

TABLE 1. STABLE CL, COSMOGENIC ^{36}CL AND CALCIUM CONCENTRATIONS, THICKNESS, TOP AND BOTTOM POSITION OF THE SAMPLES OF STRIP A OF SCARP OF THE PRIENE-SAZLI SCARP

Sample name	Top position cm	Bottom position cm	Thickness cm	^{36}Cl* 10^5 at/g	^{36}Cl uncertainty*, 10^5 at/g	Cl $_{total}$*, ppm	Cl $_{total}$ uncertainty*, ppm	Ca+, ppm
PRI-A01	732	722	2.0	3.558	0.133	6.1	0.06	360205
PRI-A02	722	712	2.0	3.070	0.139	9.7	0.10	353058
PRI-A03	712	702	2.5	3.036	0.089	9.1	0.09	348056
PRI-A04	702	692	2.0	2.950	0.132	9.6	0.10	344482
PRI-A05	692	682	2.0	2.871	0.126	13.6	0.14	367352
PRI-A06	682	672	2.0	2.922	0.133	14.8	0.15	363064
PRI-A07	672	662	3.0	2.628	0.091	4.9	0.05	378073
PRI-A08	662	652	2.5	2.411	0.098	6.3	0.06	368782
PRI-A09	652	642	2.0	2.479	0.110	10.0	0.10	379502
PRI-A10	642	632	2.0	2.685	0.098	15.5	0.15	380217
PRI-A11	632	622	2.0	2.411	0.105	11.2	0.11	367352
PRI-A12	622	612	2.5	2.436	0.087	7.3	0.07	373785
PRI-A13	612	602	3.0	2.586	0.115	8.6	0.09	368782
PRI-A14	602	592	3.0	2.521	0.102	4.4	0.04	380217
PRI-A15	592	582	2.5	2.360	0.108	2.6	0.03	375214
PRI-A16	582	572	2.0	2.536	0.115	4.4	0.04	354488
PRI-A17	572	562	2.0	2.402	0.083	4.7	0.05	366638
PRI-A18	562	552	2.5	2.367	0.098	2.0	0.02	380932
PRI-A19	552	541	2.5	2.705	0.118	3.6	0.04	376643
PRI-A20	541	531	5.0	2.397	0.105	7.0	0.07	369496
PRI-A21	531	521	2.5	2.591	0.134	8.4	0.08	365923
PRI-A22	521	511	2.0	2.313	0.087	7.6	0.08	368782
PRI-A23	511	501	2.0	2.250	0.119	7.6	0.08	351629
PRI-A24	501	491	2.5	2.180	0.118	7.4	0.07	358061
PRI-A25	491	481	2.5	2.077	0.093	6.7	0.07	353773
PRI-A26	481	471	2.0	2.382	0.111	7.2	0.07	359491
PRI-A27	471	461	2.0	1.919	0.076	8.6	0.09	363064
PRI-A28	461	451	2.0	2.177	0.107	10.1	0.10	355917
PRI-A29	451	441	2.5	2.162	0.119	2.6	0.03	369496
PRI-A30	441	431	2.0	2.121	0.082	2.7	0.03	381646
PRI-A31	431	421	2.5	2.192	0.093	3.4	0.03	385220
PRI-A32	421	411	2.0	2.088	0.079	7.0	0.07	382361
PRI-A33	411	401	2.5	2.171	0.091	8.8	0.09	362350
PRI-A34	401	391	2.0	2.208	0.104	4.8	0.05	382361
PRI-A35	391	381	2.5	2.033	0.085	5.1	0.05	371641
PRI-A36	381	371	2.0	2.229	0.112	12.6	0.13	349485
PRI-A37	371	361	2.0	1.791	0.079	12.3	0.12	358061
PRI-A38	361	351	2.0	1.821	0.097	12.4	0.12	372355
PRI-A39	351	341	2.0	1.526	0.086	8.8	0.09	365923
PRI-A40	341	331	2.0	1.843	0.081	7.0	0.07	363779
PRI-A41	331	321	2.0	1.797	0.097	6.5	0.06	348056
PRI-A42	321	311	2.0	1.524	0.067	4.3	0.04	335906
PRI-A43	311	301	2.0	1.839	0.093	4.8	0.05	330188

PRI-A44	301	291	2.0	1.815	0.097	6.1	0.06	357347
PRI-A45	291	281	2.0	1.771	0.087	8.3	0.08	358776
PRI-A46	281	271	2.0	1.804	0.092	7.3	0.07	360205
PRI-A47	271	261	2.0	1.599	0.061	6.4	0.06	348770
PRI-A48	261	251	2.5	1.672	0.093	7.9	0.08	350914
PRI-A49	251	241	1.5	1.742	0.102	7.6	0.08	365923
PRI-A50	241	231	2.0	1.744	0.079	7.2	0.07	363064
PRI-A51	231	221	2.5	1.493	0.097	4.8	0.05	330903
PRI-A52	221	211	2.0	1.316	0.054	4.2	0.04	358776
PRI-A53	211	201	2.0	1.510	0.095	2.8	0.03	357347
PRI-A54	201	191	2.5	1.681	0.075	2.9	0.03	358776
PRI-A55	191	180	2.5	1.328	0.066	4.0	0.04	345197
PRI-A56	180	170	2.0	1.317	0.063	4.6	0.05	328759
PRI-A57	170	160	2.0	1.394	0.065	3.6	0.04	343053
PRI-A58	160	150	2.0	1.280	0.058	2.6	0.03	353773
PRI-A59	150	140	2.0	1.659	0.081	2.8	0.03	339479
PRI-A60	140	130	2.0	1.313	0.068	1.7	0.02	355203
PRI-A61	130	120	2.5	1.357	0.065	2.3	0.02	355203
PRI-A62	120	110	1.5	1.179	0.056	3.9	0.04	345197
PRI-A63	110	100	2.0	1.222	0.066	4.1	0.04	350914
PRI-A64	100	90	2.0	1.340	0.060	8.0	0.08	367352
PRI-A65	90	80	3.0	1.166	0.074	4.6	0.05	332332
PRI-A66	80	70	2.0	1.127	0.051	4.7	0.05	325900
PRI-A67	70	60	2.0	0.928	0.068	6.1	0.06	295883
PRI-A68	60	50	2.0	1.083	0.047	5.0	0.05	325185
PRI-A69	50	40	2.0	1.058	0.052	3.8	0.04	343053
PRI-A70	40	30	2.0	1.126	0.059	6.6	0.07	357347
PRI-A71	30	20	1.5	1.170	0.056	10.1	0.10	372355
PRI-A72	20	10	2.5	1.268	0.065	9.5	0.09	368067
PRI-A73	10	0	2	1.154	0.060	6.8	0.07	373785

*Measured with accelerator mass spectrometry (AMS).
†Measured with ICP95A in SGS mineral services, Canada.

TABLE 2. STABLE CL, COSMOGENIC ^{36}CL AND CALCIUM CONCENTRATIONS, THICKNESS, TOP AND BOTTOM POSITION OF THE SAMPLES OF STRIP B OF SCARP OF THE PRIENE-SAZLI SCARP

Sample name	Top position cm	Bottom position cm	Thickness cm	^{36}Cl* 10^5 at/g	^{36}Cl uncertainty*, 10^5 at/g	Cl $_{total}$*, ppm	Cl $_{total}$ uncertainty*, ppm	Ca†, ppm
PRI-B01	160	150	2.0	1.362	0.069	7.7	0.08	380932
PRI-B02	150	140	2.0	1.254	0.066	6.6	0.07	380932
PRI-B03	140	130	1.5	1.270	0.073	6.2	0.06	388793
PRI-B04	130	120	2.0	1.194	0.066	6.1	0.06	389508
PRI-B05	120	110	3.0	1.337	0.085	6.2	0.06	388078
PRI-B06	110	100	1.5	1.198	0.076	4.7	0.05	384505
PRI-B07	100	90	2.0	1.374	0.069	5.5	0.06	395225
PRI-B08	90	80	2.5	1.348	0.068	4.9	0.05	392367
PRI-B09	80	70	2.0	1.224	0.072	5.1	0.05	386649
PRI-B10	70	60	2.5	1.133	0.064	6.1	0.06	371641
PRI-B11	60	50	2.0	1.210	0.066	4.6	0.05	373785
PRI-B12	50	40	2.0	1.138	0.058	4.6	0.05	379502
PRI-B13	40	30	2.0	1.350	0.078	4.4	0.04	381646
PRI-B14	30	20	2.0	1.043	0.061	4.3	0.04	384505
PRI-B15	20	10	3.0	1.255	0.074	4.6	0.05	385934
PRI-B16	10	0	2.0	1.017	0.053	3.9	0.04	380932

*Measured with accelerator mass spectrometry (AMS).
†Measured with ICP95A in SGS mineral services, Canada.

TABLE 3. STABLE CL, COSMOGENIC ^{36}CL AND CALCIUM CONCENTRATIONS, THICKNESS, TOP AND BOTTOM POSITION OF THE SAMPLES OF STRIP C OF SCARP OF THE PRIENE-SAZLI SCARP

Sample name	Top position cm	Bottom position cm	Thickness cm	^{36}Cl* 10^5 at/g	^{36}Cl uncertainty*, 10^5 at/g	Cl $_{total}$*, ppm	Cl $_{total}$ uncertainty*, ppm	Ca†, ppm
PRI-C01	179	169	2.0	1.181	0.062	9.0	0.09	324471
PRI-C02	169	159	2.0	1.272	0.059	8.3	0.08	330903
PRI-C03	159	149	3.0	1.287	0.067	6.6	0.07	351629
PRI-C04	149	139	2.0	1.344	0.078	7.1	0.07	335191
PRI-C05	139	129	2.0	1.155	0.061	9.1	0.09	326615
PRI-C06	129	119	2.0	1.261	0.058	9.0	0.09	331618
PRI-C07	119	109	3.0	1.227	0.056	7.3	0.07	338050
PRI-C08	109	100	2.0	1.243	0.076	8.4	0.08	340909
PRI-C09	100	90	2.0	1.096	0.056	10.4	0.10	344482
PRI-C10	90	80	2.0	1.111	0.050	7.5	0.07	335906
PRI-C11	80	70	2.0	1.111	0.056	7.1	0.07	336621
PRI-C12	70	60	2.0	1.329	0.079	8.0	0.08	357347
PRI-C13	60	50	2.0	1.205	0.055	7.6	0.08	354488
PRI-C14	50	40	2.0	1.258	0.050	6.7	0.07	360205
PRI-C15	40	30	2.0	1.176	0.060	5.7	0.06	383790
PRI-C16	30	20	2.0	1.060	0.052	9.0	0.09	383076
PRI-C17	20	10	2.0	1.281	0.059	11.5	0.11	385220
PRI-C18	10	0	2.0	1.119	0.063	6.0	0.06	380932

*Measured with accelerator mass spectrometry (AMS).
†Measured with ICP95A in SGS mineral services, Canada.

TABLE 4. STABLE CL, COSMOGENIC ^{36}CL AND CALCIUM CONCENTRATIONS, THICKNESS, TOP AND BOTTOM POSITION OF THE SAMPLES OF STRIP D OF SCARP OF THE PRIENE-SAZLI SCARP

Sample name	Top position cm	Bottom position cm	Thickness cm	^{36}Cl* 10^5 at/g	^{36}Cl uncertainty*, 10^5 at/g	Cl $_{total}$*, ppm	Cl $_{total}$ uncertainty*, ppm	Ca†, ppm
PRI-D01	102	91	2.5	1.171	0.053	12.3	0.12	350914
PRI-D02	91	81	2.0	1.161	0.067	9.6	0.10	352344
PRI-D03	81	71	2.5	1.241	0.060	25.8	0.26	362350
PRI-D04	71	61	2.0	1.279	0.079	30.9	0.31	373785
PRI-D05	61	51	3.0	1.177	0.067	20.7	0.21	363779
PRI-D06	51	41	2.0	1.111	0.057	13.5	0.13	345912
PRI-D07	41	30	2.5	1.081	0.066	20.7	0.21	345912
PRI-D08	30	20	1.5	1.101	0.066	19.8	0.20	347341
PRI-D09	20	10	2.0	0.918	0.052	18.7	0.19	330188
PRI-D10	10	0	2.0	0.987	0.061	19.2	0.19	333762

*Measured with accelerator mass spectrometry (AMS).
†Measured with ICP95A in SGS mineral services, Canada.

Among these scenarios, the scenario of four earthquake events showed the best fit with the beginning of the exposure at ca. 21 ka. The ages of the four earthquake events are: 8.1 ± 2.0 ka, 6.0 ± 1.5 ka, 3.7 ± 0.9 ka and 2.2 ± 0.5 ka with the vertical components of associated slip of 3.4 ± 0.5 m, 1.5 ± 0.2 m, 1.4 ± 0.2 m and 1.5 ± 0.2 m, respectively (Figs. 11 and 12). The distances between ruptures indicates mean values of vertical slip rates of greater than 0.3, 0.7, 0.6 and 1.0 mm/yr

from the oldest to the youngest modeled earthquake during the episodic activity period of the fault (Figs. 11 and 12). For calculating the long-term slip rate, about 4.4 m of slip is taken as having occurred in the time interval between the oldest and the youngest modeled rupture. This result yields a long-term vertical slip rate of 0.7 mm/yr. The recurrence interval of approximately 2000 years was calculated for the activity period of the fault.

TABLE 5. MEAN CHEMICAL COMPOSITION OF THE PRIENE-SAZLI SAMPLES AND COLLUVIUM

P	Cl (%)	O (%)	C (%)	CaO (%)	MgO (%)	Al_2O_3 (%)	SiO_2 (%)	P_2O_5 (%)	K_2O (%)
PRI-A02	0.000966	50.83965	10.46729	51.50	2.46	0.57	1.41	0.02	0.14
PRI-A11	0.001121	48.98633	10.89106	53.80	1.41	0.63	1.57	0.01	0.16
PRI-A16	0.000444	50.65485	10.50966	55.40	0.57	0.56	1.37	0.02	0.14
PRI-A25	0.000667	50.74729	10.48847	52.00	2.54	0.83	1.75	0.02	0.19
PRI-A32	0.000697	47.04093	11.33603	55.20	0.60	0.60	1.41	0.01	0.14
PRI-A48	0.000792	51.11780	10.40372	51.60	0.74	1.61	3.37	0.02	0.33
PRI-A57	0.000365	52.13746	10.17064	50.10	4.38	1.13	2.60	0.02	0.24
PRI-A67	0.000609	58.25266	8.77217	42.70	9.33	0.51	1.62	0.02	0.13
PRI-B07	0.000555	45.37323	11.71743	53.60	0.44	0.18	0.43	0.01	0.04
PRI-B12	0.000464	47.41180	11.25127	51.80	1.02	0.37	0.82	0.01	0.08
PRI-C05	0.000907	54.26806	9.68329	44.10	5.94	0.74	2.14	0.01	0.18
PRI-C18	0.000599	47.22635	11.29365	54.10	0.89	0.41	1.01	0.01	0.09
PRI-D02	0.000956	50.93232	10.44610	50.30	1.32	0.31	4.86	0.01	0.08
PRI-D08	0.001981	51.57990	10.29777	48.60	4.66	0.58	1.13	0.01	0.17
Average	*0.000660	50.11646	10.63273	51.05	2.59	0.65	1.82	0.01	0.15

	TiO_2 (%)	MnO (%)	Fe_2O_3 (%)	B (ppm)	Sm (ppm)	Gd (ppm)	U (ppm)	Th (ppm)
PRI-A02	0.03	0.02	0.81	6.00	0.70	0.50	2.82	0.90
PRI-A11	0.03	0.04	0.60	8.00	0.70	0.50	2.36	0.80
PRI-A16	0.03	0.02	1.10	8.00	1.10	0.50	2.84	1.30
PRI-A25	0.04	0.02	0.83	8.00	0.70	1.00	2.79	0.90
PRI-A32	0.03	0.02	1.00	7.00	1.40	0.50	2.45	1.10
PRI-A48	0.09	0.03	2.09	13.00	2.30	2.00	3.45	2.70
PRI-A57	0.06	0.04	0.86	12.00	1.50	1.00	5.01	1.70
PRI-A67	0.03	0.04	0.37	6.00	1.00	0.50	2.74	0.70
PRI-B07	0.01	0.02	0.12	2.50	0.50	0.50	1.72	0.20
PRI-B12	0.02	0.02	0.44	2.50	0.80	0.50	1.94	0.70
PRI-C05	0.04	0.04	0.80	7.00	1.30	0.50	2.39	1.10
PRI-C18	0.02	0.02	0.37	2.50	0.60	0.50	2.10	0.50
PRI-D02	0.01	0.01	0.16	2.50	3.10	2.00	1.15	0.30
PRI-D08	0.01	0.04	0.19	2.50	3.50	3.00	0.63	0.50
Average	0.03	0.03	0.69	6.25	1.37	0.96	2.45	0.95

* Average of values presented in Tables 1-4 are used for modeling.

TABLE 6. PARAMETERS OF THE SAMPLED FAULT SCARP

Latitude	37° 38.895' N			
Longitude	27° 15.421' E			
Altitude	52 m			
	Strip A	Strip B	strip C	Strip D
Scarp strike	N66°E	N45°E	N68°E	N60°E
Scarp dip	52°	55°	52°	50°
Colluvium dip	20°			
Scarp height	8.5 m			
Top surface dip	31°			
Rock density	2.4 g/cm^3			
Colluvium density	1.5 g/cm^3			
Rock water content	0.2 %			
Colluvium water content	1 %			

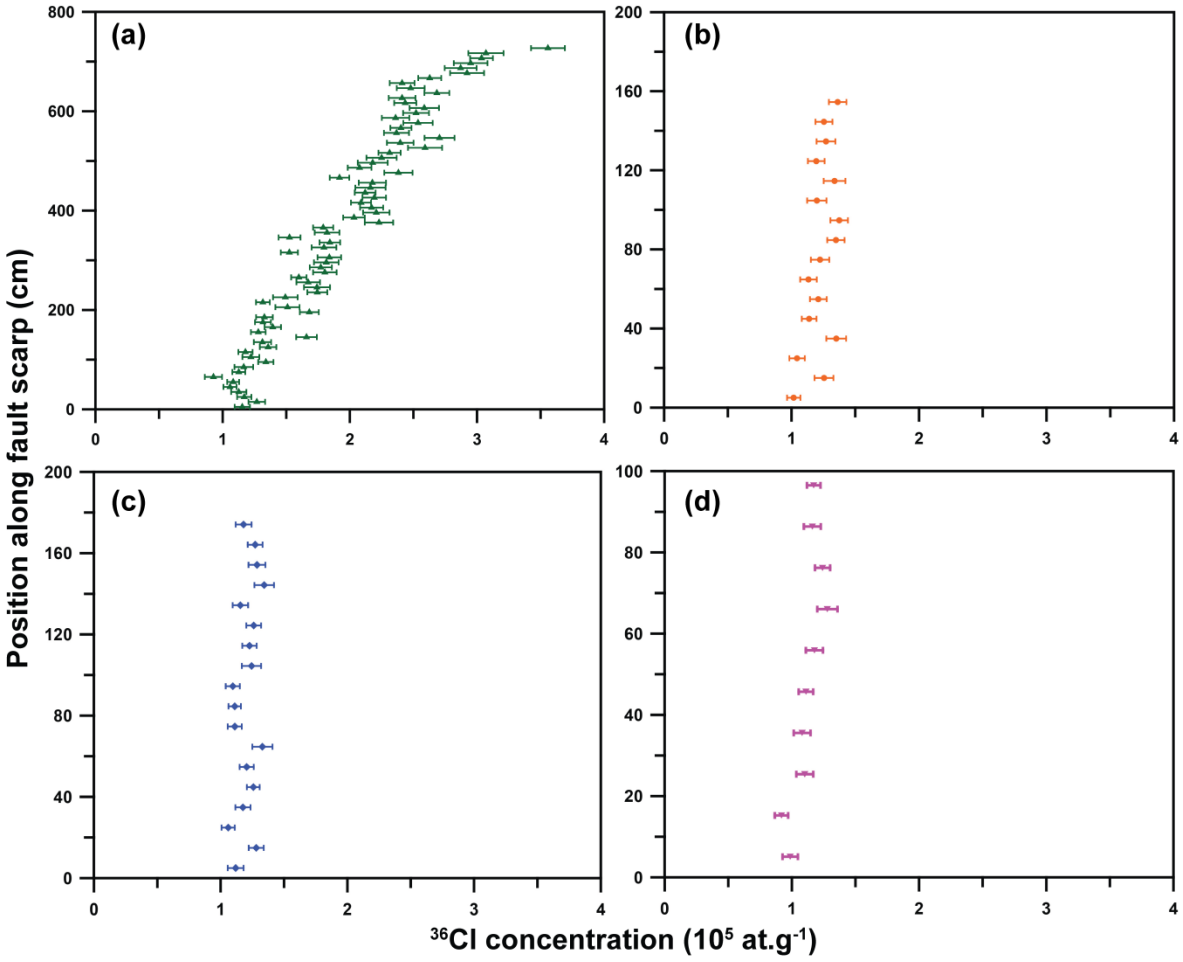

Fig. 9. Cosmogenic ^{36}Cl concentrations with 1σ uncertainties versus height along: (a) strip A; (b) strip B; (c) strip C; and (d) strip D.

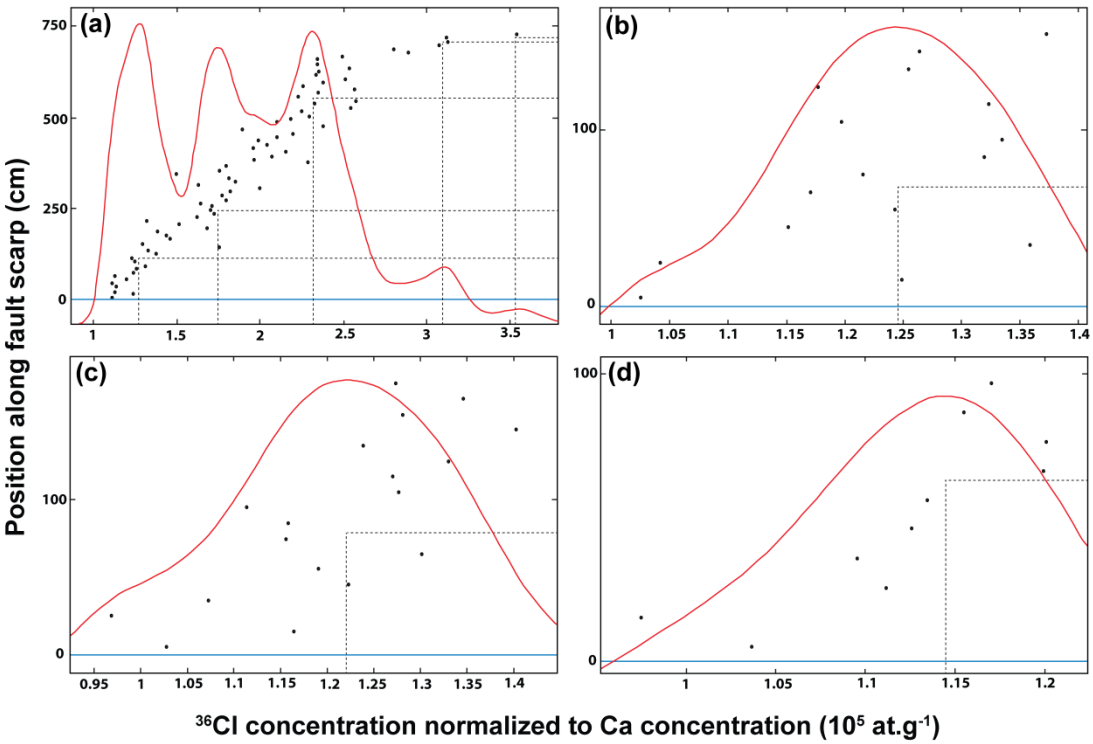

Fig. 10. The PDF (Probability Density Function) plot of ^{36}Cl concentrations normalized to Ca concentrations of: (a) strip A; (b) strip B; (c) strip C; and (d) strip D.

TABLE 7. OUTPUT RESULTS FOR THE DATA SET OF STRIP A OF THE PRIENE-SAZLI FAULT SCARP ALONG WITH STATISTICAL CRITERION

Event number	Beginning of exposure (ka)	Age (ka)	Slip (m)	
4	21	8.1 6.0 3.7 2.2	3.4 1.5 1.4 1.5	**X^2 = 2.9** **RMSw = 1.6** **AICc = 291**
5	22	7.3 5.8 3.7 2.1 0.07	4.0 1.1 1.4 1.7 0.0	X^2 = 3.0 RMSw = 1.6 AICc = 297
6	19	7.9 5.6 3.6 2.3 0.1 0.01	3.6 1.8 1.1 1.4 0.1 0.0	X^2 = 3.1 RMSw = 1.6 AICc = 301

Chi-squared Value (X^2)
Weighted root mean square (RMSw)
Akaike information criterion (AICc)

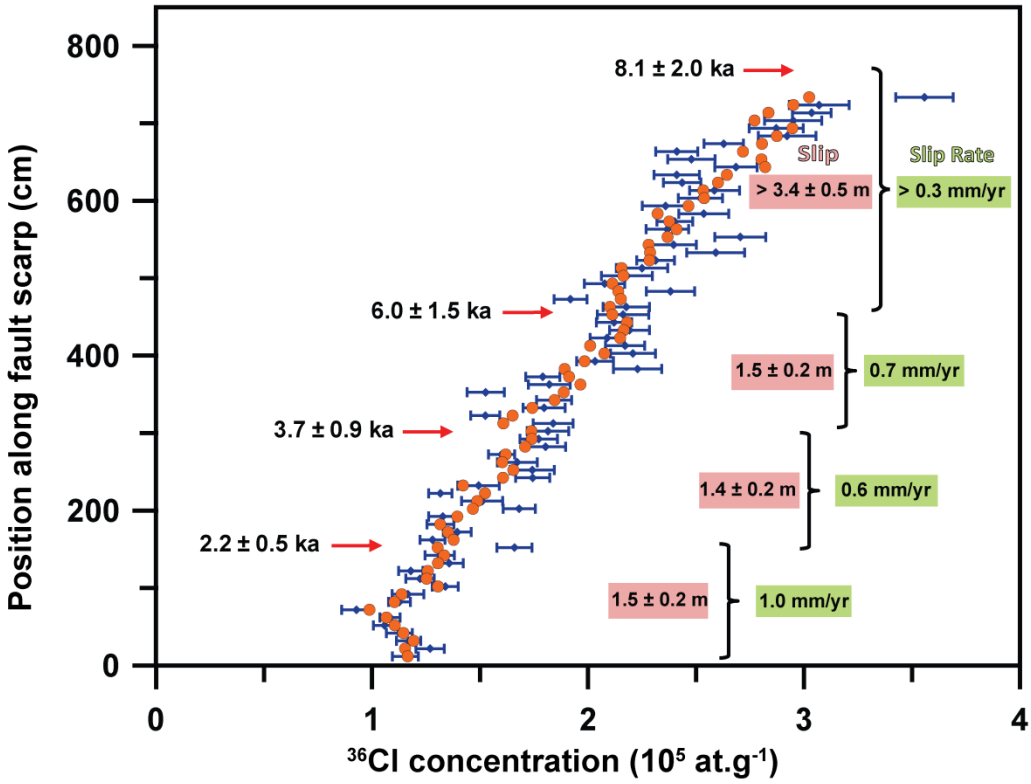

Fig. 11. Best fit (orange circles) of strip A of the Priene-Sazlı Fault scarp data with a four rupture model. Blue dots with 1σ uncertainties are measured ^{36}Cl concentrations. Red arrows mark the colluvium positions before the modeled ruptures. Slip rates are calculated individually for each earthquake, based on the slip value and the time period between two successive earthquakes.

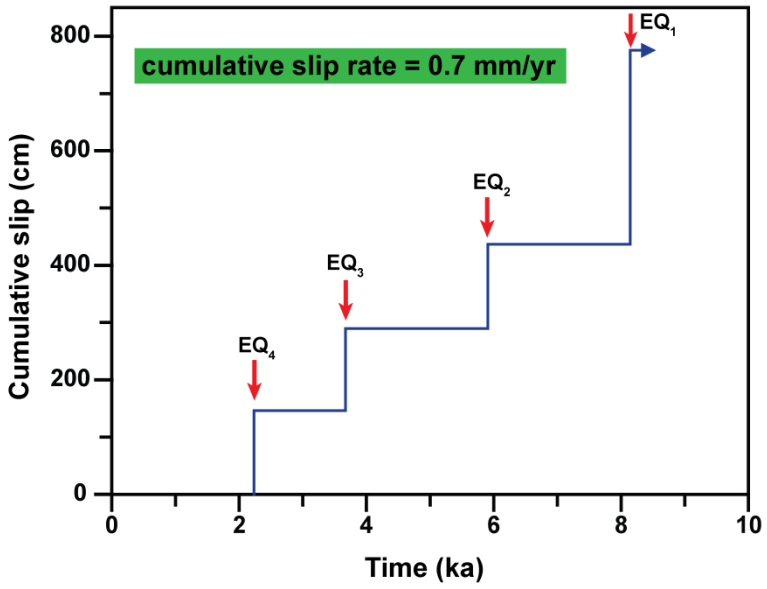

Fig. 12. Time versus cumulative slip amount obtained from modeling of the Priene-Sazlı Fault scarp. The average slip rate is 0.7 mm/yr.

5. Discussion

It is important to be considered the seismic exhumation history of major faults in order to estimate the approximate timing and size of their probable activity and minimize future probable damage (e.g., Scholz, 2002). We have recovered the time-slip history of the fault in order to present the past rupture pattern and the chronology of fault activity. The Priene-Sazlı Fault in the Büyük Menderes Graben is one of the major structures in the seismically active region of western Anatolia, which had two significant ruptures recorded over the past 2000 years in 68 AD and in 1955. Our analysis reveals four major events, which indicates that the Priene-Sazlı Fault is an active fault that was displaced vertically by at least 7.8 m during the Holocene (Fig. 11). It should be mentioned that the number of modeled earthquakes is the minimum, since the code is unable to identify small ruptures, which were not able to displace the fault. In addition, differentiation of earthquakes clustered close in time within 25% and 15% of uncertainties for the age and slip, respectively, is not possible (Tikhomirov, 2014). Accordingly, the calculated slip value is the upper bound. The recurrence interval of the paleoearthquakes is obtained by taking into account the time of the ruptures. The vertical slip rate for each earthquake is calculated based on the amount of the slip.

5. 1. Modeled past ruptures

As the PDF of cosmogenic ^{36}Cl concentrations of strip A, which is the longest sampled strip, indicates more than one peak, it has been used to analyze and modeling the past rupture history (Fig. 10). Without any simulation, at least three notable discontinuities are recognizable in strip A (Fig. 9a), which reveals episodic activity of the fault through time.

Based on our modeling, the ground level was at G_0 position before the occurrence of the first earthquake (Fig. 13). ***Event 1,*** the oldest modeled earthquake, occurred at ca. 8.1 ka ago with a slip value of ca. 3.4 m (S_1) (Fig. 11). However, we consider this value as a minimum amount of slip, due to the uppermost 1.2 m of the fault scarp, which was not suitable for sampling. The mode led colluvium position before this rupture was estimated to be about 40 cm higher than the top of the

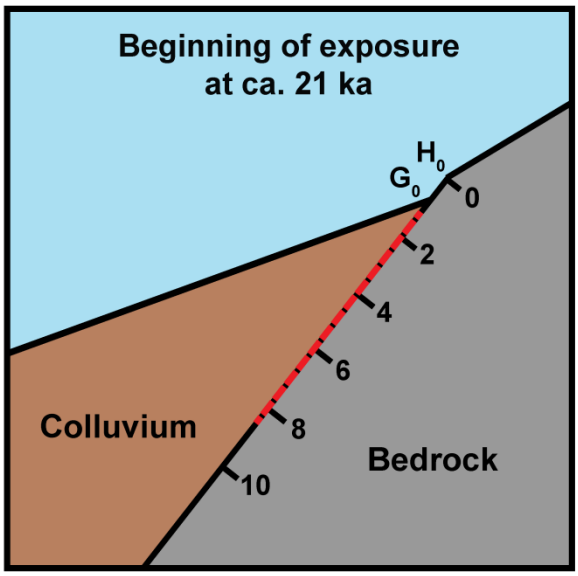

Fig. 13. Schematic sketch of the Priene-Sazlı Fault scarp before its activity period. Red dashed line shows the sampled surface. The fault surface grade is in meters. H_0 and G_0 show scarp height and ground level prior to the first rupture. Note that the 1.2 m uppermost part of the fault scarp was not sampled.

uppermost sample (G_0) at about 7.8 m up scarp (Fig. 13), which moved to G_1 after the rupture (Fig. 14a). To calculate the slip rate until the timing of the first modeled event, we considered the time interval between 21 ka and 8.1 ka. The calculated slip rate is 0.3 mm/yr, which we consider as a lower boundary, since the upper part of the scarp was not sampled and also if there was an earthquake before the first modeled rupture; it would be younger than 21 ka, which would result in a higher slip rate value. ***Event 2,*** the second rupture, was identified at the height of ca. 4.4 m on the fault scarp, 2.2 ka after the first event (Fig. 11). Thus, the fault experienced a rupture at ca. 6.0 ka ago with a slip amount of ca. 1.5 m (S_2). The ground level shifted from G_1 to G_2 (Fig. 14b). However, the main discontinuity is identified in the PDF plot at the height of about 5.5 m, which is higher than the height of the modeled event (Fig. 10a). This difference is explained by an approximate nature of the PDF approach, which can be used for initial points of simulation (Fig. 10a). Slip of ca. 1.5 m over the time span between the first and second ruptures results in mean slip rate of ca. 0.7 mm/yr. Before the occurrence of ***Event 3,*** the fault remained quiet for ca. 2.2 ka. The subsequent earthquake struck at ca. 3.7 ka ago (Fig. 11), causing a fault rupture with ca. 1.4 m of slip (S_3) and the ground level to move to G_3 (Fig. 14c). This discontinuity at the height of about 2.8 m fits very well with the second peak of the PDF plot with about 40 cm of difference in the height (Fig. 10a). Average slip rate of about 0.6 mm/yr were obtained by taking into account the related quiescence phase since the occurrence of the previous rupture to this event. ***Event 4,*** the last modeled earthquake, occurred in 2.2 ka ago, after a 1.4 ka phase of inactivity, and with 1.5 m of slip (S_4) (Fig. 11), which caused ground level displacement to the modern level (G) (Fig. 14d). This event fits exactly with the discontinuity shown in the PDF graph (Fig. 10a). The mean slip value of 1.0 mm/yr was calculated for the time span between the

third and last modeled earthquakes. This event correlates with the destructive historical earthquake of 68 AD, which had an intensity of VII (Ergin et al., 1967).

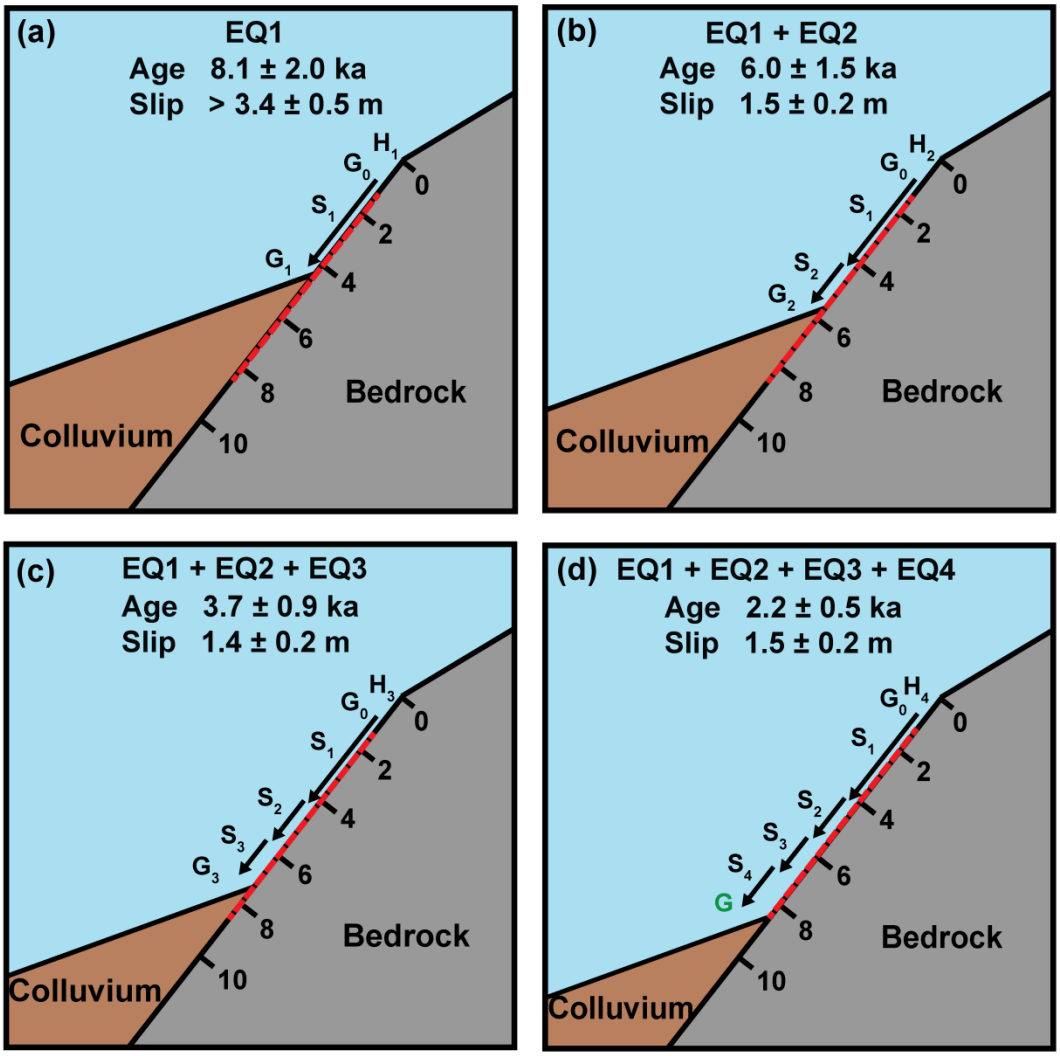

Fig. 14. Schematic sketch of the Priene-Sazlı Fault scarp showing colluvium position and episodic fault exposure during four modeled earthquake events. Red dashed line shows the sampled surface. The fault surface grade is in meters. H_1 to H_4 (Height of the fault scarp) following earthquakes of 1 to 4, respectively; G_0 (Ground level just before the first rupture), G_1 to G_3 are ground level before the second, third and fourth ruptures, and G is the current ground level. S_1 to S_4 represent the slip amounts of the four earthquakes related to the past to recent events.

Earthquake of July 1955. The destructive earthquake of July 1955 was not identified by the fault scarp dating method. In the best fit solution of five and six event scenarios, the slip amounts of the youngest modeled earthquake were either zero or very small (Table 7). But for a fault with a length of at least 30 km, a much higher slip amount than a few decimeters is expected (see sec. 5. 2. and Table 8). The surface of this rupture along strip A, which is supposed to have been exposed by the last earthquake, should still be under colluvium. It is probable that the lower part was

covered by collapsed colluvium from the top surface. However, the three strips of B, C and D with constant distributions of cosmogenic ^{36}Cl in the samples might represent the recent earthquake (Figs. 9b, 9c and 9d). This uniform value of ^{36}Cl along the entire length of these three stripes might reveal that the lowest part of the fault has had the same exposure history. Taking into account the earthquake of July 1955, the inactivity periods between each two successive events are between 1.5 - 2.2 ka. Thus, we can deduce that the major earthquakes on the Priene-Sazlı Fault repeat in a roughly similar seismic cycle of approximately 2000 years.

5. 2. Magnitude of future ruptures

Definitive prediction of future earthquake magnitudes is not possible by any of the present seismological methods. But the potential maximum magnitudes of earthquakes can be estimated by empirical relationships as a logarithmic factor of fault surface length (SRL) in order to analyze an earthquake hazard assessment (e.g., Wells & Coppersmith 1994; Ambraseys and Jackson, 1998; Pavlides & Caputo, 2004).

First, we refer to the study conducted by Pavlides and Caputo (2004), who specifically focused on dip-slip normal faults in the Aegean region, including western Anatolia and the Priene-Sazlı Fault (Table 8, equation. 1). If we consider a 30 km fault length (Altunel et al., 2009) as the SRL for the Priene-Sazlı Fault, an earthquake with magnitude of 6.8 is expected, if the fault is activated. Pavlides and Caputo (2004) consider the Priene-Sazlı Fault length is ca. 38 km, while the SRL is ca. 35 km based on the active fault map of Turkey (Şaroğlu et al., 1992). This also yields an earthquake with a magnitude of 6.9. If we consider a 37 km fault length (Sümer et al., 2013), the probable earthquake magnitude would still be 6.9. Finally, if consider the longest length of 40 km for the fault (Duman et al., 2011; Emre et al., 2013), an earthquake with magnitude of 7.0 is expected (Table 8).

Second, we considered the equation of Wells and Coppersmith (1994), which was compiled based on diverse normal faults worldwide (Table 8, equation 3). The probable magnitude is similar by taking into account either of these equations if any particular length of the fault is considered (Table 8). In the first relationship (equation

1), Ms (Surface wave magnitude), which is computed from Rayleigh surface waves that travel primarily along the uppermost layers of the Earth, is considered, whereas in the second, M (moment magnitude) is observed, which is measured from low-frequency seismic data within the zone ruptured following an earthquake. No systematic relationship between M and Ms is indicated, but according to Wells and Coppersmith (1994), their value differences are negligible for earthquakes of greater than Ms of 5.7. Likewise, Kanamori (1983) confirmed that these parameters are nearly identical for the earthquakes within the range of 5 to 7.5 in Ms, similar to the recorded and expected magnitude for the Priene fault.

The Priene-Sazlı Fault is classified as a seismogenic fault, which is characterized by having the potential to produce earthquakes with values larger than magnitude 5 (McCalpin, 2009). An earthquake with a 6.9 magnitude is large enough to leave considerable damage in a highly populated area like western Anatolia.

TABLE. 8. REGRESSION OF SRL (SURFACE RUPTURE LENGTH), MAGNITUDE (Ms/M) AND VERTICAL DISPLACEMENT (MVD/MD) CALCULATED FOR THE PRIENE-SAZLI FAULT. Unit of slip, MVD and MD is in meters.

	SRL/FL	30 km Altunel et al. (2009)	35 km Pavlides & Caputo (2004)	37 km Sümer et al. (2013)	40 km Duman et al. (2011) Emre et al. (2013)
Pavlides & Caputo (2004)	Ms = 0.9 x Log (SRL) + 5.48 (equation 1)	6.8	6.9	6.9	7.0
	Log (MVD) = 1.14.Ms - 7.82 (equation 2)	MVD = 0.9 Slip = 1.1	MVD = 1.1 Slip = 1.4	MVD = 1.1 Slip = 1.4	MVD = 1.4 Slip = 1.8
Wells & Coppersmith (1994)	M = 4.86 + 1.32 x log (SRL) (equation 3)	6.8	6.9	6.9	7.0
	Log (MD) = - 5.90 + 0.89 x M (equation 4)	MD (Slip) = 1.4	MD (Slip) = 1.7	MD (Slip) = 1.7	MD (Slip) = 2.1

5. 3. Magnitude of the modeled events and plausibility of modeling

We used empirical relationships, which connect the displacement value with the corresponding earthquake magnitude. According to the relationship of Pavlides and Caputo (2004), which represents the MVD (maximum vertical displacement) value on Ms (Table 8, equation 2), for an earthquake with magnitude of 6.8 - 7.0, which is expected for the Priene-Sazlı Fault, the maximum vertical displacement is 0.9 - 1.4 m, and equates to 1.1 - 1.8 m of slip. Since in our modeling the slip value (=

MD) is recovered, we convert it to MVD by accounting for a dip of θ = 52° for the fault scarp surface along A strip (Fig. 1b).

Sin (θ) = vertical displacement /Slip

Based on Wells and Coppersmith (1994), (Table 8, equation 4), maximum displacement (MD) resulting from an earthquake with magnitude of 6.8 - 7.0 results in 1.4 - 2.1 m of MD.

TABLE. 9. REGRESSION OF MAGNITUDE (Ms/M) AND VERTICAL DISPLACEMENT (MVD/MD) FOR THE PRIENE-SAZLI FAULT. * MODELED BY THE CODE.

		Event	Slip* (m)	MVD (m)	Ms
Pavlides & Caputo (2004)	Ms = 0.59 x Log (MVD) + 6.75 (equation 5)		**Lowest X^2**	**Average**	**Average**
		1	**3.4 ± 0.5**	**2.7 ± 0.4**	**7.0**
		2	**1.5 ± 0.2**	**1.2 ± 0.2**	**6.8**
		3	**1.4 ± 0.2**	**1.1 ± 0.2**	**6.8**
		4	**1.5 ± 0.2**	**1.2 ± 0.2**	**6.8**
		Event	**MD (=Slip*) (m)**		**M**
Wells & Coppersmith (1994)	M= 6.61 + 0.71 x log (MD) (equation 6)		**Lowest X^2**		**Average**
		1	**3.4 ± 0.5**		**7.0**
		2	**1.5 ± 0.2**		**6.7**
		3	**1.4 ± 0.2**		**6.7**
		4	**1.5 ± 0.2**		**6.7**

The magnitude values of the modeled earthquakes were calculated using the relationship of Pavlides and Caputo (2004) (Table 9, equation 5). The equation of Wells and Coppersmith (1994) was also used to estimate the modeled earthquake magnitudes (Table 9, equation 6).

Event 1, the vertical displacement of 2.7 ± 0.4 m is obtained for the oldest movement with average modeled slip of 3.4 ± 0.5 m. Based on either equation (5) or (6), an earthquake with magnitude of at least 7 is required to produce such a large amount of displacement. Thus, we conclude that probably in a short period of time the fault experienced a cluster of smaller ruptures rather than an individual earthquake. The FSDT code recognizes earthquakes, which occur within a short time

interval, as a single event. However, minor discontinuities might be recognizable between the main curves, which indicate smaller earthquakes that are not distinguished by the code within the uncertainties of the study (Fig. 11). In addition, taking into account either equations (2) or (4), the fault needs to experience at least two or three ruptures of 6.8 - 7.0 to be exposed on average about 3.4 m at once. Thus, this modeled rupture is interpreted as several smaller sub-events rather than a unique event. ***Event 2,*** the second modeled rupture with 1.5 ± 0.2 m of slip equates to 1.2 ± 0.2 m of MVD, which was likely produced by an earthquake of magnitude 6.7 - 6.8, based on equations (5) and (6). Based on equations (2) and (4), depending on the length of the fault, one or two earthquake(s) is responsible for producing this amount of slip. ***Event 3,*** the third modeled earthquake caused a fault rupture of 1.4 ± 0.2 m of slip, which equates to 1.1 ± 0.2 m of MVD. An earthquake with magnitude 6.7 - 6.8 is able to generate this amount of slip, based on equations (5) and (6). Taking into account equations (2) and (4), one to two earthquake(s) are required to expose the fault with this amount of slip. ***Event 4,*** the last modeled earthquake with 1.5 ± 0.2 m of slip equates to MVD of 1.2 ± 0.2 m. An earthquake with magnitude of 6.7 - 6.8 is able to generate this amount of slip, based on equations (5) and (6). Also, taking into account equations (2) and (4), one to two earthquake(s) could produce this amount of displacement.

6. Conclusions

We studied the Priene-Sazlı Fault within the Büyük Menderes Graben in western Anatolia in order to provide the long-term modeling of associated paleoearthquakes. The measured cosmogenic ^{36}Cl in 117 samples along the fault were analyzed using FSDT (Tikhomirov, 2014).

- Our best fit results show that the fault experienced at least four seismic events during Holocene time, with its maximum movement in ca. 8.1 ka ago.
- Vertical components of slips were 1.4 to 3.4 m following the seismic events, mostly as a series of earthquakes struck within a short time span.
- The average earthquake return period of 2000 years was calculated for the Priene-Sazlı Fault seismic activity.

- Mean values of vertical slip rates of greater than 0.3, 0.7, 0.6 and 1.0 mm/yr from the oldest to the youngest modeled ruptures during the periodic activity of the fault were calculated.
- Long-term slip rate of the fault is estimated to be 0.7 mm/yr.
- Since, the Priene-Sazlı Fault has periods of high seismic activity in its history that occur as a series of earthquakes close in time, the occurrence of a large earthquake clustered with the 1955 earthquake, occurring in the near future is not beyond reasonable expectation.

Cosmogenic ^{36}Cl fault scarp dating as a direct method has high potential to improve our knowledge for seismic risk assessment, where major normal faults in carbonate bedrock dominate in a region similar to western Anatolia. The long-term slip rate, slip per event, rupture length, magnitude of possible earthquake and recurrence interval of the fault allows us to consider the Priene-Sazlı Fault as a low to moderate (class 3) active fault based on the activity classification of faults by Cluff and Cluff (1984) for earthquake engineering. According to the Modified Mercalli Intensity Scale (MM) an earthquake with this value of intensity causes very strong shaking on the Earth's surface. The fault is considered a seismogenic fault that should be assigned a more severe alert status due to its capacity to generate earthquakes with large magnitudes. Our findings and data still under analysis might shed light on the contribution of seismic hazard assessment of the active region of western Anatolia accompanied with the pre-existing seismic records. The importance of the study is highlighted further when the high population density of up to 500 person per km^2 in western Anatolia (European Environment Agency, 2010) is considered.

Acknowledgments

We are grateful to Dr. Hans-Arno Synal and the team at the Laboratory of Ion Beam Physics, ETH Zurich, for their support with the AMS measurements. We wish to thank Dr. Çağlar Özkaymak for his collaboration with sample preparation. We would also like to thank the students and technicians of Dokuz Eylül University, who helped us during our sampling campaign. This study was jointly funded by the Dokuz Eylül University (Research Project No. 2006.KB.FEN.008), the Surface Exposure Dating Laboratory at the University of Bern, the Bern University Research Foundation and Swiss National Science Foundation (Project No. 200021-147065).

References

- Akçar, N., Tikhomirov, D., Özkaymak, Ç., Ivy-Ochs, S., Alfimov, V., Sözbilir, H., Uzel, B., Schlüchter, Ch., 2012. ^{36}Cl Exposure Dating of Paleoearthquakes in the Eastern Mediterranean: First Results from Western Anatolian Extensional Province, Turkey. GSA Bulletin 124, no. 11/12, 1724-1735.
- Alfimov, V., Ivy-Ochs, S., 2009. How well do we understand production of Cl-36 in limestone and dolomite?: Quaternary Geochronology, 4(6), 462-474.
- Altunel, E., 1998. Evidence for damaging historical earthquakes at Priene, Western Turkey. Turkish Journal of Earth Sciences 7, 25-35.
- Altunel, E., Akyüz, S., Meghraoui, M., Kiyak, N.G., Karabacak, V., Yalçiner, Ç., 2009. Büyük Menderes Fay Zonunun Arkeosismolojisi ve Paleosismolojisi.
- Ambraseys, N.N., 1971. Value of historical records of earthquakes, Nature, 232, 375-379.
- Ambraseys, N.N., 1975. Studies in Historical Siesmicity and Tectonics. Geodynamics Today, Chap. 2, The Royal Soc., London.
- Ambraseys, N., 2009. Earthquakes in the Mediterranean and Middle East: a multidisciplinary study of seismicity up to 1900. Cambridge University Press, 947 p.
- Ambraseys, N.N., Jackson, J.A., 1998. Faulting associated with historical and recent earthquakes in the Eastern Mediterranean region: Geophysical Journal International 133, no. 2, 390-406.
- Barnett, J.A.M., Mortimer, J., Rippon, J.H., Walsh, J.J., Watterson, J., 1987. Displacement geometry in the volume containing a single normal fault. American Association of Petroleum Geologists Bulletin 71, 925-937.
- Benedetti, L., Finkel, R., King, G., Armijo, R., Papanastassiou, D., Ryerson, F.J., Flerit, F., Farber, D., Stavrakakis, G., 2003. Motion on the Kaparelli fault (Greece) prior to the 1981 earthquake sequence determined from Cl-36 cosmogenic dating: Terra Nova, v. 15, no. 2, p. 118-124.
- Benedetti, L., Finkel, R., Papanastassiou, D., King, G., Armijo, R., Ryerson, F., Farber, D., Flerit, F., 2002. Post-glacial slip history of the Sparta fault (Greece) determined by Cl-36 cosmogenic dating: Evidence for non-periodic earthquakes, Geophysical Research Letters, 29, no. 8, 1246, doi:10.1029/2001GL014510.
- Benedetti, L., Manighetti, I., Gaudemer, Y., Finkel, R., Malavieille, Y., Pou, Kh., Arnold, M., Aumaître, G., Bourlès, D., Keddadouche, K., 2013. Earthquake synchrony and clustering on Fucino faults (Central Italy) as revealed from in situ ^{36}Cl exposure dating. Journal of Geophysical Reasearch, Solid Earth 118, 4948-4974.
- Broughton, T.R.S., 1938. An Economic Survey of Ancient Roma. Vol. IV, The Johns Hopkins Press, Baltimore.
- Boğaziçi University Kandilli Observatory and Earthquake Research Institute (KOERI). Retreived from (www.koeri.boun.edu.tr/scripts/lst4.asp)
- Calvi, V.S., 1941. Erdbebenkatalog der Turkei und Einiger Benaehbarter Gabiete. Yayınlanmış, Rapor No. 276, MTA Enstitüsü, 1941, Ankara.
- Cannıtez, N., Üçer, S.B., 1967. Computer determinations for the fault plane solutions in and near Anatolia, Tectonophysics, 4 (3), 235-244.
- Caputo, R., Pavlides, S., Papadopoulos, G., Helly, B., 1998. Palaeoseismological researches in northern Thessaly, Greece. Preliminary Results: XXVI. General assembly of the ESC, Tel Aviv, August 23–28, 1998. Abstracts, p. 25.
- Cluff, L.S., Cluff, J.L., 1984. Importance of assessing degrees of fault activity for engineering decisions, Proceeding 8th World Conference on Earthquake Engineering, vol. 2, 629-636.
- Collection Academique. Tome VI de la Partie Entrange et Premier Tome de la Physique Experimentale Separee. 1766.
- Cowie, P.A., Phillips, R.J., Roberts, G.P., McCaffrey, K., Zijerveld, L.J.J., Gregory, L.C., Faure Walker, J., Wedmore, L.N.J., Dunai, T.J., Binnie, S.A., Freeman, S.P.H.T. , Wilcken, K., Shanks, R.P., Huismans, R.S., Papanikolaou, I., Michetti, A.M., Wilkinson, M., 2017. Orogen-scale uplift in the central Italian Apennines drives episodic behaviour of earthquake faults, Scientific Reports 7, Article number 44858.

- Desilets, D., Zreda, M., Almasi, P.F., Elmore, D., 2006. Determination of cosmogenic Cl-36 in rocks by isotope dilution: Innovations, validation and error propagation, Chemical Geology 233, no. 3-4, 185-195.
- Dewey, J.F., Şengör, A.M.C., 1979. Aegean and surrounding region: complex multiplate and continuum tectonics in a convergent zone. Geological Society of America Bulletin 90, 84–92.
- Dikmen, G., 1952. Nazilli, Tarih ve Cografyası (Nazilli, History and Geography), Aydın İl Halk Kütüphanesi.
- Duman, T.Y., Emre, Ö., Özalp, S., Elması, H., 2011. Active fault map series of Turkey (scale 1:250,000), General Direct. Mineral Res. Explor., Aydın (NJ 35-11).
- Elmore, D., Ma, X., Miller, T., Mueller, K., Perry, M., Rickey, F., Sharma, P., Simms, P., Lipschutz, M., Vogt, S., 1997. Status and plans for the PRIME Lab AMS facility: Nuclear Instruments and Methods in Physics Research Section B-Beam Interactions with Materials and Atoms, 123(1-4), 69-72.
- Emre, Ö., Duman, T.Y., Özalp, S., Elması, H., Olgun, Ş., Şaroğlu, F., 2013. Active fault map of Turkey (scale 1:250,000), General Direct. Mineral Res. Explor., Special Publication Series - 30.
- Ergin, K., Güçlü, U., Uz, Z., 1967. A catalog of Earthquake for Turkey and Surrounding Area (11 A.D. to 1964 A.D.). ITU Faculty of Mining Engineering, Istanbul, Turkey.
- Evans, J. M., Stone, J. O. H., Fifield, L. K., Cresswell, R. G., 1997. Cosmogenic chlorine-36 production in K-feldspar: Nuclear Instruments and Methods in Physics Research Section B-Beam Interactions with Materials and Atoms, 123(1-4), 334-340.
- Fink, D., Vogt, S., Hotchkis, M., 2000. Cross-sections for Cl-36 from Ti at E-p=35-150 MeV: Applications to in-situ exposure dating: Nuclear Instruments and Methods in Physics Research Section B-Beam interactions with materials and atoms, 172, 861-866.
- Gosse, J. C., Phillips, F. M., 2001. Terrestrial in situ cosmogenic nuclides: theory and application, Quater. Sci. Rev., 20, 1475-1560.
- Guidoboni, E., Comastri, A., Traina, G., 1994. Catalogue of Ancient Earthquakes in the Mediterranean Area up to 10th Century. Ist. Naz. di Geofis. e Vulcanol., Storia Geofis. Ambiente, Bologna, Italy. 504.
- Gürer, Ö.F., Bozcu, M., Yılmaz, K., Yımaz, Y., 2001. Neogene basin development around Söke-Kuşadası (western Anatolia) and its bearing on tectonic development of the Aegean region. Geodinamica Acta, 14, 57-69.
- Gürer, Ö.F., Sarica-Filoreau, N., Özburan, M., Sangu, E., Doğan, B., 2009. Progressive development of the Büyük Menderes Graben based on new data, western Turkey, Geological Magazine 146, Issue 5, 652-673.
- Hancock, P.L., Barka, A.A., 1987. Kinematic indicators on active faults in western Turkey, Journal of Structural Geology 9, No. 5/6, 573-584.
- Harvard Centroid –Moment Tensor Project CMT, Harvard University, MA, USA (1977–2015). (www.globalcmt.org/CMTsearch).
- Istituto Nazionale di Geofisica e Vulcanologia, Italy (istituto.ingv.it).
- Ivy-Ochs, S., Poschinger, A. V., Synal, H. A., Maisch, M., 2009. Surface exposure dating of the Flims landslide, Graubunden, Switzerland, Geomorphology, 103(1), 104-112.
- Ivy-Ochs, S., Synal, H. A., Roth, C., Schaller, M., 2004. Initial results from isotope dilution for Cl and Cl-36 measurements at the PSI/ETH Zurich AMS facility: Nuclear Instruments and Methods in Physics Research Section B-Beam Interactions with Materials and Atoms, 223-24, 623-627.
- Kalafat, D., 1998. Anadolu'nun Tektonik Yapılarının Deprem Mekanizmaları Açısından irdelenmesi, Deprem Araştırma Bülteni, Sayı 77, 1-217, Temmuz 1998 (in Turkish).
- Kalafat, D., Kekovalı, K., Güneş, Y., Yılmazer, M., Kara, M., Deniz, P., Berberoğlu, M., 2009. Türkiye ve Çevresi Faylanma-Kaynak Parametreleri (MT) Kataloğu (1938–2008): A Catalogue of Source Parameters of Moderate and Strong Earthquakes for Turkey and its Surrounding Area (1938–2008). Boğaziçi University Publication, 1026.
- Kanamori, H., 1983. Magnitude scale and quantification of earthquakes, Tectonophysics 93, 185-199.
- Karnik, V., 1971. Siesmicity of the European Area 2.D. Reidel Publishing Company/Dordrecht, Holland.
- Kim, Y.-S., Sanderson, D.J., 2005. The relationship between displacement and length of faults: A review, Earth-Science Reviews 68, 317-334.

- Lee, W.H.K., Wu, F.T., Jacobsen, C., 1976. A catalog of historical earthquakes in China compiled from recent Chinese publications, Bulletin of the Seismological Society of America 66, 2003-2017.
- Liu, B.L., Phillips, F.M., Fabrykamartin, J.T., Fowler, M.M., Stone, W.D., 1994. Cosmogenic ^{36}Cl accumulation in unstable landforms, 1. Effects of the thermal neutron distribution: Water Resources Research, 30(11), 3115-3125.
- Marrett, R., Allmendinger, R.W., 1991. Estimates of strain due to brittle faulting: sampling of fault populations. Journal of Structural Geology 13, 735-738.
- McCalpin, J.P., ed, 2009, Paleoseismology, London, Academic, 629 p.
- McKenzie, D., 1972. Active tectonics of the Mediterranean region. Geophysical Journal International, 30, 109-185.
- Mitchell, S.G., Matmon, A., Bierman, P.R., Enzel, Y., Caffee, M., Rizzo, D., 2001. Displacement history of a limtesone normal fault scarp, northern Israel, from cosmogenic ^{36}Cl, J. geophys. Res., 106(B3), 4247- 4264.
- Molnar, P., 1979. Earthquake recurrence intervals and plate tectonics, Bull. seism. Soc. Am., 69(1), 115–133.
- Mouslopoulou, V., Moraetis, D., Benedetti, L., Guillou, V., Bellier, O., Hristopulos, D., 2014. Normal faulting in the forearc of the Hellenic subduction margin: Paleoearthquake history and kinematics of the Spili Fault, Crete, Greece. - Journal of Structural Geology 66, 298-308.
- National Observatory of Athens, Greece (bbnet.gein.noa.gr).
- Öcal, N., 1958. Söke-Balat zelzelesi (Söke-Balat earthquake), Ist. Kandili Rasathanesi Sismoloji Yay., 2.
- Öcal, N., 1968. Türkiyenin Sismisitesi ve Zelzele Coğrafyası, 1850-1960 Yılları İçin Zelzele Kataloğu. Kandilli Rasathanesi Yayınları No. 8, İstanbul.
- Palumbo, L., Benedetti, L., Bourles, D., Cinque, A., Finkel, R., 2004. Slip history of the Magnola fault (Apennines, Central Italy) from ^{36}Cl surface exposure dating: evidence for strong earthquake over the Holocene, Earth planet. Sci. Lett., 225, 163–176.
- Pantosti, D., D'Adezzio, G., Cinti, F.R., 1996. Paleoseismicity of the Ovindo-Pezza fault, central Apennines, Italy: a history including a large, previously unrecorded earthquake in the Middle Ages (860-1300 A.D.). J. geophys. Res., 101(B3), 5937–5959.
- Pavlides, S., 1996. First palaeoseismological results from Greece. Annali di Geofisica. 39, 545-555.
- Pavlides, S., Caputo, R., 2004. Magnitude versus faults' surface parameters: Quantitative relationships from the Aegean Region. Tectonophysics, 380, 159-188.
- Phillips, F.M., Stone, W.D., Fabryka-Martin, J.T., 2001. An improved approach to calculating low-energy cosmic-ray neutron fluxes near the land/atmosphere interface: Chemical Geology, 175 (3-4), 689-701.
- Phillips, F.M., Zreda, M.G., Flinsch, M. R., Elmore, D., Sharma, P., 1996. A reevaluation of cosmogenic Cl-36 production rates in terrestrial rocks: Geophysical Research Letters, 23(9), 949-952.
- Pınar, N., Lahn, E., 1952. Türkiye Depremleri İzahlı Kataloğu T.C. Bayındırlık Bak. Yapı ve İmar İş. Reis. Y. Seri 6, Sayı 36.
- Republic of Turkey Prime Ministry Disaster & Emergency Management Presidency-Earthquake Research Department (AFAD-ERD) (www.afad.gov.tr/en/).
- Şaroğlu, F., Emre, Ö., Kuşçu, I., 1992. Active Fault Map of Turkey (scale 1:1,000,000). General Direct. Mineral Res. Explor. (MTA), Ankara, Turkey.
- Schimmelpfennig, I., Benedetti, L., Finkel, R., Pik, R., Blard, P.H., Bourles, D., Burnard, P., Williams, A., 2009. Sources of in-situ Cl-36 in basaltic rocks. Implications for calibration of production rates, Quaternary Geochronology, 4(6), 441-461.
- Schlagenhauf, A., Gaudemer, Y., Benedetti, L., Manighetti,I., Palumbo, L., Schimmelpfennig, I., Finkel, R., Pou, K., 2010. Using in situ chlorine-36 cosmonuclide to recover past earthquake histories on limestone normal fault scarps: A reappraisal of methodology and interpretations, Geophysical Journal International, v. 182, no. 1, p. 36-72.
- Schlagenhauf, A., Manighetti, I., Benedetti, L., Gaudemer, Y., Finkel, R., Malavieille, J., Pou, K., 2011. Earthquake supercycles in Central Italy, inferred from ^{36}Cl exposure dating. Earth and Planetary Science Letters, 307(3-4), 487-500.

- Scholz, Ch.H., 2002. The Mechanics of Earthquakes and Faulting. Second Edition, Cambridge University Press, 464 p.
- Şengör, A.M.C., 1987. Cross-faults and differential stretching of hanging walls in regions of low-angle normal faulting: examples from western Turkey. *In* Coward, M.P., Dewey, J.F., Hancock, P.L. (Eds.), Continental Extensional Tectonics. Geological Society of London, Special Publication 28, 575-589.
- Şengör, A.M.C., Görür, N., Şarğlu, F., 1985. Strike-slip faulting and related basin formation in zones of tectonic escape: Turkey as a case study. *In* Biddle, K., Christie-Blick, N. (Eds.), Strike-Slip Deformation, Basin Formation and Sedimentation. Society of Economic Paleontologists and Mineralogists, Special Publications 37, 227-264.
- Shebalin, N.V., Karnik, V., Hadzievski, D. (eds.), 1974. Catalogue of earthquakes of the Balkan region. I, UNDP- UNESCO Survey of the seismicity of the Balkan region. Skopje, 600 p.
- Soysal, H., Sipahioğlu, S., Kolçak, D., Altınok, Y., 1981. Historical earthquake catalogue of Turkey and surrounding area (2100 B.C. – 1900 A.D.). Technical Report, TUBİTAK, No: TBAG-341.
- Stone, J.O., 2000. Air pressure and cosmogenic isotope production. Journal of Geophysical Research 105 (B10), 23753-23759.
- Stone, J.O., 2005. Terrestrial chlorine-36 production from spallation of iron. In: 10th International Conference on Accelerator Mass Spectrometry. Berkeley, California.
- Stone, J.O., Allan, G.L., Fifield, L.K., Cresswell, R.G., 1996. Cosmogenic chlorine-36 from calcium spallation, Geochimica Cosmochimica Acta 60, 679-692.
- Stone, J.O., Evans, J.M., Fifield, L.K., Allan, G.L., Cresswell, R.G., 1998. Cosmogenic chlorine-36 production in calcite by muons: Geochimica et Cosmochimica Acta, 62(3), 433-454.
- Sümer, Ö., Inci, U., Sözbilir, H., 2012. Tectono-sedimentary evolution of an Early Pleistocene shallow marine fan-deltaic succession at the western coast of Turkey. Geodinamica Acta 25, Nos. 3-4, 112-131.
- Sümer, Ö., Inci, U., Sözbilir, H., 2013. Tectonic evolution of the Söke Basin: Extension-dominated transtensional basin formation in western part of the Büyük Menderes Graben, Western Anatolia, Turkey. Journal of Geodynamics 65, 148-175.
- Synal, H.A., Bonani, G., Dobeli, M., Ender, R.M., Gartenmann, P., Kubik, P.W., Schnabel, C., Suter, M., 1997. Status report of the PSI/ETH AMS facility: Nuclear Instruments and Methods in Physics Research Section B-Beam Interactions with Materials and Atoms, 123(1-4), 62-68.
- Tan, O., Taymaz, T., 2001. Source Parametres of November 6, 1992 Doğanbey (İzmir) Earthquake (Mw=6.0) Obtained From Inversion of Teleseismic Body-WaveforAD. Fourth International Turkish Geology Symposium: Work in Progress on the Geology of Turkey and Its Surroundings, Çukurova University – Adana, Abstracts, p. 171.
- Tan, O., Taymaz, T., 2003. Seismotectonics of Karaburun Peninsula and Kufladası Gulf: source parameters of April 2, 1996. Kuşadası Gulf and April 10, 2003 Seferihisar (İzmir) earthquakes. International Workshop on the North Anatolian, East Anatolian and Dead Sea Fault SysteAD: Recent Progress in Tectonics and Paleoseismology and Field Training Course in Paleoseismology, Middle East Technical University (METU) – Ankara, Abstracts, p. 147.
- Taymaz, T., 1993. The source parameters of Çubukdağ (W. Turkey) earthquake of 1986 October 11. Geophysical Journal International 113, 260–267.
- Taymaz, T., Tan, O., Yolsal, S., 2004. Seismotectonics of western Turkey: a synthesis of source parameters and rupture histories of recent earthquakes. AGU Fall Meeting, Session T14, San Francisco-California, EOS Transactions 85 (47).
- Tikhomirov, D., 2014. PhD thesis, University of Bern, An advanced model for fault scarp dating and paleoearthquake reconstruction, with a case study of the Gediz Graben formation (Turkey).
- Tikhomirov, D., Akçar, N., Ivy-Ochs, S., Alfimov, V., Schlüchter, C., 2014. Calculation of shielding factors for production of cosmogenic nuclides in fault scarpes. Quaternary Geochronology, 19, 181-193.
- United States Geological Survey National Earthquake Information Center (USGS-NEIC) (earthquake.usgs.gov/contactus/golden/neic.php).
- Walsh, J.J., Bailey, W.R., Childs, C., Nicol, A., Bonson, C. G., 2003. Formation of segmented normal faults: a 3-D perspective. Journal of Structural Geology 25, 1251-1262.

- Walsh, J.J., Watterson, J., 1987. Distributions of cumulative displacement and seismic slip on a single normal fault surface. Journal of Structural Geology 9, 1039-1046.
- Walsh, J.J., Watterson, J., 1988. Analysis of the relationship between the displacements and dimensions of faults. Journal of Structural Geology 10, 239-247.
- Wells, D.L., Coppersmith, J.K., 1994. New empirical relationships among magnitude, rupture length, rupture width, rupture area, and surface displacement. Bulletin of the Seismological Society of America 84, 974-1002.
- Yönlü, Ö., Altunel, E., Karabacak, V., Akyüz, S., Yalçıner, Ç., 2010. Offset archaeological relics in the western part of the Büyük Menderes Graben, (western Turkey) and their tectonic implications. The Geological Society of America 471, 269-279 (Special Publications).
- Zreda, M.G., Phillips, F.M., Elmore, D., Kubik, P.W., Sharma, P., Dorn, R.I., 1991. Cosmogenic chlorine-36 production rates in terrestrial rocks. Earth and Planetary Science Letters 105, 94-109.
- Zreda, M., Noller, J., 1998. Ages of prehistoric earthquakes revealed by cosmogenic chlorine-36 in a bedrock fault scarp at Hebgen Lake. Science, 282, 1097-1099.

Chapter 3

The propagation and linkage of normal faults: Insights from fault scarp dating in western Anatolia

Nasim Mozafari Amiri[1], Dmitry Tikhomirov[1], Ökmen Sümer[2], Çağlar Özkaymak[3], Bora Uzel[2], Serdar Yesilyurt[1], Susan Ivy-Ochs[4], Christof Vockenhuber[4], Hasan Sözbilir[2] and Naki Akçar[1]

[1]Institute of Geological Sciences, University of Bern, 3012 Bern, Switzerland
[2]Dokuz Eylül University, Geological Engineering Department, 35160 İzmir, Turkey
[3]Department of Geological Engineering, Afyon Kocatepe University, 03200 Afyonkarahisar, Turkey
[4]Institute for Particle Physics, ETH Hönggerberg, 8093 Zürich, Switzerland

Submitted to Journal of EPSL

The propagation and linkage of normal faults: Insights from fault scarp dating in western Anatolia

Abstract

Carbonate fault scarps, if well-preserved, include precise evidence of past earthquakes. Using cosmogenic ^{36}Cl dating, the timing and vertical component of slip of paleoearthquakes are recoverable beyond the historical and instrumental earthquake archives. One of the more appropriate seismically active regions to apply ^{36}Cl dating is western Anatolia, where the complex deformation is influenced by an approximately N-S extensional regime since early Miocene, and where the horst-graben structures are characterized by normal faults in carbonates.

We have studied the Kalafat and Yavansu fault scarps with opposite-faces of limestones in the western end of the Büyük Menderes Graben within western Anatolia. The distribution of cosmogenic ^{36}Cl against height along the vertical component of slip on the fault surfaces indicates that both faults experienced at least three high seismically active phases in the past. The recovered ages of high seismic activity are 15.3 ± 3.8 ka, 8.4 ± 2.1 ka, and 3.6 ± 0.9 ka, with vertical components of slip of 0.7 ± 0.1 m, 0.9 ± 0.1 and 3.1 ± 0.5 m, respectively, for the Kalafat Fault, and 7.9 ± 2.0 ka, 3.4 ± 0.8 ka, and 2.0 ± 0.5 ka with vertical components of slip of 0.6 ± 0.1 m, 3.5 ± 0.5 m, and 2.6 ± 0.4 m, respectively, for the Yavansu Fault. The recurrence interval of recovered seismically active periods is generally becoming shortened over time. The ruptures mostly occurred as clusters of earthquakes close in time with magnitudes of 6.5 to 7.1. The vertical slip rates of > 0.1, 0.1, and 1.5 mm/yr, and > 0.1, 0.8, and 1.9 mm/yr were calculated for the Kalafat and Yavansu faults, respectively. Long-term slip rates were also estimated about 1.0 and 0.6 mm/yr for the Kalafat and Yavansu faults, respectively. Considering the fault lengths, both faults are capable of producing earthquakes with magnitudes larger than 5, and are considered to be seismogenic faults.

Key words: Fault scarp, Dating, Eastern Mediterranean, Neotectonic, Fault linkage

1. Introduction

The western Anatolian Extensional Province is one of the most seismically active regions in the world, where large-scale horst-graben structures control its tectonic behavior (e.g., Dewey and Şengör, 1979; Şengör et al., 1985). The collision of the African and Eurasian plates with an approximately N-S extensional regime since early Miocene is responsible for this complex deformation (e.g., Dewey and Şengör, 1979). The graben systems are characterized by normal faults occasionally occurring in carbonates (Fig. 1), which are ideal to apply exposure dating using cosmogenic ^{36}Cl. Reconstruction of paleoearthquakes in terms of their timing and magnitude is crucial to estimate the timing and magnitude of probable future earthquakes (e.g., McCalpin, 2009). The occurrence of many destructive historical and instrumental earthquakes in the active region of western Anatolia sheds light on the importance of paleoseismic studies in order to reduce the potential damage following significant earthquakes.

The potential of cosmogenic ^{36}Cl dating method has been proven worldwide on carbonate normal faults during the last 20 years (Zreda and Noller, 1998; Mitchell et al., 2001; Benedetti et al., 2002; 2003; 2013; Palumbo et al., 2004; Schlagenhauf et al., 2010; 2011; Akçar et al., 2012; Tikhomirov, 2014; Mouslopoulou et al., 2014; Cowie et al., 2017; Mozafari et al., *submitted*). In this dating method, measured cosmogenic ^{36}Cl concentrations in the outermost couple of centimeters of the fault scarp surface are considered as a function of scarp height. Cyclic seismic activity of a fault causes a non-linear profile in cosmogenic ^{36}Cl concentrations, which enables determination of the timing of past ruptures and the vertical component of their slips. Based on the magnitude of associated ruptures, the short-term and long-term slip rates can be calculated. Each rupture exposes at the surface a section of the scarp previously covered by colluvium. Consequently, the exposed section accumulates ^{36}Cl at a higher rate during the period of quiescence. As long as a fault section is covered by hanging-wall colluvium sediments, secondary cosmic rays create an exponential pattern of cosmogenic ^{36}Cl reducing with depth. In a successive seismic pattern, each sharp discontinuity in the cosmogenic ^{36}Cl concentration profile indicates an activity period of the fault, whereas the convex intervals of ^{36}Cl profile

mark the dormancy periods. The distance between two adjacent inactivity marks is the vertical component of slip (for further information see Mozafari et al., *submitted*).

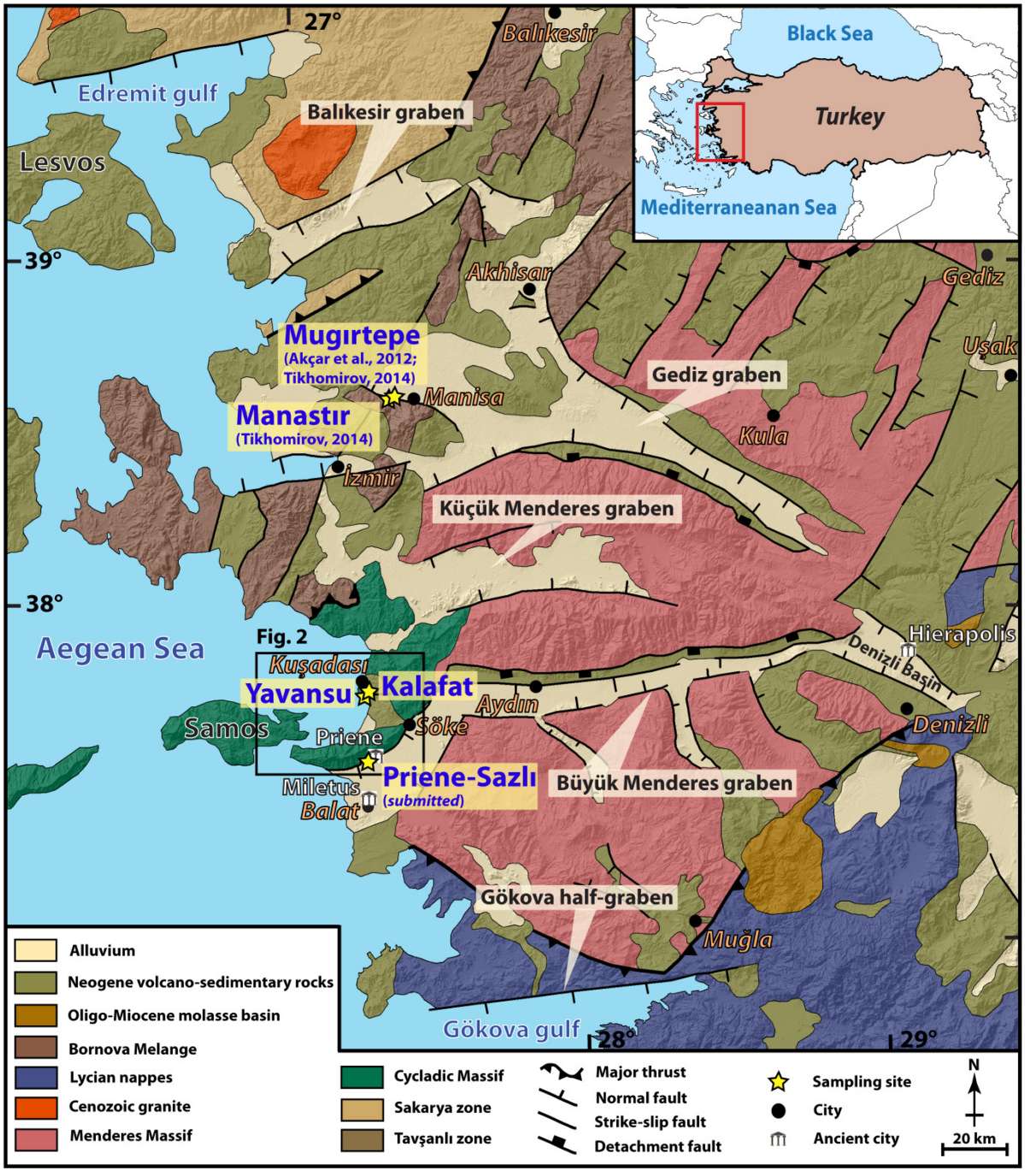

Fig. 1. Simplified geological map of western Anatolia (modified after Akçar et al., 2012; Sümer et al., 2013; Hancock and Barka, 1987). The yellow stars show the locations of the sampling sites of this study in Kalafat and Yavansu Faults along with Priene-Sazlı Fault, Mugırtepe Fault (Akçar et al., 2012) and Manastır Fault (Tikhomirov, 2014) within Manisa Fault Zone. The black box gives location of Fig 2.

Kuşadası City is located in the western part of the Büyük Menderes Graben, one of the main graben systems of western Anatolia, where many active faults potentially threaten thousands of lives (Fig. 2). The adjacent Kalafat and Yavansu faults are two such faults in the southeast of Kuşadası. There is no historical or instrumental earthquake directly attributed to these two faults. However, the oldest known historical earthquake closest to the two faults is dated back to 1751 AD (e.g., Soysal et al., 1981). There were also instrumental earthquakes in the surrounding area, among which the greatest occurred in 1955, and is related to Priene-Sazlı Fault. However, in order to evaluate the seismic pattern of earthquakes on any particular fault, more seismic data over a wider time span is needed. In this study, we modeled the time-slip history of the Kalafat and Yavansu faults over a large time-scale (Figs. 1 and 2). Our goals were to reconstruct the age and vertical components of slip of past earthquakes, calculate the slip rates through time and estimate the magnitude of future earthquakes. To accomplish this, a total 122 samples were collected from both fault scarp surfaces for cosmogenic ^{36}Cl analysis. Our results show the occurrence of at least three periods of high seismic activity with earthquakes from 6.5 to 7.0 in magnitude on both faults during the Late Pleistocene -Holocene. Given the length of the faults, earthquakes with magnitudes of 5.4 to 7.0 are expected, if the faults become activated.

2. Study area

Büyük Menderes Graben is one of the main horst-graben systems in western Anatolia. This structure extends approximately 140 km (Gürer et al., 2009) between Denizli Basin in the east with an E-W trending and continues with a change in strike to a NE-SW trend towards the Aegean Sea in the west (Fig. 1). The Menderes Massif borders the Büyük Menderes Graben to the north and south (Fig. 1). The horst-graben structure of the Büyük Menderes is heavily dominated by many faults of varying scales.

Kuşadası City is located in the northwest part of the Büyük Menderes graben (Figs. 1 and 2). The fault zone in the Kuşadası area has a dominant trend of ENE to NE-SW. The ENE-trending part of the fault zone follows the trend of Büyük Menderes graben greater length (Hancock and Barka, 1987). This fault zone can be

considered as the northern boundary of a second-order graben, whose southern boundary is the Dilek Fault (Hancock and Barka, 1987) (Fig. 2). The Kalafat Fault is generally a WNW-trending normal fault with a minor component of dextral movement on the northern side of the Kalafat Mountain (Figs. 2 and 3a). The Cycladic Massif constitutes its footwall, while the hanging wall is made up of volcano-sedimentary rocks of Miocene age, covered by a few ten meters of colluvium in front of the fault. The fault length is given at approximately 15 km in the

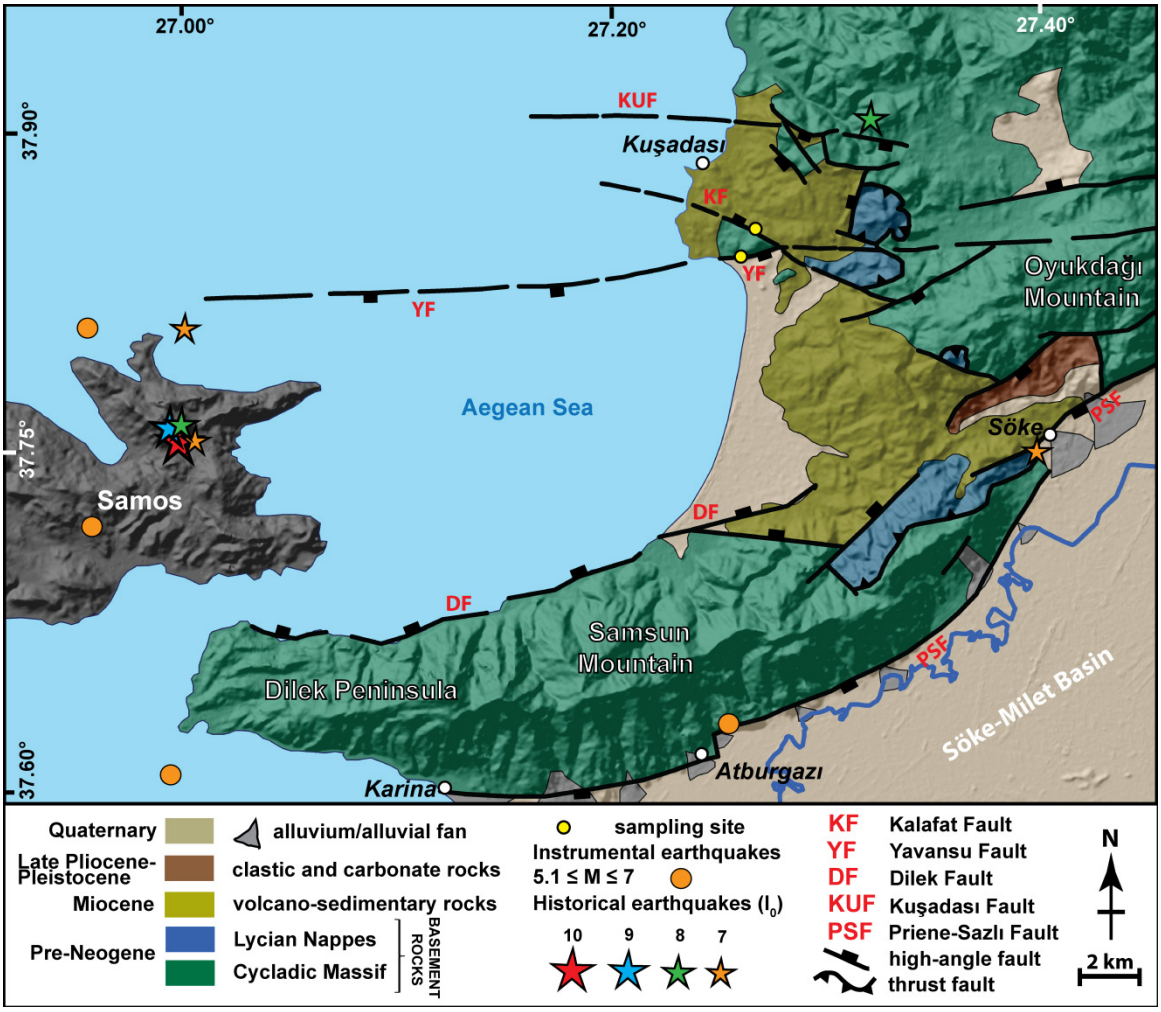

Fig. 2. Geological map of Kuşadası area, including location of historical and instrumental earthquakes (modified after Hancock and Barka, 1987; Passchier et al., 2013; Sümer et al., 2012b).

geology map of western Turkey (Çakmakoğlu, 2006). The Yavansu Fault is basically an E-W-trending normal fault, located on the southern side of the Kalafat Mountain, which juxtaposes Quaternary sediments in the hanging-wall against Cycladic Massif in the footwall (Fig. 4a). Based on Hancock and Barka (1987), the fault is projected to extend north of Samos Island (Fig. 2), with a length of roughly 50 km. According

to Sümer et al. (2012a), the Menderes Fault Zone in its continuation towards the west divides into smaller faults, which the Kalafat and Yavansu faults are part of. Sümer et al. (2013) consider the Yavansu Fault to be 2.5 km in length, and is linked to the Kalafat Fault eastwards. Emre et al. (2013; 2016), however, define the Kuşadası Fault Zone, including the Yavansu Fault, as a distinct structure from the Büyük Menderes Graben, with the 19 km long normal Kuşadası Fault as its main structure.

The Kuşadası area was seismically active in the time span of 1751-1893 AD (e.g., Soysal et al., 1981). Most of the seismic events occurred in the western segment of the Yavansu Fault that extended to Samos Island (Fig. 2). The largest instrumental earthquake close to the study area was 1955 Söke-Balat earthquake, related to the Priene-Sazlı Fault, whose trend is sub-parallel to the Yavansu Fault (Fig. 2). A comparison of the focal mechanism solution of the 1955 earthquake with the Yavansu Fault structural measurements indicates the similarity of their structural patterns (Hancock and Barka, 1987). The activity of the Yavansu Fault was proven by several pieces of evidence, which indicate the occurrence of at least one slip during the Quaternary (Hancock and Barka, 1987). These are documented by: (1) brecciated colluvium in the vicinity of the uppermost slip planes; (2) brecciated colluvium affected by several sub-ordinate slip surfaces; (3) matrix and clasts occasionally cut by comb-fractures in patches of colluvium; (4) occasional striations of colluvium material located in corrugations; and (5) locally displaced colluvium layering by small reverse faults, which cut the slip planes of normal dip-slip lineations.

3. Sampling

Our sampling sites are located on opposite slopes of the Kalafat Mountain, SE of Kuşadası along the Kalafat and Yavansu normal fault scarps within the Kuşadası Fault Zone (Fig. 2). Appropriate sampling sites were selected following the instructions of Mitchell et al. (2001) and Tikhomirov (2014). We sampled the well-exposed N82E, 82°- 85° NW-dipping Kalafat Fault (Figs. 3a and 3b). In total, 54 samples measuring 15 cm wide by 10 cm high were collected with a chisel and hammer. A total of 4.6 m in height of the fault surface was sampled parallel to the

slip direction. We ignored the top 1.6 m of the fault surface due to heavy erosion and weathering. The boundary between the exposed part of the fault scarp and the part covered by colluvium was evidenced by the freshness of the fault surface and determined to be approximately 10 cm above the recent ground level (Fig. 3c). From the Kalafat Fault surface, 45 of the samples were collected along a main strip (KAL). Nine additional samples were also taken from a parallel strip (KALA) at the same heights corresponding samples on part of the KAL, and within approximately one meter of horizontal separation (Fig. 3d).

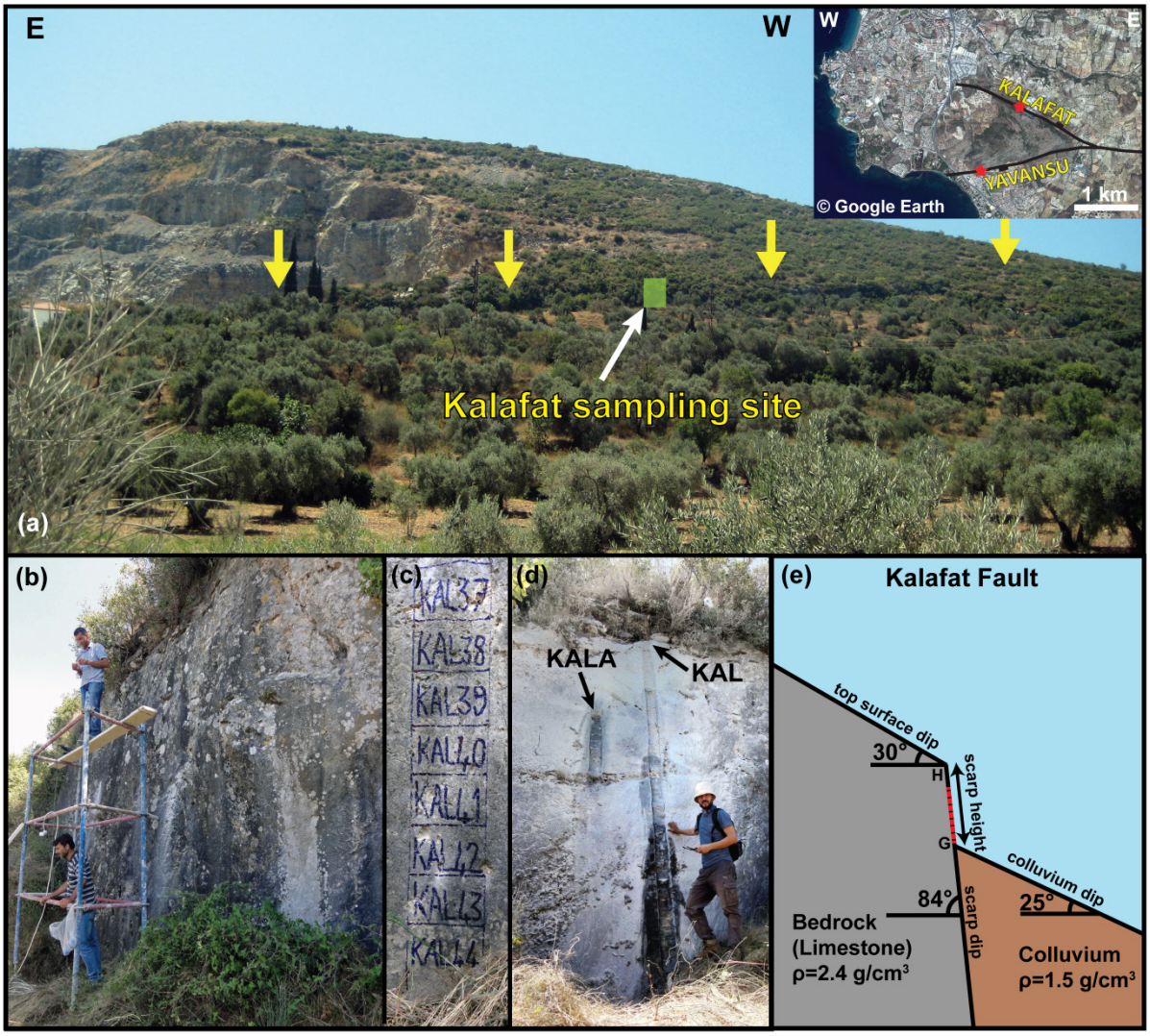

Fig. 3. (a) Field view of the Kalafat Fault and sampling site; The yellow arrows trace the fault exposed surface; (b) Approximately vertical Kalafat Fault surface; (c) Fault scarp surface showing the lowest marked sampling slabs to be cut and collected; (d) KAL and KALA strips after the sample collections; and (e) Schematic sketch of Kalafat Fault showing important parameters of the fault scarp for modeling, including scarp height, scarp dip, colluvium dip, top surface dip and density of the bedrock and colluvium. Red dashed line shows the sampled surface.

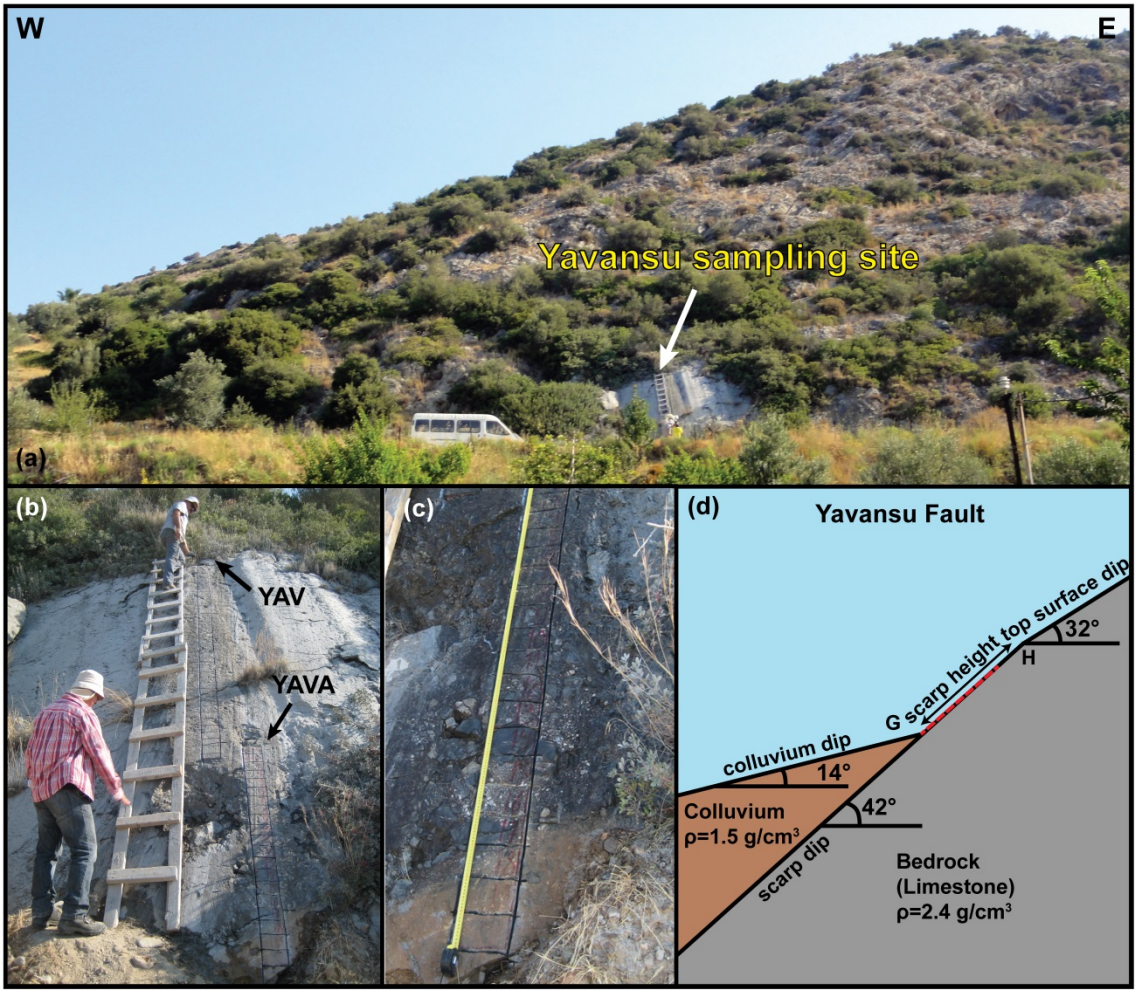

Fig. 4. (a) Field view of the Yavansu Fault and sampling site; (b) YAV and YAVA continuous strips before sample collections; (c) More detailed view of YAVA sampling strip showing the colluvium level; and (d) Schematic sketch of Yavansu Fault showing important parameters of the fault scarp for modeling, including scarp height, scarp dip, colluvium dip, top surface dip and density of the bedrock and colluvium. Red dashed line shows the sampled surface.

On the other side of the mountain, from the N74W, 40°- 44° SW-dipping scarp surface in the lowermost part of the Yavansu normal fault escarpment (Fig 4a), samples were taken from heights of about approximately 6.6 m to the ground level, along two strips, YAV and YAVA, parallel to the slip direction (Fig. 4b). In total, 68 slabs were collected from the fault scarp. The top 60 cm of the fault surface was not sampled, due to weathering and vegetation. Similar to the Kalafat Fault, the colluvium position was determined based on the difference in freshness of the exposed and already covered surface at about 40 cm above the recent ground level (Fig. 4c). As the modeled concentration profile specifically depends on the geometry of the fault scarp, therefore, the scarp dip, scarp height, top surface dip and colluvium dip were measured (Figs. 3e and 4d) (Tikhomirov, 2014). The specific position of each sample along the sampling strips was recorded. Furthermore, the

density of the colluvium was measured with a defined volume bucket and a balance in the field.

4. Cosmogenic ^{36}Cl analysis

We analyzed the Kalafat and Yavansu fault data with the FSDT Matlab® code, which denotes -Fault Scarp Dating Tool- (Tikhomirov, 2014). The fault scarp shielding model (Tikhomirov et al., 2014) was used to calculate the cosmogenic ^{36}Cl accumulation. In order to reconstruct a realistic time-slip history, the Monte-Carlo method was used. All samples were prepared at the Surface Exposure Dating Laboratory of University of Bern, following the protocol of Stone et al. (1996) and Ivy-Ochs et al. (2004; 2009), and an appropriate isotope dilution method (Elmore et al., 1997; Ivy-Ochs et al., 2004; Desilets et al., 2006). First, the slabs were cut parallel to the surface to a thickness of 2.5-3 cm. After crushing, they were sieved into a 0.25-0.4 mm size fraction. A hand magnet was used to separate any metal-chips from crushing material. The crushed material was leached in 75 ml of 2M of HNO_3 overnight, and they rinsed four times with ultrapure water (18.2 MΩ.cm) to remove non-in situ Cl (Zreda et al., 1991). The same leaching procedure was repeated. The samples were dried on a hotplate at 60 °C. Approximately 12 g of each sample, one meter apart along the height of the fault scarp, were taken as proxies, and analyzed for major and trace elements at Actlabs Analytical Services, Canada. Additionally, the Ca concentration of each sample was also measured.

Samples were prepared in batches of 15 samples, and were accompanied with one full process blank to be processed at once. Samples were spiked with around 2.5 mg of pure ^{35}Cl in order to measure the total Cl concentration (^{35}Cl, ^{37}Cl) (Ivy-Ochs et al., 2004; 2009), and were dissolved with HNO_3. Determination of the Cl concentration is required in order to calculate (1) ^{36}Cl concentration in the sample; (2) ^{36}Cl production rate by low-energy neutron capture on ^{35}Cl; and (3) non-cosmogenic subsurface production of ^{36}Cl. The samples were then centrifuged to remove impurities. In order to precipitate AgCl, 10 ml of $AgNO_3$ was added to the supernatant at 200 °C in the dark. After collection of the precipitated AgCl, dissolution was achieved with 2 ml of NH_4OH. The samples were centrifuged in order to eliminate cations. Afterwards, $BaSO_4$ was precipitated by addition of

$Ba(NO_3)_2$ to the supernatant, in order to avoid interference of ^{36}S isobar with ^{36}Cl during Accelerator Mass Spectrometry (AMS) measurements. AgCl was precipitated for the second time. In the final step, the AgCl decant was recovered and rinsed with ultrapure water. AgCl sample tablets were pressed into copper targets for AMS measurements.

The measurements of total Cl and ^{36}Cl concentrations were done from a single target at ETH AMS facility following the isotope dilution method (Synal et al., 1997; Ivy-Ochs et al., 2004), which results in high precision and sensitivity of the ^{36}Cl concentration measurements (Ivy-Ochs et al., 2004; Desilets et al., 2006). The stable ratio of $^{37}Cl/^{35}$ Cl was normalized to the neutral ratio $^{37}Cl/^{35}$ Cl = 31.98 % of K382/4N standard and the machine blank. Ratios of $^{36}Cl/^{35}Cl$ derived from the measurements were normalized to the ETH internal standard K382/4N with a value of $^{36}Cl/Cl = 17.36 \times 10^{-12}$ (normalized to Nishiizumi standard in 2009). The sulfur correction of the measured $^{36}Cl/^{35}Cl$ ratio was insignificant. Furthermore, measured $^{36}Cl/^{35}Cl$ ratios of the sample were corrected for a procedure blank of 6×10^{-15}, which was less than 2.5 % for the samples.

5. Results

The position of the samples along the scarp height, the sample thickness, the cosmogenic ^{36}Cl concentration and its uncertainty, the natural chlorine concentration, as well as calcium, oxygen and carbon concentrations of the samples from the Kalafat and Yavansu fault scarps are given in the Tables 1 and 2. Major and trace elements were measured in eight and seven proxy samples in the Kalafat and Yavansu fault scarps, respectively, whose average values were used for modeling (Tables 3 and 4). The fault scarp parameters are given in Table 5. The density of the colluvium was measured as 1.5 g/cm^3 in the field and density of the scarp limestone is considered to be 2.4 g/cm^3. Measured cosmogenic ^{36}Cl concentrations with their corresponding 1σ errors were plotted versus height for each strip (Figs. 5 and 6). The concentration of cosmogenic ^{36}Cl varies between $(1.049 \pm 0.046) \times 10^5$ at.g^{-1} to $(3.111 \pm 0.114) \times 10^5$ at.g^{-1} along the Kalafat Fault (Fig. 5) and between $(0.793 \pm 0.047) \times 10^5$ at.g^{-1} to $(2.593 \pm 0.126) \times 10^5$ at.g^{-1} along the Yavansu Fault (Fig. 6).

Table 1. Stable Cl, Cosmogenic ^{36}Cl and calcium concentrations, thickness, top and bottom position of the samples of the Kalafat Fault scarp

Sample name	Top position cm	Bottom position cm	Thickness cm	^{36}Cl* 10^5 at/g	^{36}Cl uncertainty*, 10^5 at/g	Cl $_{total}$*, ppm	Cl $_{total}$ uncertainty*, ppm	Ca†, ppm
KAL-1	443	433	3.0	2.929	0.160	11.6	0.12	321000
KAL-2	432	422	3.0	3.111	0.114	9.8	0.10	348000
KAL-3	422	412	2.5	3.083	0.111	11.7	0.12	337000
KAL-4	412	402	3.0	2.750	0.110	12.0	0.12	326000
KAL-5	402	392	3.0	2.881	0.117	10.3	0.10	324000
KAL-6	391	382	3.0	2.805	0.139	9.7	0.10	330000
KAL-7	381	372	2.5	2.754	0.094	9.2	0.09	342000
KAL-8	371	361	2.5	2.760	0.152	4.6	0.05	363000
KAL-9	361	351	2.5	2.896	0.097	5.6	0.06	364000
KAL-10	351	341	3.0	2.810	0.088	8.2	0.08	356000
KAL-11	341	332	3.0	2.316	0.084	8.2	0.08	340000
KAL-12	331	322	3.0	2.356	0.085	9.4	0.09	329000
KAL-13	321	311	3.0	2.139	0.082	9.8	0.10	332000
KAL-14	311	301	3.0	2.304	0.082	9.8	0.10	313000
KAL-15	300	291	3.0	2.318	0.084	11.2	0.11	341000
KAL-16	290	280	3.0	2.325	0.092	7.4	0.07	354000
KAL-17	279	271	3.0	2.135	0.115	8.2	0.08	343000
KAL-18	270	260	3.0	2.053	0.099	10.2	0.10	345000
KAL-19	260	250	3.0	1.906	0.084	11.8	0.12	354000
KAL-20	249	240	3.0	1.786	0.070	6.2	0.06	359000
KAL-21	239	230	2.5	1.880	0.084	6.8	0.07	358000
KAL-22	230	220	2.5	1.610	0.059	6.5	0.07	349000
KAL-23	220	211	2.5	1.686	0.063	5.3	0.05	360000
KAL-24	210	200	2.0	1.483	0.065	2.6	0.03	364000
KAL-25	200	191	3.0	1.644	0.058	5.2	0.05	360000
KAL-26	190	181	2.5	1.538	0.052	4.1	0.04	354000
KAL-27	180	170	2.5	1.489	0.063	6.6	0.07	343000
KAL-28	169	160	2.5	1.477	0.062	5.3	0.05	360000
KAL-29	159	152	2.5	1.468	0.058	7.1	0.07	362000
KAL-30	151	141	3.0	1.588	0.087	5.8	0.06	363000
KAL-31	140	131	2.5	1.558	0.105	4.9	0.05	358000
KAL-32	130	120	3.0	1.423	0.052	5.9	0.06	375000
KAL-33	120	110	2.5	1.446	0.058	6.3	0.06	360000
KAL-34	110	99	2.5	1.290	0.093	5.4	0.05	365000
KAL-35	99	90	3.0	1.133	0.058	12.1	0.12	304000
KAL-36	89	79	3.0	1.049	0.046	5.0	0.05	313000
KAL-37	79	69	3.0	1.177	0.088	4.6	0.05	372000
KAL-38	69	59	2.5	1.611	0.060	5.9	0.06	361000
KAL-39	58	49	2.5	1.387	0.060	4.7	0.05	369000
KAL-40	49	40	2.5	1.405	0.051	5.9	0.06	346000
KAL-41	40	30	2.0	1.201	0.065	3.3	0.03	358000
KAL-42	29	20	2.5	1.207	0.052	6.6	0.07	350000
KAL-43	19	10	2.5	1.255	0.059	4.5	0.05	363000
KAL-44	10	0	3.0	1.169	0.067	5.9	0.06	373000
KAL-45	0	-10	2.5	1.423	0.070	5.2	0.05	371000
KALA-1	290	280	2.5	2.290	0.094	5.7	0.06	367000
KALA-2	279	270	2.5	2.171	0.080	6.4	0.06	361000
KALA-3	269	260	2.5	2.367	0.075	5.1	0.05	361000
KALA-4	259	250	2.5	2.299	0.071	5.6	0.06	355000
KALA-5	249	239	2.5	2.056	0.076	5.8	0.06	349000
KALA-6	239	229	2.5	1.928	0.073	6.0	0.06	348000
KALA-9	209	200	3.0	1.679	0.082	6.4	0.06	328000

*Measured with accelerator mass spectrometry (AMS). †Measured with ICP in Actlabs Analytical services, Canada.

Table 2. Stable Cl, Cosmogenic ^{36}Cl and calcium concentrations, thickness, top and bottom position of the samples of the Yavansu Fault scarp

Sample name	Top position cm	Bottom position cm	Thickness cm	^{36}Cl* 10^5 at/g	^{36}Cl uncertainty*, 10^5 at/g	Cl $_{total}$*, ppm	Cl $_{total}$ uncertainty*, ppm	Ca†, ppm
YAV-1	622	612	2	2.140	0.075	3.9	0.04	389000
YAV-2	612	603	2	2.593	0.126	0.6	0.01	398000
YAV-3	602	593	2	2.127	0.170	0.5	0.01	397000
YAV-4	592	583	2.5	2.313	0.113	2.0	0.02	396000
YAV-5	582	573	2	2.198	0.089	2.5	0.02	392000
YAV-6	572	563	3	1.970	0.097	2.1	0.02	371000
YAV-7	562	553	2	1.852	0.088	3.4	0.03	324000
YAV-8	552	543	2	2.094	0.104	2.7	0.03	350000
YAV-9	542	533	2	1.895	0.129	2.9	0.03	372000
YAV-10	532	523	1.5	1.876	0.110	1.8	0.02	386000
YAV-11	522	513	2.5	1.956	0.105	1.1	0.01	384000
YAV-12	512	503	2	1.965	0.147	1.0	0.01	388000
YAV-13	503	492	2	1.821	0.125	1.7	0.02	377000
YAV-14	492	483	2	1.848	0.110	0.9	0.01	389000
YAV-15	482	474	2.5	1.899	0.081	0.8	0.01	386000
YAV-16	473	463	3	1.673	0.394	1.1	0.01	381000
YAV-17	462	453	2	1.582	0.083	1.5	0.01	374000
YAV-18	452	442	2	1.687	0.066	1.5	0.02	390000
YAV-19	442	433	2.5	1.663	0.077	5.4	0.05	394000
YAV-20	432	423	2	1.624	0.090	2.4	0.02	375000
YAV-21	423	413	2	1.564	0.096	0.9	0.01	379000
YAV-22	412	403	2.5	1.479	0.079	1.2	0.01	380000
YAV-23	402	393	2.5	1.508	0.086	1.3	0.01	380000
YAV-24	393	383	3	1.425	0.090	1.0	0.01	386000
YAV-25	382	373	2.5	1.523	0.081	1.2	0.01	386000
YAV-26	372	363	2.5	1.263	0.084	1.2	0.01	386000
YAV-27	362	353	2.5	1.402	0.072	1.2	0.01	380000
YAV-28	352	343	2	1.419	0.063	1.5	0.02	381000
YAV-29	342	333	2	1.113	0.055	1.0	0.01	305000
YAV-30	332	323	3	1.350	0.133	1.5	0.01	373000
YAV-31	322	313	2.5	1.449	0.089	1.0	0.01	384000
YAV-32	312	302	2.5	1.535	0.071	1.7	0.02	389000
YAV-33	302	293	2.5	1.483	0.068	1.6	0.02	391000
YAV-34	292	282	2.5	1.481	0.072	1.9	0.02	391000
YAV-35	282	272	2.5	1.337	0.065	1.9	0.02	387000
YAV-36	272	263	2.5	1.366	0.071	1.4	0.01	400000
YAV-37	262	253	2.5	1.303	0.074	1.8	0.02	392000
YAV-38	252	243	3	1.286	0.074	2.4	0.02	383000
YAV-39	243	233	3	1.348	0.067	1.4	0.01	380000
YAV-40	232	223	3	1.244	0.063	1.2	0.01	383000
YAV-41	222	213	2	1.185	0.066	1.4	0.01	393000
YAV-42	212	203	2	1.171	0.073	1.2	0.01	388000
YAV-43	202	192	2.5	1.245	0.059	1.1	0.01	387000
YAV-44	192	183	3	1.221	0.057	1.5	0.02	386000
YAV-45	183	173	2.5	1.132	0.059	1.4	0.01	380000
YAV-46	172	163	2	1.277	0.063	0.7	0.01	390000
YAV-1	169	160	2.5	1.098	0.069	1.4	0.01	381000
YAV-47	163	157	3	1.148	0.060	0.8	0.01	387000
YAVA-2	160	150	2.5	1.102	0.051	1.2	0.01	384000
YAVA-3	149	140	3	1.178	0.063	1.2	0.01	378000
YAVA-4	139	130	3	1.089	0.071	1.2	0.01	373000
YAVA-5	129	120	3	0.883	0.062	1.2	0.01	377000

YAVA-6	119	110	2.5	1.080	0.081	1.2	0.01	377000
YAVA-7	109	100	2.5	0.823	0.085	1.2	0.01	378000
YAVA-8	99	90	2.5	0.959	0.055	1.2	0.01	383000
YAVA-9	90	80	2.5	1.086	0.061	1.1	0.01	383000
YAVA-10	79	70	3	1.107	0.056	1.5	0.02	378000
YAVA-11	69	61	3	0.919	0.048	2.7	0.03	360000
YAVA-12	60	50	2.5	0.893	0.077	1.9	0.02	365000
YAVA-13	49	40	3	0.901	0.078	0.9	0.01	377000
YAVA-14	39	29	3	1.035	0.096	7.9	0.08	387000
YAVA-15	29	20	2.5	0.975	0.063	7.9	0.08	387000
YAVA-16	19	10	2.5	0.920	0.048	1.5	0.01	387000
YAVA-17	9	0	3	0.981	0.058	1.4	0.01	386000
YAVA-18	-1	-10	3	0.949	0.106	1.1	0.01	384000
YAVA-19	-11	-20	2.5	0.839	0.049	1.1	0.01	376000
YAVA-20	-21	-31	3	0.793	0.047	1.5	0.01	373000
YAVA-21	-32	-38	2.5	1.051	0.054	1.1	0.01	382000

*Measured with accelerator mass spectrometry (AMS). †Measured with ICP in Actlabs Analytical services, Canada.

The FSDT Matlab® code (Tikhomirov, 2014) was used to analyze the measured cosmogenic ^{36}Cl concentrations in order to reconstruct past earthquakes. The method considers all factors leading to produce ^{36}Cl, which are high energy neutrons, fast and negative muons, as well as thermal and epithermal neutrons (Liu et al., 1994; Phillips et al., 1996; 2001; Stone et al., 1996; 1998; Alfimov and Ivy-Ochs, 2009; Schimmelpfennig et al., 2009). The model considers the given scenario in terms of number of ruptures, timing and associated slips, beginning of exposure and erosion rate. The code applies default rates of ^{36}Cl by high-energy neutron spallation on Ca of 48.8 ± 3.5 at g^{-1} yr^{-1} (Stone et al., 1996), on K of 170 ± 25 at g^{-1} yr^{-1} (Evans et al., 1997), on Ti of 13 ± 3 at g^{-1} yr^{-1} (Fink et al., 2000), and on Fe of 1.9 ± 0.2 at g^{-1} yr^{-1} (Stone, 2005). It also applies defaults for the production rate of epithermal neutrons from fast neutrons in the atmosphere at the land/atmosphere interface of 760 ± 150 n/g^{-1} yr^{-1} (Alfimov and Ivy-Ochs 2009); while the default scaling scheme of Stone (2000) is also used. The model output is displayed as the ^{36}Cl concentrations of the samples versus position along fault scarp in meters, in which each discontinuity defines a distinct period of activity of the fault. The measured data are compared with the modeled data, and a best fit model, which is more consistent with the measured data, is accepted. The number of earthquakes modeled by FSDT is the minimum number, because the program only detects earthquakes with high magnitudes that are capable of displacing the faults. Furthermore, the separation of the earthquakes occurred within a short time interval,

which their uncertainty can be estimated as 25 % of recovered age is not possible (Tikhomirov, 2014). An uncertainty of 15 % was estimated for the amount of slip.

Table 3. Mean chemical composition of the Kalafat Fault samples and colluvium

	Cl (%)	O (%)	C (%)	CaO (%)	MgO (%)	Al_2O_3 (%)	SiO_2 (%)	P_2O_5 (%)	K_2O (%)
KAL-1	0.001161	51.66720	9.516833	45.36	9.30	0.30	1.46	0.02	0.05
KAL-11	0.000817	50.32508	10.08013	46.94	6.29	0.28	2.31	0.01	0.05
KAL-21	0.000684	49.71608	10.61379	49.36	4.62	0.29	1.52	0.01	0.05
KAL-31	0.000492	49.96332	10.61379	49.34	4.21	0.26	1.55	0.02	0.05
KAL-41	0.000328	50.61337	10.61379	50.65	3.02	0.26	1.71	0.01	0.04
KALA-1	0.000566	49.40657	10.88062	50.54	2.47	0.27	2.43	0.02	0.04
KALA-9	0.000640	51.76509	9.724365	46.33	7.18	0.29	1.88	0.02	0.04
Average	*0.000725	50.32400	10.36475	48.36	5.30	0.28	1.84	0.01	0.05
	Na_2O (%)	TiO_2 (%)	MnO (%)	Fe_2O_3 (%)	B (ppm)	Sm (ppm)	Gd (ppm)	U (ppm)	Th (ppm)
KAL-1	0.04	0.010	0.024	0.11	1.0	0.4	0.4	3.1	0.3
KAL-11	0.03	0.011	0.023	0.14	1.0	0.5	0.5	3.6	0.5
KAL-21	0.04	0.009	0.030	0.19	1.0	0.5	0.6	10.0	0.5
KAL-31	0.03	0.009	0.027	0.10	1.0	0.5	0.5	4.6	0.4
KAL-41	0.03	0.008	0.034	0.12	1.0	0.5	0.5	3.6	0.3
KALA-1	0.03	0.008	0.027	0.10	1	0.4	0.4	3.3	0.3
KALA-9	0.02	0.010	0.025	0.09	1	0.6	0.7	3.4	0.5
Average	0.03	0.009	0.027	0.12	1.0	0.48	0.5	4.5	0.4

* Average of values presented in Tables 1 is used for modeling.

Table 4. Mean chemical composition of the Yavansu Fault samples and colluvium

	Cl (%)	O (%)	C (%)	CaO (%)	MgO (%)	Al_2O_3 (%)	SiO_2 (%)	P_2O_5 (%)	K_2O (%)
YAV-1	0.000385	47.42710	11.53286	53.82	0.28	0.49	1.64	0.03	0.06
YAV-11	0.000105	48.35410	11.38462	52.90	1.57	0.31	0.88	0.04	0.03
YAV-21	0.000092	48.50208	11.23638	52.56	1.04	0.62	1.79	0.05	0.06
YAV-31	0.000101	48.36969	11.38462	53.07	0.93	0.45	1.32	0.05	0.04
YAV-41	0.000142	47.17666	11.65145	52.99	0.78	0.44	1.43	0.05	0.04
YAVA-2	0.000120	48.28426	11.38462	53.03	1.11	0.34	1.54	0.04	0.05
YAVA-12	0.000192	49.59739	10.82132	50.92	3.20	0.38	1.30	0.05	0.05
YAVA-21	0.000115	48.78046	11.32533	53.54	1.02	0.37	1.06	0.03	0.03
Average	*0.000173	48.30754	11.29037	52.85	1.24	0.42	1.37	0.04	0.04
	Na_2O (%)	TiO_2 (%)	MnO (%)	Fe_2O_3 (%)	B (ppm)	Sm (ppm)	Gd (ppm)	U (ppm)	Th (ppm)
YAV-1	0.05	0.028	0.012	0.38	2.00	0.3	0.2	3.1	0.5
YAV-11	0.02	0.011	0.011	0.25	1.00	0.5	0.4	4.0	1.2
YAV-21	0.03	0.022	0.017	0.57	6.00	0.4	0.4	5.1	0.8
YAV-31	0.03	0.016	0.015	0.47	1.00	0.5	0.4	7.5	1.0
YAV-41	0.03	0.017	0.011	0.37	1.00	0.4	0.3	6.0	0.6
YAVA-2	0.02	0.014	0.011	0.29	1.00	0.5	0.3	4.2	0.8
YAVA-12	0.03	0.013	0.011	0.32	1.00	0.3	0.3	5.6	0.4
YAVA-21	0.02	0.013	0.015	0.33	1.00	0.5	0.4	6.3	0.8
Average	0.03	0.017	0.013	0.37	1.75	0.4	0.3	5.2	0.8

* Average of values presented in Tables 2 is used for modeling.

Table 5. Parameters of the sampled Kalafat and Yavansu fault scarps

	Kalafat Fault	Yavansu Fault
Latitude	37.83469° N	37.82499° N
Longitude	27.27087° E	27.26412° E
Altitude	160 m	36 m
Scarp strike	N82°E	N74°W
Scarp dip	84°	42°
Colluvium dip	25°	14°
Scarp height	6.2 m	7.2 m
Top surface dip	30°	32°
Rock density	2.4 g/cm^3	2.4 g/cm^3
Colluvium density	1.5 g/cm^3	1.5 g/cm^3
Rock water content	0.2 %	0.2 %
Colluvium water content	1 %	1 %

In the first step of modeling using FSDT, different scenarios with different numbers of earthquakes, age and slip as well as erosion rates were tested. Afterwards, the scenarios with the best statistical criteria were focused upon. The best fit solutions for each scenario tested for the faults are summarized in Tables 6. The scenarions with three earthquakes show the lowest statistics with RMSw = 1.7492, X^2 = 3.6007 and AICc = 233.9766 for the Kalafat Fault, and with RMSw = 1.1422, X^2 = 1.4768 and AICc = 346.8627 for the Yavansu Fault. The scenario of three earthquake events for the Kalafat Fault gave the best fit, with the beginning of the exposure of ca. 22 ka. The ages of the three earthquake events are ca. 15.3 ± 3.8 ka, 8.4 ± 2.1 ka, and 3.6 ± 0.9 ka, with vertical components of associated slip of 0.7 ± 0.1 m, 0.9 ± 0.1, and 3.1 ± 0.5 m. (Fig. 7). The average slip rates from the oldest to youngest reconstructed rupture were estimated to be > 0.1, 0.1 and 1.5 mm/yr (Fig. 9a), while the long-term slip rate was calculated to be 0.6 mm/yr. The fault does not follow a regular recurrence interval with ca. 6.9 and 4.8 ky difference in the time span between earthquakes.

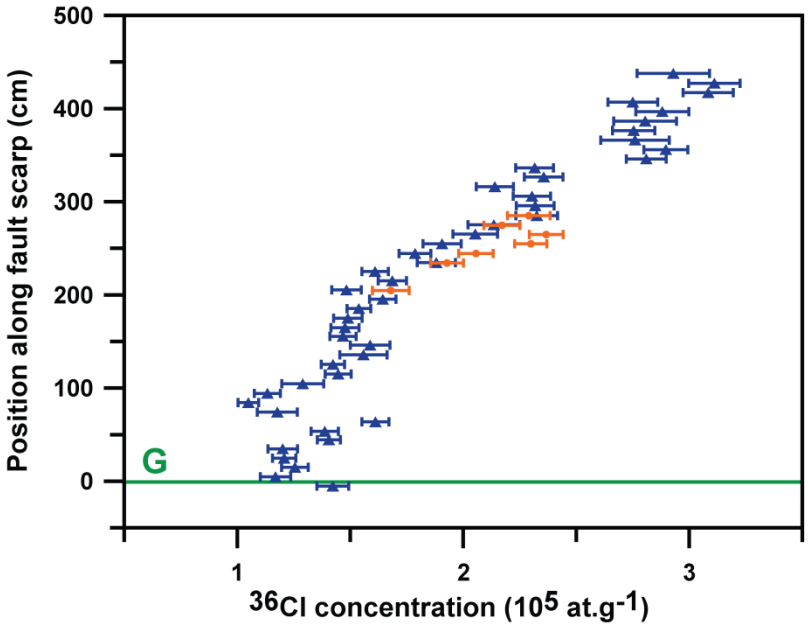

Fig. 5. Cosmogenic ^{36}Cl concentrations with 1σ uncertainties versus height along Kalafat Fault scarp surface; Blue and orange colors indicate KAL and KALA samples, respectively.

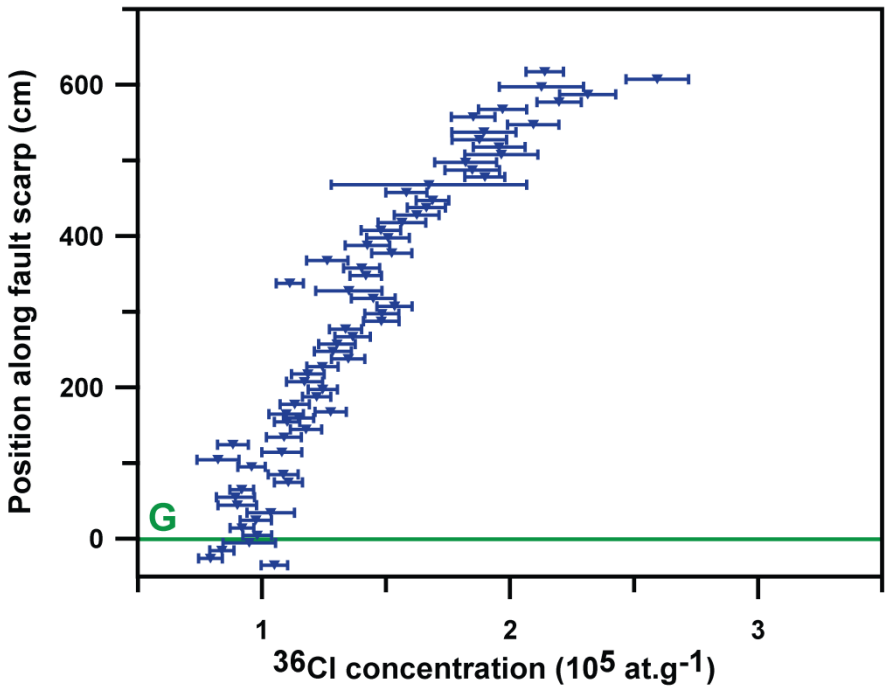

Fig. 6. Cosmogenic ^{36}Cl concentrations with 1σ uncertainties versus height along Yavansu Fault scarp surface.

Table. 6. Results for the data set of the Kalafat and Yavansu fault scarps along with statistical criterion

	Event number	Beginning of exposure (ka)	Age (ka)	Slip (m)	Statistical criterion
Kalafat Fault	3	22	15.3 8.4 3.6	0.7 0.9 3.1	**X^2 = 3.6** **RMSw = 1.7** **AICc = 233**
	4	20	20.0 16.0 8.6 3.9	1.3 0.2 0.9 3.1	X^2 = 3.7 RMSw = 1.7 AICc = 239
	5	24	11.0 10.0 6.0 3.4 0.2	0.4 0.6 0.4 3.0 0.0	X^2 = 4.0 RMSw = 1.7 AICc = 245
Yavansu Fault	3	12	7.9 3.4 2.0	0.6 3.5 2.6	**X^2 = 1.47** **RMSw = 1.1** **AICc = 346**
	4	12	8.8 3.5 2.1 0.7	1.0 3.4 2.8 0.0	X^2 = 1.53 RMSw = 1.1 AICc = 351
	5	11	9.4 8.9 5.1 3.3 2.0	0.1 0.7 0.4 3.3 2.2	X^2 = 1.61 RMSw = 1.1 AICc = 356

Chi-squared Value (X^2)
Weighted root mean square (RMSw)
Akaike information criterion (AICc)

The scenario of three earthquake events for the Yavansu Fault gave the best fit, with the beginning of the exposure of ca. 12 ka. The ages of the three earthquake events are 7.9 ± 2.0 ka, 3.4 ± 0.8 ka, and 2.0 ± 0.5 ka with vertical components of associated slip of 0.6 ± 0.1 m, 3.5 ± 0.5 m, and 2.6 ± 0.4 m, respectively (Fig. 8). The vertical distances between ruptures give an average value of vertical slip rates greater than 0.1 mm/yr for the oldest earthquake and 0.8 and 1.9 mm/yr for the second and third earthquakes during the seismic activity of the Yavansu Fault (Fig. 9b). The long-term slip rate

was calculated to be ca. 1 mm/yr, taking into account ca. 6.1 m of slip occurred in the time span between the oldest and the youngest modeled ruptures. The irregular intervals between earthquakes are ca. 4.5 and 1.4 ky.

6. Discussion

The geochronology of seismic activity of faults can provide essential findings in terms of helping to reduce the potential damages during destructive earthquakes (e.g., Scholz, 2002). The reconstruction of the age and slip amounts of major paleoearthquakes can make a significant contribution in the field of seismic risk assessment, particularly in the highly populated region of western Anatolia and Kuşadası. The activity of faults prior to the seismic archives in this region has already been documented by the powerful fault scarp dating method on the Priene-Sazlı Fault (Mozafari et al., *submitted*), as well as the Manastır and Mugırtepe faults in the Manisa Fault Zone (Akçar et al., 2012; Tikhomirov; 2014). This study examined the past seismic activity of the Kalafat and Yavansu faults in western Anatolia using cosmogenic ^{36}Cl.

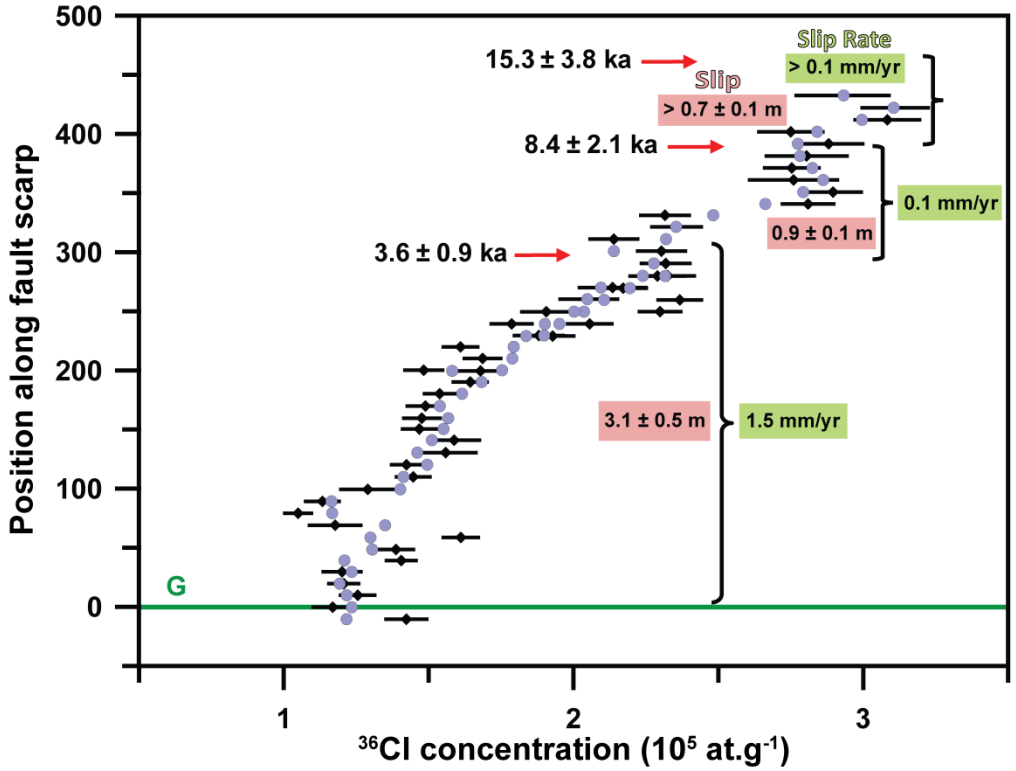

Fig. 7. Best fit (blue circles) of the samples of the Kalafat Fault scarp data with a three rupture model. Black dots with 1σ uncertainties are measured ^{36}Cl concentrations. Red arrows mark the colluvium positions before the modeled ruptures. Slip rates are calculated individually for each earthquake, based on the slip value and the time period between two successive earthquakes.

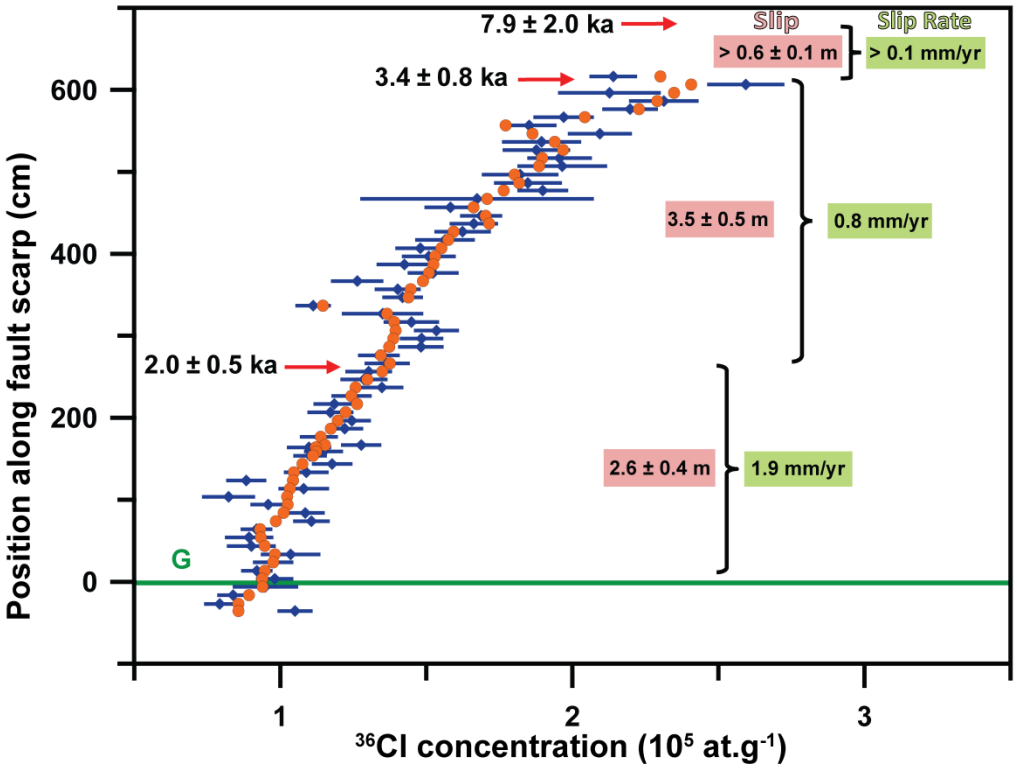

Fig. 8. Best fit (orange circles) of the samples of the Yavansu Fault scarp data with a three rupture model. Blue dots with 1σ uncertainties are measured ^{36}Cl concentrations. Red arrows mark the colluvium positions before the modeled ruptures. Slip rates are calculated individually for each earthquake, based on the slip value and the time period between two successive earthquakes.

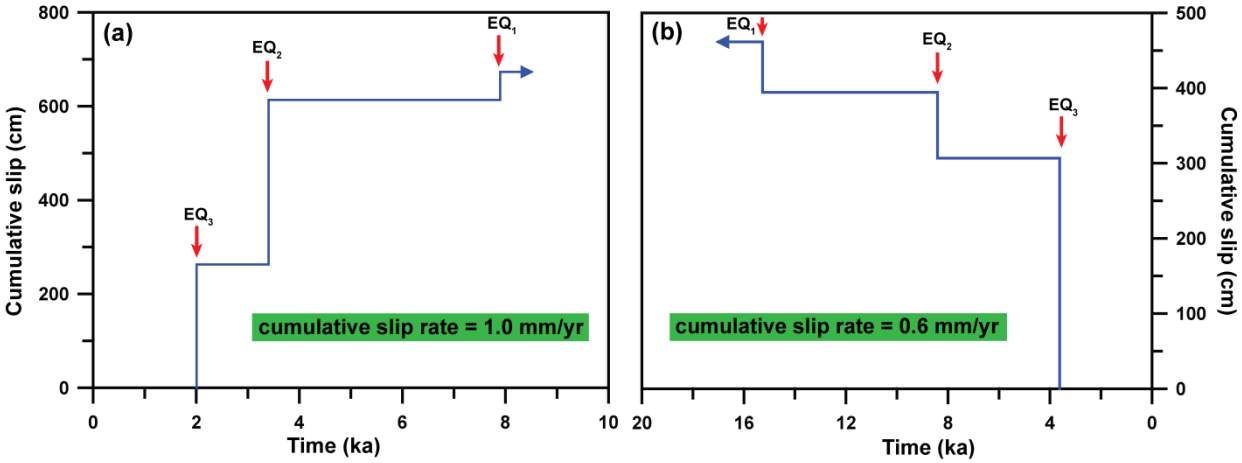

Fig. 9. Time versus cumulative slip amount obtained from modeling of (a) the Kalafat Fault scarp; The average slip rate is 1.0 mm/yr; and (b) the Yavansu Fault scarp; The average slip rate is 0.6 mm/yr.

6. 1. Future earthquakes

Seismological methods are not yet explicitly able to predict the magnitude of future earthquakes. However, an approximation of probable magnitude is possible by empirical relationships, which logarithmically connect fault surface length (SRL) to the size of earthquakes (e.g., Wells and Coppersmith, 1994; Ambraseys and Jackson, 1998; Pavlides and Caputo, 2004). To accomplish this, we used the formula of Pavlides and Caputo (2004), which is specifically based on dip-slip normal faults in the Aegean region (equation 1 in Table 7). The formula of Wells and Coppersmith (1994), which is based on a worldwide investigation on different normal faults, was also used (equation 3 in Table 7). By considering the 15 km length, the Kalafat Fault can produce an earthquake of magnitude 6.5 on average (equation 1 in Table 7). Based on the formula of Wells and Coppersmith (1994) the occurrence of an earthquake with magnitude of 6.4 is possible (equation 3 in Table 7). The probable length of about 50 km for the Yavansu Fault yields an earthquake capacity of magnitude 7.0 or 7.1 in magnitude according to equations (1) and (3), respectively, in Table 7. If the fault is 2.5 km long, the probable earthquake would have a magnitude of 5.8 or 5.4 according to equations 1 and 3, respectively, in Table 7, respectively. Since both faults are able of producing earthquakes of greater than magnitude 5, they can be classified as seismogenic faults (McCalpin, 2009).

The empirical relationships that connect the displacement value with the earthquake magnitude were also used to estimate the average slip value as a consequence of probable rupture (i.e., equations 2 and 4 in Table 7). The magnitude of earthquakes based on the length of the Kalafat Fault was estimated to be 6.5 (equation 1 in Table 7). This results in a maximum vertical displacement (MVD) and slip of 0.4 m (equation 2 in Table 7). Based on Wells and Coppersmith (1994), the maximum displacement (MD) or slip resulting from an earthquake with magnitude 6.4 is 0.6 m (equation 4 in Table 7). The 2.5 and 50 km length of the Yavansu Fault yielded earthquakes with magnitudes 5.8 and 7.0, respectively (equation 1 in Table 7). The MVD were estimated to be 0.1 and 1.4 m, respectively, and based on dip of the fault surface ($\theta = 42°$), yield slips of 0.1 and 1.7 m, respectively (equation 2 in Table 7). Considering the formula of Wells and

Coppersmith (1994), the maximum displacement (MD) or slip resulting from earthquakes of magnitude 5.4 and 7.1 would be 0.1 and 2.6 m, respectively (equation 4 in Table 7).

Table 7. Regression of SRL (surface rupture length), magnitude (M_s/M) and vertical displacement (MVD/MD) calculated for the Kalafat and Yavansu Faults.

	SRL/FL	15 km (Cakmakoglu, 2007)	50 km (Hancock & Barka, 1987)	2.5 km (Sümer et al., 2013)
		KALAFAT FAULT	YAVANSU FAULT	
Pavlides & Caputo (2004)	Ms = 0.9 x Log (SRL) + 5.48 (equation 1)	6.5	7.0	5.8
	Log (MVD) = 1.14.Ms - 7.82 (equation 2)	MVD = 0.4 Slip = 0.5	MVD = 1.4 Slip = 1.7	MVD = 0.1 Slip = 0.1
Wells & Coppersmith (1994)	M = 4.86 + 1.32 x log (SRL) (equation 3)	6.4	7.1	5.4
	Log (MD) = - 5.90 + 0.89 x M (equation 4)	MD (Slip) = 0.6	MD (Slip) = 2.6	MD (Slip) = 0.1

6. 2. Earthquake history

In the following paragraphs, we discuss the seismic activity and breakage history of the Kalafat and Yavansu faults based on our modeling, as well as the plausibility of magnitude values of earthquakes that produced the associated amount of slip. We used the same empirical approaches in order to estimate the magnitude values of the reconstructed earthquakes (Pavlides and Caputo, 2004; Wells and Coppersmith 1994; equations 5 and 6 in Table 8).

Table 8. Regression of magnitude (M_s/M) and vertical displacement (MVD/MD) for the Kalafat and Yavansu Faults. Unit of slip, MVD and MD is in meters. * Modeled by the code.

			KALAFAT FAULT (θ = 84°)			YAVANSU FAULT (θ = 42°)		
Sin (θ) = vertical displacement /Slip		Event	Slip* (m)	MVD (m)	Ms	Slip* (m)	MVD (m)	Ms
Pavlides & Caputo (2004)	Ms = 0.59 x Log (MVD) + 6.75 (equation 5)		Lowest X^2	Average	Average	Lowest X^2	Average	Average
		EQ1	0.7 ± 0.1	0.7 ± 0.1	6.6	0.6 ± 0.1	0.4 ± 0.1	6.5
		EQ2	0.9 ± 0.1	0.9 ± 0.1	6.8	3.5 ± 0.5	2.3 ± 0.4	7.0
		EQ3	3.1 ± 0.5	3.1 ± 0.5	7.0	2.6 ± 0.4	1.8 ± 0.3	6.9
		Event	MD (= Slip*) (m)		M	MD (= Slip*) (m)		M
Wells & Coppersmith (1994)	M = 6.61 + 0.71 x log (MD) (equation 6)		Lowest X^2		Average	Lowest X^2		Average
		EQ1	0.7 ± 0.1		6.5	0.6 ± 0.1		6.5
		EQ2	0.9 ± 0.1		6.6	3.5 ± 0.5		7.0
		EQ3	3.1 ± 0.5		7.0	2.6 ± 0.4		6.9

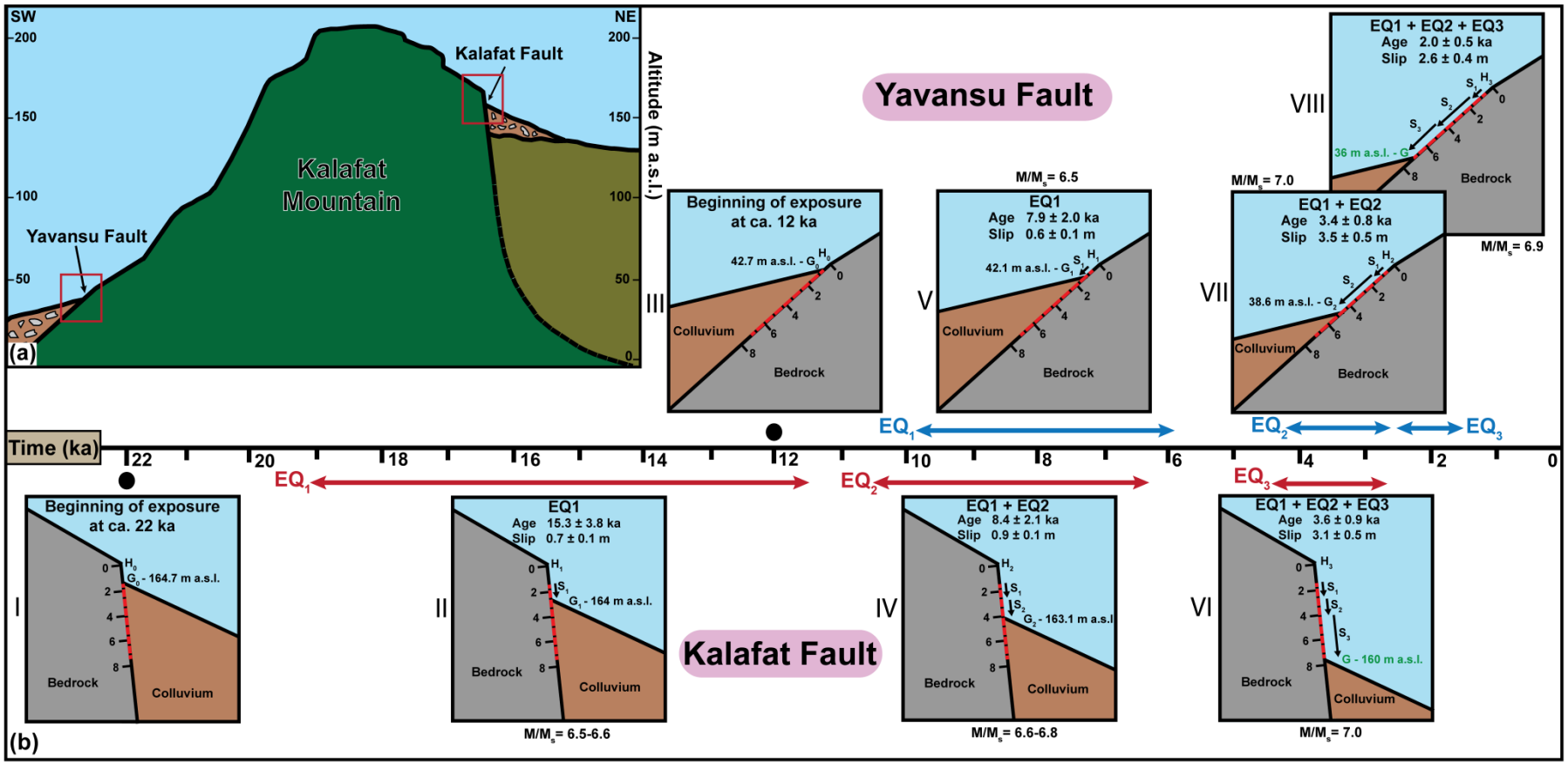

Fig. 10. (a) Schematic sketch of the Yavansu and Kalafat Fault scarps on the opposite sides of the Kalafat Mountain; The horizontal scale is 1:5 (Our sampling sites on the Kalafat and Yavansu Fault surfaces are about 1.4 km apart); (b) I to VIII; A detailed view of the fault situation through time, showing colluvium position and episodic fault exposure during three modeled earthquake events, from the beginning of exposure of the Kalafat and Yavansu Faults (left to right). In the insets, red dashed lines show the sampled surfaces. The fault surface grade is in meters. H_0 shows scarp heights prior to first rupture. H_1 to H_3 are height of the fault scarp following earthquakes of 1 to 3, respectively; G_0 is ground level just before the first rupture, G_1 and G_2 are ground levels before the second and third ruptures; and G mark the current ground level. S_1 to S_3 represent the associated amounts of slip of three earthquakes from past to recent events. M/M_s show magnitude of earthquake with capacity of displacing the fault with the modeled slip amount. Double-heading arrows represent the uncertainty of earthquake ages.

The locations of our sampling sites on opposite sides of Kalafat Mountain is illustrated in the schematic cross-section shown in Figure 10a, which shows approximately 120 m of difference in elevation (Fig. 10a). The sampled part of the scarp of the Kalafat Fault began its exposure at ca. 22 ka. The position of the ground level cannot be defined at this time, due to an unsampled part of the scarp. But it was at about 165 m a.s.l. (above sea level) or higher (point G_0 in inset I in Fig. 10b), before the first seismic activity of the Kalafat Fault at 15.3 ± 3.8 ka with a slip value of 0.7 ± 0.1 m (S_1). This event caused movement of the ground level from G_0 to G_1 (Fig. 7 and inset II in Fig. 10b). For this interval, a slip rate of 0.1 mm/yr was calculated. However, this value is considered as the lower limit, because if the upper part of scarp was sampled, it might result in a higher slip value. In addition, one should note that we cannot exclude additional older earthquakes, which similarly results in a shorter interval and higher slip rate (e.g., Schlagenhauf et al., 2010). This amount of slip indicates an earthquake with an order of magnitude of 6.5 to 6.6 (equations 5 and 6 in Table 8). Two earthquakes are required to move the fault to produce this amount of slip (equations 2 and 4 in Table 7). This phase of activity probably occurred as clustered events in a short time span rather than a single earthquake. In the South of Kalafat Mountain**,** the exposure of the Yavansu Fault appears to be much younger than the Kalafat Fault exposure at ca. 12 ka (inset III in Fig. 10b). Meanwhile the Kalafat Fault ruptured for the second time at 8.4 ± 2.1 ka, after a long phase of inactivity of ca. 6.9 ka. Afterwards, the ground ground level moved from G_1 to G_2, as a result of 0.9 ± 0.1 m of slip (S_2) (Fig. 7 and inset IV in Fig. 10b). This amount of slip over the time span between the first and second ruptures results in mean slip rate of ca. 0.1 mm/yr. This rupture is likely to be produced by an earthquake of magnitude 6.6-6.8 (equations 5 and 6 in Table 8). Two earthquakes are required to expose the fault surface with this amount of slip (equations 2 and 4 in Table 7). The Yavansu Fault started rupture approximately simultaneous with the second rupture of the Kalafat at 7.9 ± 2.0 ka, with a minimum slip of 0.6 ± 0.1 m (S_1). This caused the initial ground level (G_0) to move to G_1, which was already at the elevation of 43 m a.s.l. or higher before the occurrence of the first rupture (Fig. 8 and insets III and V in Fig. 10b). Similar to the Kalafat Fault, the slip rate of this phase of activity is calculated to be a minimum of 0.1 mm/yr. This slip amount equals to an MVD of ca. 0.4 m, which can be produced by an earthquake

with magnitude of 6.5 (equations 5 and 6 in Table 8). If the 50 km length of the fault is considered, one earthquake could be severe enough to produce this rupture. However, several earthquakes would be required, if the fault length is 2.5 km (equations 2 and 4 in Table 7). The last earthquake on the Kalafat Fault occurred at 3.6 ± 0.9 ka after ca. 4.8 ky period of quiescence. This rupture caused a hanging-wall slip of 3.1 ± 0.5 m (S_3) to the recent ground level of 160 m a.s.l. (Fig. 7 and inset VI in Fig. 10b). The mean slip rate of approximately 1.5 mm/yr was obtained by taking into account the slip amount and the corresponding phase of inactivity from the occurrence of the preceding rupture to the last rupture. An earthquake with magnitude 7 on average is capable of generating this slip (equations 5 and 6 in Table 8). Considering the length of the fault, several earthquakes are required to produce about three meters of displacement. This phase of activity can also be considered as several sub-events occurring as a series of ruptures close in time. The second rupture of the Yavansu Fault occurred highly coincident with the last rupture on the Kalafat Fault at 3.4 ± 0.8 ka, after ca. 4.5 ky period of quiescence. In total, 3.5 ± 0.5 m of slip (S_2) caused the ground level to move from G_1 to G_2 (Fig. 8 and inset 10b in Fig. VII). The calculated slip rate for this time interval is ca. 0.8 mm/yr, which is much higher than in the past phase of activity. The slip amount equates to ca. 2.3 m of MVD, which can be produced by an earthquake of magnitude 7 (equations 5 and 6 in Table 8). More likely, two or more earthquakes were needed to expose the fault with this amount of slip. We conclude that this phase of activity involved a series of ruptures close in time, based on the 50 km length of the fault (equations 2 and 4 in Table 7). If the fault is short as 2.5 km long, too many earthquakes are needed to cause this amount of slip, which we consider implausible. After a period of quiescence of ca. 1.4 ky, the last earthquake on the Yavansu Fault occurred at 2.0 ± 0.5 ka ago. This resulted in 2.6 ± 0.4 m of slip (S_3) and the ground level to move to G, the recent ground level of ca. 36 m a.s.l. (Fig. 8 and inset VIII in Fig. 10b). The mean slip rate was about 1.9 mm/yr for this time interval. The slip equals to 1.8 ± 0.3 m MVD, which can be created by an earthquake of magnitude 6.9 (equations 5 and 6 in Table 8). One earthquake can cause this slip, where the fault length is considered to be 50 km. However, if the fault length is as short as 2.5 km, a large number of earthquakes are responsible for

the exposure of the fault in the corresponding period of activity (equations 2 and 4 in Table 7).

The youngest identified earthquake by our modeling dates back to ca. 2 ka on the Yavansu Fault. However, there are historical and instrumental earthquakes reported mostly recorded on Samos Island since 1751 AD, none of which are directly linked to either the Yavansu or Kalafat faults, (Fig. 2). Therefore, our modeling suggests that the western extension of the Yavansu Fault possibly is an individual segment, which is not fully linked to the Yavansu Fault on mainland Turkey.

In the Kuşadası region, the cycles of quiescence between successive events along the Kalafat and Yavansu faults through time until the occurrence of the last ruptures of both faults are generally shortening, from ca. 6.9 to 4.8 ky for the Kalafat Fault and ca. 4.5 to 1.4 ky for the Yavansu Fault. However, the Kalafat and Yavansu faults had their last activity in ca. 3.6 and 2 ka, respectively. However, both faults have the potential to produce earthquakes of magnitude 5 and larger in the future. If we assume the historical and instrumental earthquakes recorded in Samos Island (Fig. 2) are related to activity on the Yavansu Fault, and these are not identified by our modeling, an interval of ca. 1.7 ky is obtained from the last modeled rupture for the Yavansu Fault.

Further south, fault scarp dating of the Priene-Sazlı Fault revealed evidence of four phases of high seismic activity between 8.1 to 2.2 ka (Mozafari et al., *submitted*). Comparison of the timing of the modeled earthquakes on the Kalafat, Yavansu and Priene-Sazlı faults indicates similar timing of high seismic activities in this region at ca. 3.5 and 8 ka, once all three of the faults were active. In addition, at ca. 2 ka, the Priene-Sazlı and Yavansu faults were spontaneously ruptured with a very similar time interval. These data can indicate the high amount of interaction between the nearby faults, which is reflected in their seismic behavior as a portion of the larger fault setting. The Kalafat and Yavansu faults are connected in the middle of their strikes, to the east of our sampling sites, according to geological map (Fig. 2). Based on our results, the Kalafat Fault was exposed ca. 10 ky prior to the first exposure of the Yavansu Fault, and even had its first significant activity before the

Yavansu Fault was exposed (Fig 10b). This may indicate the possibility of the Yavansu Fault exposure and subsequent activity interacted with the pre-existing and older Kalafat Fault as its opposite-facing antithetic pair, which eventually linked to each other through more activities. Evidence for this can be seen by the increasing slip rates on both faults over time (Figs. 7, 8 and 9). Acceleration of slip rates of normal faults can indicate either a cause or an outcome of linkage (e.g., Abruzzo, central Italy; Cowie et al., 2007). In our case study, the increase of the slip rates could cause incremental growth of the Kalafat and Yavansu faults, and ease their linkage. Linkage can be triggered, particularly when an active fault, like Kalafat is located in the middle of a larger fault setting, as in our case between the neighboring Yavansu and Kuşadası faults (Cowie et al., 2007). However, fault seismic activity and growth are not solely dependent on the local pattern of nearby structures, but are more related to the regional tectonic framework and how the structures are interacted, which might result in either fault lockage or release of accommodated strain. Regarding the cumulative slip rates, slip per event, rupture lengths, magnitude of probable earthquakes and recurrence intervals of the Kalafat and Yavansu faults, both faults can be considered as low to moderate (Class 3) active faults using the activity classification of faults for earthquake engineering of Cluff and Cluff (1984).

7. Conclusions

Fault scarp dating using cosmogenic ^{36}Cl distributions is a powerful technique to recover the history of paleoearthquakes, and develop earthquake hazard assessment in extensional tectonic settings. We have explored the long-term paleoearthquake history of two faults in the Kuşadası area within the northwestern end of the Büyük Menderes Graben prior to and within the available earthquake archives by analyzing cosmogenic ^{36}Cl in 122 samples and using FSDT (Tikhomirov, 2014). At least six high seismically active periods were recovered, of which two events on each fault happened synchronously with a seismic event on the other fault. Both faults can be considered as seismic-prone and active faults, which should be given more serious attention in order to reduce the earthquake associated risks. Our findings are summarized as follow:

- Both faults experienced at least three seismic events during late Pleiostocene - Holocene time basically as clusters of earthquakes occurring close in time.
- Vertical components of slips were modeled ranging from 0.7 to 3.1 m for the Kalafat Fault, and from 0.6 to 3.5 m for the Yavansu Fault at the cessation of the seismic events.
- Average slip rates of greater than 0.1, 0.1, and 1.5 mm/yr for the Kalafat Fault and greater than 0.1, 0.8, and 1.9 mm/yr for the Yavansu Fault were estimated from the oldest to youngest modeled ruptures, respectively.
- Long-term slip rates were calculated as 0.6 and 1.0 mm/yr for the Kalafat and Yavansu faults, respectively.
- The recurrence intervals of earthquakes on neither of the faults follow a regular pattern, but are generally getting shorter over time.
- Both Kalafat and Yavansu faults can be considered as seismogenic faults, due to having the potential to generate earthquakes of greater than magnitude 5.
- At around 3.5 and 8 ka, the three faults of Kalafat, Yavansu and Priene-Sazlı were ruptured, which indicates the occurrence of high seismically active periods in the western part of the Büyük Menderes Graben.

Acknowledgments

We warmly acknowledge Dr. Hans-Arno Synal and the team at the Laboratory of Ion Beam Physics, ETH Zurich for their supports with the AMS measurements. We are thankful to Cihan Bayrakdar for his collaboration with sample preparation. We would also like to thank the students and technicians of Dokuz Eylül University, who helped us during our sampling campaign. Our work has been funded by the Dokuz Eylül University (Research Project No. 2006.KB.FEN.008), the Surface Exposure Dating Laboratory at the University of Bern, the Bern University Research Foundation and the Swiss National Science Foundation (Project No. 200021-147065).

References

- Akçar, N., Tikhomirov, D., Özkaymak, Ç., Ivy-Ochs, S., Alfimov, V., Sözbilir, H., Uzel, B., Schlüchter, Ch., 2012. ^{36}Cl Exposure Dating of Paleoearthquakes in the Eastern Mediterranean: First Results from Western Anatolian Extensional Province, Turkey. GSA Bulletin 124, no. 11/12, 1724-1735.
- Alfimov, V., Ivy-Ochs, S., 2009. How well do we understand production of Cl-36 in limestone and dolomite?: Quaternary Geochronology, 4(6), 462-474.

- Ambraseys, N.N., Jackson, J.A., 1998. Faulting associated with historical and recent earthquakes in the Eastern Mediterranean region: Geophysical Journal International 133, no. 2, 390-406.
- Benedetti, L., Finkel, R., King, G., Armijo, R., Papanastassiou, D., Ryerson, F.J., Flerit, F., Farber, D., Stavrakakis, G., 2003. Motion on the Kaparelli fault (Greece) prior to the 1981 earthquake sequence determined from Cl-36 cosmogenic dating: Terra Nova, v. 15, no. 2, p. 118-124.
- Benedetti, L., Finkel, R., Papanastassiou, D., King, G., Armijo, R., Ryerson, F., Farber, D., Flerit, F., 2002. Post-glacial slip history of the Sparta fault (Greece) determined by Cl-36 cosmogenic dating: Evidence for non-periodic earthquakes: Geophysical Research Letters, 29, no. 8, 1246, doi: 10.1029/2001GL014510.
- Benedetti, L., Manighetti, I., Gaudemer, Y., Finkel, R., Malavieille, Y., Pou, Kh., Arnold, M., Aumaître, G., Bourlès, D., Keddadouche, K., 2013. Earthquake synchrony and clustering on Fucino faults (Central Italy) as revealed from in situ ^{36}Cl exposure dating. Journal of Geophysical Reasearch, Solid Earth 118, 4948-4974.
- Çakmakoğlu, A., 2006. Dilek yarımadası-söke ve selçuk çevresinin Jeolojisi.
- Cluff, L.S., Cluff, J.L., 1984. Importance of assessing degrees of fault activity for engineering decisions, Proceeding 8th World Conference on Earthquake Engineering, vol. 2, 629-636.
- Cowie, P.A., Phillips, R.J., Roberts, G.P., McCaffrey, K., Zijerveld, L.J.J., Gregory, L.C., Faure Walker, J., Wedmore, L.N.J., Dunai, T.J., Binnie, S.A., Freeman, S.P.H.T. , Wilcken, K., Shanks, R.P., Huismans, R.S., Papanikolaou, I., Michetti, A.M., Wilkinson, M., 2017. Orogen-scale uplift in the central Italian Apennines drives episodic behaviour of earthquake faults, Scientific Reports 7, Article number 44858.
- Cowie, P.A., Roberts, G.P., Mortimer, E., 2007. Strain localization within fault arrays over timescales of 10^0-10^7 years (Observations, explanations, and debates). *In* Tectonic faults: agents of change on a dynamic earth. Edited by M.R., Handy, G., Hirth, N., Hovius, MIT Press, Cambridge, Mass., 47-78.
- Desilets, D., Zreda, M., Almasi, P.F., Elmore, D., 2006. Determination of cosmogenic Cl-36 in rocks by isotope dilution: Innovations, validation and error propagation, Chemical Geology 233, no. 3-4, 185-195.
- Dewey, J.F., Şengör, A.M.C., 1979. Aegean and surrounding region: complex multiplate and continuum tectonics in a convergent zone. Geological Society of America Bulletin 90, 84–92.
- Elmore, D., Ma, X., Miller, T., Mueller, K., Perry, M., Rickey, F., Sharma, P., Simms, P., Lipschutz, M., Vogt, S., 1997. Status and plans for the PRIME Lab AMS facility: Nuclear Instruments and Methods in Physics Research Section B-Beam Interactions with Materials and Atoms, 123(1-4), 69-72.
- Emre, Ö., Duman, T.Y., Özalp, S., Elması, H., Olgun, Ş., Şaroğlu, F., 2013. Active fault map of Turkey (scale 1:250,000), General Direct. Mineral Res. Explor., Special Publication Series - 30.
- Emre, Ö., Duman, T.Y., Özalp, S., Şaroğlu, F., Olgun, Ş., Elması, H., Tolga, Ç., 2016. Active fault database of Turkey, Bull. Earthquake Eng., DOI 10.1007/s10518-016-0041-2
- Evans, J. M., Stone, J. O. H., Fifield, L. K., Cresswell, R. G., 1997. Cosmogenic chlorine-36 production in K-feldspar: Nuclear Instruments and Methods in Physics Research Section B-Beam Interactions with Materials and Atoms, 123(1-4), 334-340.
- Fink, D., Vogt, S., Hotchkis, M., 2000. Cross-sections for Cl-36 from Ti at E-p=35-150 MeV: Applications to in-situ exposure dating: Nuclear Instruments and Methods in Physics Research Section B-Beam interactions with materials and atoms, 172, 861-866.
- Gürer, Ö.F., Sarica-Filoreau, N., Özburan, M., Sangu, E., Doğan, B., 2009. Progressive development of the Büyük Menderes Graben based on new data, western Turkey, Geological Magazine 146, Issue 5, 652-673.
- Hancock, P.L., Barka, A.A., 1987. Kinematic indicators on active faults in western Turkey, Journal of Structural Geology 9, No. 5/6, 573-584.
- Ivy-Ochs, S., Poschinger, A. V., Synal, H. A., Maisch, M., 2009. Surface exposure dating of the Flims landslide, Graubunden, Switzerland, Geomorphology, 103(1), 104-112.
- Ivy-Ochs, S., Synal, H. A., Roth, C., Schaller, M., 2004. Initial results from isotope dilution for Cl and Cl-36 measurements at the PSI/ETH Zurich AMS facility: Nuclear Instruments and Methods in Physics Research Section B-Beam Interactions with Materials and Atoms, 223-24, 623-627.

- Liu, B.L., Phillips, F.M., Fabrykamartin, J.T., Fowler, M.M., Stone, W.D., 1994. Cosmogenic ^{36}Cl accumulation in unstable landforms, 1. Effects of the thermal neutron distribution: Water Resources Research, 30(11), 3115-3125.
- McCalpin, J.P., ed, 2009, Paleoseismology, London, Academic, 629 p.
- Mitchell, S.G., Matmon, A., Bierman, P.R., Enzel, Y., Caffee, M., Rizzo, D., 2001. Displacement history of a limtesone normal fault scarp, northern Israel, from cosmogenic ^{36}Cl, J. geophys. Res., 106(B3), 4247- 4264.
- Mozafari, N., Sümer, Ö., Tikhomirov, D., Ivy-Ochs, S., Alfimov, V., Vockenhuber, Ch., İnci, U., Sözbilir, H., Akçar, N., *submitted*. Holocene seismic activity of the Priene-Sazlı Fault revealed by cosmogenic ^{36}Cl, western Anatolia, Turkey.
- Mouslopoulou, V., Moraetis, D., Benedetti, L., Guillou, V., Bellier, O., Hristopulos, D., 2014. Normal faulting in the forearc of the Hellenic subduction margin: Paleoearthquake history and kinematics of the Spili Fault, Crete, Greece. - Journal of Structural Geology 66, 298-308.
- Palumbo, L., Benedetti, L., Bourles, D., Cinque, A., Finkel, R., 2004. Slip history of the Magnola fault (Apennines, Central Italy) from ^{36}Cl surface exposure dating: evidence for strong earthquake over the Holocene, Earth planet. Sci. Lett., 225, 163–176.
- Passchier, C.W., Wiplinger, G., Güngör, T., Sürmelihindi, G., 2013. Normal fault displacement dislocating a Roman aqueduct of Ephesos, western Turkey, Terra Nova, Vol 25, No. 4, 292-297.
- Pavlides, S., Caputo, R., 2004. Magnitude versus faults' surface parameters: Quantitative relationships from the Aegean Region. Tectonophysics, 380, 159-188.
- Phillips, F.M., Stone, W.D., Fabryka-Martin, J.T., 2001. An improved approach to calculating low-energy cosmic-ray neutron fluxes near the land/atmosphere interface: Chemical Geology, 175 (3-4), 689-701.
- Phillips, F.M., Zreda, M.G., Flinsch, M. R., Elmore, D., Sharma, P., 1996. A reevaluation of cosmogenic Cl-36 production rates in terrestrial rocks: Geophysical Research Letters, 23(9), 949-952.
- Schimmelpfennig, I., Benedetti, L., Finkel, R., Pik, R., Blard, P.H., Bourles, D., Burnard, P., Williams, A., 2009. Sources of in-situ Cl-36 in basaltic rocks. Implications for calibration of production rates, Quaternary Geochronology, 4(6), 441-461.
- Schlagenhauf, A., Gaudemer, Y., Benedetti, L., Manighetti,I., Palumbo, L., Schimmelpfennig, I., Finkel, R., Pou, K., 2010. Using in situ chlorine-36 cosmonuclide to recover past earthquake histories on limestone normal fault scarps: A reappraisal of methodology and interpretations, Geophysical Journal International, v. 182, no. 1, p. 36-72.
- Schlagenhauf, A., Manighetti, I., Benedetti, L., Gaudemer, Y., Finkel, R., Malavieille, J., Pou, K., 2011. Earthquake supercycles in Central Italy, inferred from ^{36}Cl exposure dating. Earth and Planetary Science Letters, 307(3-4), 487–500.
- Scholz Ch. H., 2002. The Mechanics of Earthquakes and Faulting. Second Edition, Cambridge University Press, 464 p.
- Şengör, A.M.C., Görür, N., Şarğlu, F., 1985. Strike-slip faulting and related basin formation in zones of tectonic escape: Turkey as a case study. *In* Biddle, K., Christie-Blick, N. (Eds.), Strike-Slip Deformation, Basin Formation and Sedimentation. Society of Economic Paleontologists and Mineralogists, Special Publications 37, 227-264.
- Soysal, H., Sipahioğlu, S., Kolçak, D., Altınok, Y., 1981. Historical earthquake catalogue of Turkey and surrounding area (2100 B.C.-1900 A.D.). Technical Report, TUBİTAK, No: TBAG-341.
- Stone, J.O., 2000. Air pressure and cosmogenic isotope production. Journal of Geophysical Research 105 (B10), 23753-23759.
- Stone, J.O., 2005. Terrestrial chlorine-36 production from spallation of iron. In: 10th International Conference on Accelerator Mass Spectrometry. Berkeley, California.
- Stone, J.O., Allan, G.L., Fifield, L.K., Cresswell, R.G., 1996. Cosmogenic chlorine-36 from calcium spallation, Geochimica Cosmochimica Acta 60, 679-692.
- Stone, J.O., Evans, J.M., Fifield, L.K., Allan, G.L., Cresswell, R.G., 1998. Cosmogenic chlorine-36 production in calcite by muons, Geochimica et Cosmochimica Acta, 62(3), 433-454.
- Sümer, Ö, İnci, U., Sözbilir, H., 2012a. Büyük Menderes Grabeni kuzey sınırını oluşturan aktif Menderes Fayı'nın batı ucundaki faylanma şekli ve mekanizması [The shape and

mechanism of the faulting at the western end of the active Menderes Fault, which forms the northern boundary of Büyük Menderes Graben], ATAG 16 abstract book, 44-45.

- Sümer, Ö., Inci, U., Sözbilir, H., 2012b. Tectono-sedimentary evolution of an Early Pleistocene shallow marine fan-deltaic succession at the western coast of Turkey. Geodinamica Acta 25, Nos. 3-4, 112-131.
- Sümer Ö, İnci U., Sözbilir, H., 2013. Tectonic evolution of the Söke Basin: Extension-dominated transtensional basin formation in western part of the Büyük Menderes Graben, Western Anatolia, Turkey. Journal of Geodynamics 65, 148-175.
- Synal, H.A., Bonani, G., Dobeli, M., Ender, R.M., Gartenmann, P., Kubik, P.W., Schnabel, C., Suter, M., 1997. Status report of the PSI/ETH AMS facility: Nuclear Instruments and Methods in Physics Research Section B-Beam Interactions with Materials and Atoms, 123(1-4), 62-68.
- Tikhomirov, D., 2014. PhD thesis, University of Bern, An advanced model for fault scarp dating and paleoearthquake reconstruction, with a case study of the Gediz Graben formation (Turkey).
- Tikhomirov, D., Akçar, N., Ivy-Ochs, S., Alfimov, V., Schlüchter, C., 2014. Calculation of shielding factors for production of cosmogenic nuclides in fault scarpes. Quaternary Geochronology, 19, 181-193.
- Wells, D.L., Coppersmith, J.K., 1994. New empirical relationships among magnitude, rupture length, rupture width, rupture area, and surface displacement. Bulletin of the Seismological Society of America 84, 974-1002.
- Zreda, M.G., Phillips, F.M., Elmore, D., Kubik, P.W., Sharma, P., Dorn, R.I., 1991. Cosmogenic chlorine-36 production rates in terrestrial rocks. Earth and Planetary Science Letters 105, 94-109.
- Zreda, M., Noller, J., 1998. Ages of prehistoric earthquakes revealed by cosmogenic chlorine-36 in a bedrock fault scarp at Hebgen Lake. Science, 282, 1097-1099.

Chapter 4

Seismic activity in western Anatolia during the last 15 ka

Nasim Mozafari Amiri[1], Çağlar Özkaymak[2], Ökmen Sümer[3], Dmitry Tikhomirov[1], Bora Uzel[3], Serdar Yesilyurt[1], Susan Ivy-Ochs[4], Christof Vockenhuber[4], Hasan Sözbilir[3] and Naki Akçar[1]

[1]Institute of Geological Sciences, University of Bern, 3012 Bern, Switzerland
[2]Department of Geological Engineering, Afyon Kocatepe University, 03200 Afyonkarahisar, Turkey
[3]Dokuz Eylül University, Geological Engineering Department, 35160 İzmir, Turkey
[4]Institute for Particle Physics, ETH Hönggerberg, 8093 Zürich, Switzerland

In preparation

Seismic activity in western Anatolia during the last 15 ka

Abstract

Understanding of paleoseismic behaviors of faults and in a broader extent, recurrence interval of earthquakes in regional scales are important keys in order to improve our knowledge of future seismic activities and minimize risk of probable damages. Western Anatolia is one of the active regions of the world, whose major faults' seismic histories are unknown or poorly understood. There, the extensional tectonic regime caused formation of large-scale horst-graben systems characterized by normal faults, locally built in carbonates, which caused huge amount of uplifts. We explored the seismic history of western Anatolia based on fault scarp dating using cosmogenic ^{36}Cl. To fulfil this, we collected 584 samples from seven well-preserved fault surfaces within the Büyük Menderes Graben, Gediz Graben and Gökova half-graben. We could reconstruct at least 12 major seismic events, mainly occurred as a series of earthquakes of 5.4 to 7.1 in magnitude through the past 15 ka and beyond the existing earthquake archives. According to our results, the oldest earthquake approximated to be occurred at ca. 15 ka. The age correlation of the reconstructed palesoseismic events shows a minimum of four periods of high seismic activity western Anatolia at ca. 2.0, 3.5, 6.0 and 8.0 ka indicating a regional return period of earthquakes of about 2000 years. Regarding this time interval, the recent century, with records of abundant major earthquakes is also considered as a period of high seismic active and the next one would occur in 2000 years. This time interval is compatible with the time interval of earthquakes of several normal faults within the extensional setting of Aegean region and Italy. The acceleration of vertical slip rates, in general, from 0.1 to 1.9 mm/yr through time indicates that western Anatolia is now experiencing its most seismically active period during Holocene time.

Key words: Fault scarp, Dating, Eastern Mediterranean, Neotectonic, Recurrence interval

1. Introduction

The collision of African and Eurasian plates is responsible for the complex deformation pattern of Mediterranean region within the Alpine-Himalayan belt (e. g. Dewey and Şengör, 1979). The 300 km wide Western Anatolia Extensional Province, one of the most rapid extending and seismically active regions in the world, is part of this tectonic mega structure (Dewey and Şengör, 1979; Şengör et al., 1985), which formed in response to approximately N-S extensional tectonic regime since early Miocene. There, the horst-graben systems, namely Gediz, Küçük Menderes and Büyük Menderes grabens and Gökova half-graben are the main structures, whose activities are evidenced by normal faulting, which occasionally are built in carbonates (Fig. 1). Four models have been proposed to explain the origin and age of the present-day extension and the presence of large-scale normal faults in the western Anatolia. According to the most widely accepted “tectonic escape model”, the Anatolian plate is moving rapidly westward towards the Black Sea plate and southwestward relative to the African plate with a rate of about 28-40 mm/yr (Dewey and Şengör, 1979; Taymaz et al., 1991; Jackson and McKenzie, 1988; Le Pichon et al., 1995). This movement results in differential uplift and subsidence in response to the movement of dextral North Anatolian Fault Zone and sinistral East Anatolian Fault Zone (Dewey and Şengör, 1979; Şengör et al., 1985; Barka et al., 1994; Görür et al, 1995). In this model, the rate of extension is still under debate and speeds as low as 6 mm/yr to 8-9 mm/yr have been suggested (Oner and Dilek; 2011 and references therein). According to Eyidoğan (1988), the rate of extension increases from north to south, which its maxima occurs in southwestern part of western Anatolia with a rate of 13.5 mm/yr. The second model proposed to explain the development of the horst-graben systems is “the back-arc spreading model”, which assumes a back-arc extension as a consequence of the south-southwest migration of Helenic trench (McKenzie, 1978; Le Pichon and Angelier, 1979, 1981; Meulenkamp et al., 1988; Kissel and Laj, 1988). The third one, “the Orogenic collapse model” suggests that the extensional regime is commenced by the spreading of a thickened crust related to an earlier Paleogene compressional regime in the late Oligocene-early Miocene (Seytoğlu and Scott, 1991, 1992, 1996; Seytoğlu et al, 1992). The forth model is “the two stage graben model” which

suggests that two phases of individual extensional regimes separated by a short-term compressional tectonic activity (Koçyiğit et al., 1999).

In western Anatolia, rapid tectonic activity initiated by the extensional regime must have been caused the occurrence of destructive earthquakes. In addition to

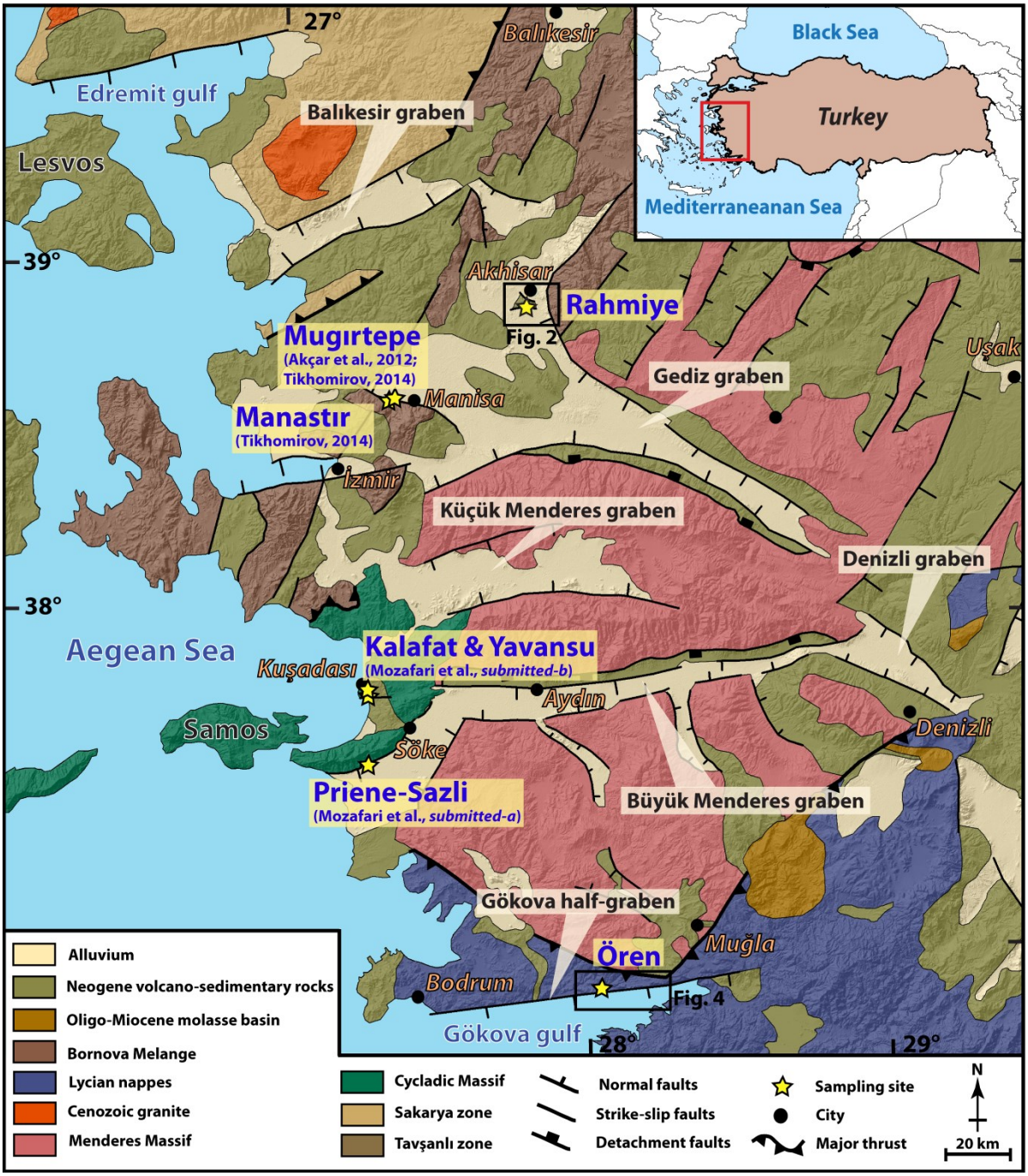

Fig. 1. Simplified geological map of western Anatolia (modified after Akçar et al., 2012; Sümer et al., 2013; Hancock and Barka, 1987). The yellow stars show the locations of the sampling sites of this study in Priene-Sazlı, Yavansu and Kalafat faults within Büyük Menderes Graben, Ören Fault in Gökova half-graben, Rahmiye Fault, Mugırtepe Fault (Akçar et al., 2012) and Manastır Fault (Tikhomirov, 2014) within Gediz Graben. The black boxes give locations of Figs. 2 and 4.

the historical and instrumental records, the occurrence of past ruptures is evidenced in several archaeological sites by heavy damages (e.g., Altunel, 1998; Yönlü et al., 2010). Several trenches have been excavated in order to date the past ruptures and associated amount of slips in western Anatolia (e.g., Özkaymak et al., 2011; Altunel et al., 2009). However, fault scarp dating is the most direct and precise method to reconstruct past earthquakes. The oldest known historical earthquake in the Eastern Mediterranean and Middle East dates back to 2100 B.C. (Shebalin et al., 1974; Soysal et al., 1981; Ambraseys, 2009) and the instrumental earthquakes have been recorded only since 1900. However, for a long-term seismic modeling, more data beyond and within the limits of available archive is required. High seismic activity of western Anatolia together with the presence of well-preserved normal faults, locally built in carbonates, give rise to make this region as an ideal target to use cosmogenic ^{36}Cl exposure dating in order to explore its paleoseismic history.

During the last decade, we focused on well-preserved normal fault scarps in western Anatolia in order to track the pace of destructive earthquakes, beyond the existing historical and instrumental data. The aims of our study were: (1) reconstruction of paleoseismic events in order to determine recurrence interval of destructive earthquakes; (2) quantify the vertical component of slips and plausibility of the magnitude of modeled ruptures; and (3) calculate short-term and long-term slip rates. These are essential data for earthquake hazard analysis in seismic-prone areas in order to reduce probable damages (e.g. Cluff and Cluff, 1984). To do this, we sampled Ören and Rahmiye faults in Gediz Graben and Gökova half-graben, respectively. A Matlab® code (Tikhomirov, 2014) was used to model the significant paleoseismic events and their timing. We provided a comprehensive story in a regional tectonic context based on analyzing of 584 samples from about 52 m long profiles, in total, including the published data of Manastır and Mugırtepe faults in Gediz Graben (Akçar et al., 2012; Tikhomirov, 2014), as well as Kalafat, Yavansu and Priene-Sazlı fault scarps in Büyük Menderes Graben (Mozafari et al., *submitted-a; submitted -b*). Our analysis yielded seismically active periods around 2.0, 3.5, 6.0 and 8.0 ka in western Anatolia, and with the occurrence of the oldest seismic activity at ca. 15 ka.

2. Fault scarp dating

For the first time, Zreda and Noller (1998) introduced fault scarp dating with cosmogenic ^{36}Cl plausibility by modeling of six seismic activity ages in the Hebgen Lake fault scarp, Montana, USA. Over the last twenty years, the seismic activity of limestone fault scarps using cosmogenic ^{36}Cl have been reconstructed in various locations in the Eastern Mediterranean and the Middle East (Mitchell et al., 2001; Benedetti et al., 2002; 2003; 2013; Palumbo et al., 2004; Schlagenhauf et al., 2010; 2011; Akçar et al., 2012; Tikhomirov, 2014; Mouslopoulou, 2014; Cowie et al., 2017). In this study, we used a Matlab® code of Fault Scarp Dating Tool -FSDT- developed by Tikhomirov (2014) to reconstruct the paleoearthquakes history in western Anatolia. The method has taken into account all parameters that could introduce the production of ^{36}Cl depending on an assumed seismic scenario regarding number of ruptures, age of ruptures, vertical component of slips related to each rupture, hanging-wall position prior to the ruptures, beginning of exposure of the fault, and erosion rate of fault surface. ^{36}Cl concentration of samples is shown versus the position along the fault scarp as a profile, in which discontinuities indicate periods of high seismic activity and the convex curves reveal phases of inactivity (for further information see Mozafari et al., *submitted-a*). The vertical distance between two succeeding discontinuities shows the related slip of the seismic event. The method enables to reconstruct seismic events with 2σ uncertainties about 25 % for the timing of ruptures and 15 % for the vertical component of slips (Tikhomirov, 2014).

3. Study sites and sampling

In this study, well-preserved fault surfaces were chosen in Gediz Graben, Büyük Menderes Graben and Gökova half-graben (Fig. 1), based on the guidelines proposed by Tikhomirov (2014) after Mitchell et al. (2001). In order to extract at least one seismically active period using FSDT (Tikhomirov2014), a minimum of two meters of sampling along the fault scarp from the ground level is necessary. An ideal sampling profile is a continuous strip parallel to the vertical component of slip. A sequence of profiles shifted horizontally is an alternative (e.g., Benedetti et al., 2002; Sclaugenhauf et al., 2011; Akçar et al., 2012), where the fault surface is

locally weathered (Tikhomirov, 2014). In total, 584 samples from seven well-preserved fault surfaces were collected in order to analysis cosmogenic ^{36}Cl.

3.1. Gediz Graben

About 150 km long WNW-ESE-trending Gediz Graben is one of the most prominent structural elements in the western Anatolia. Menderes Massif constitutes the bedrock of this structure as its horst blocks with the elevation of maximum 2000 m (Çiftçi and Bozkurt, 2009). The graben basement is also made up of the same rock, which is covered by sediments of varying ages from Miocene to Quaternary (Çiftçi and Bozkurt, 2009 and references therein). The fault scarps of Manastır and Mugırtepe in the western part of the graben were already sampled and analyzed (Akçar et al., 2012; Tikhomirov, 2014) for fault scarp dating. In addition to these, we collected samples from the Rahmiye Fault in the north part of the graben.

3.1.1. Manastır Fault

Approximately 4.5 km long and up to 140 m high Manastır Fault is a normal fault, which constitutes the southern boundary of ca. 35 km long Manisa Fault Zone. The fault contains evidence of recent activity based on landslides, sequences of screes and triangular facets (Özkaymak et al., 2011). The foot wall of the fault constitutes Mesozoic limestone against the Holocene sediments as its hanging wall. Several major paleoearthquakes were recorded in this area. Earthquake of 17 AD caused severe damages in many ancient cities within the Manisa basin, particularly, with evidence of surface rupture in Magnesia (ancient Manisa) (Guidoboni et al. 1994; Ambraseys, 1988). In addition, another earthquake with an intensity of VIII struck Magnesia and Ephesus ancient cities at 44 AD (Ergin et al. 1967; Soysal et al. 1981). There are also earthquakes reported at 926 AD, 1595 or 1664 AD and 1845 AD (e.g., Ambraseys and Jackson 1998; Ergin et al. 1967; Soysal et al. 1981). Samples of 87 were collected from a total 7 m multiple sampling strips along ca. 12 m long Manastır Fault (Akçar et al., 2012).

3.1.2. Mugırtepe Fault

About 3 km long NW-SE-trending Mugırtepe Fault is also a normal fault located in the Manisa Fault zone. The Mugırtepe Fault is the succeeding fault scarp of the Manastır Fault, located ca. 1 km towards the north. This fault is a maximum 4 meters high (Akçar et al., 2012), with the same bedrock lithology as the Manastır Fault (Özkaymak et al., 2011). The records of historical earthquakes are the same as the Manastır Fault. Two trenches were excavated perpendicular to the Mugırtepe Fault scarp in order to reconstruct the ages of paleoearthquakes (Özkaymak et al., 2011). The results showed the occurrence of earthquakes compatible with the records of historical archives at 926 AD, 1595 or 1664 AD, and 1845 AD. Slabs of 44 were collected from a total ca. 2.7 m long profile along the fault surface (Akçar et al., 2012).

3.1.3. Rahmiye Fault

E-W-trending Rahmiye Fault is at least 7 km long dextral normal fault situated in the vicinity of a village of the same name within the Gediz Graben (Fig. 2). The fault is projected to be the continuation of NNW-SSE trending Akselendi Fault (Fig.

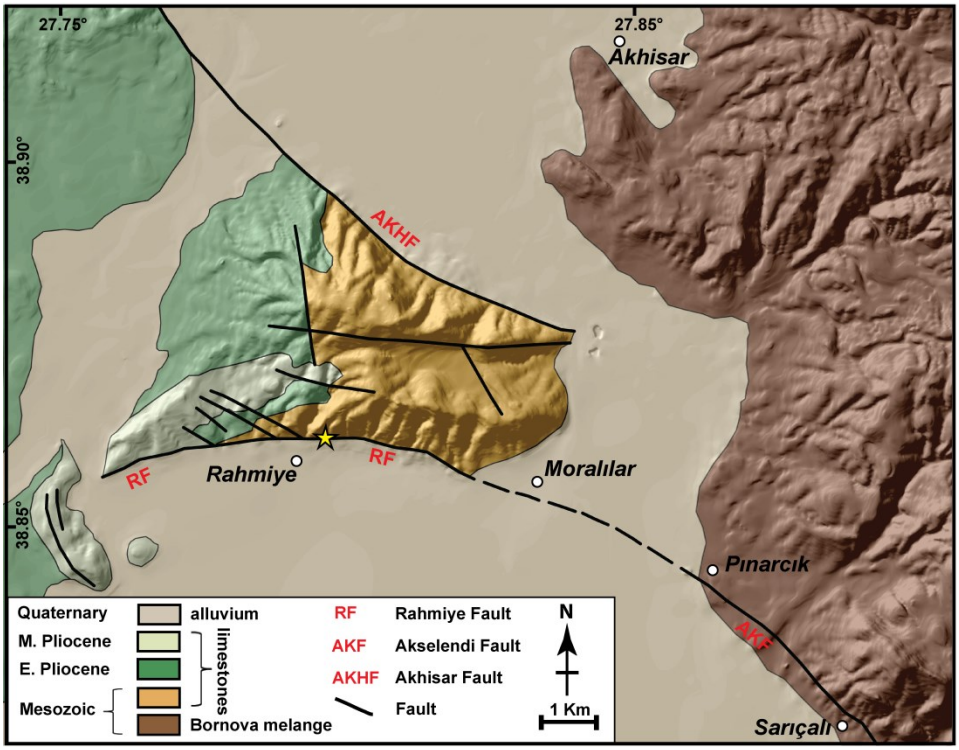

Fig. 2. Geological map of Gediz Graben around Rahmiye Fault scarp. The yellow star marks the sampling site.

2). The fault surface is highly well-preserved almost along its entire length, characterized by clear triangular facets. Foot wall of the fault in the sampling site is made up of limestone of late Jurassic versus the Quaternary sediments as the hanging wall. The largest known earthquake in surrounding area was recorded in September 9, 2016 with magnitude of 5 in about 3 km NW of Rahmiye Fault (B.Ü. KOREI). From ca. 6.5 m height of the scarp, 87 samples were collected (Fig. 3).

Fig. 3. The sampled surface of the Rahmiye Fault scarp.

3.2. Büyük Menderes Graben

Approximately 140 km long Büyük Menderes Graben starts from Denizli Basin in the east with E-W strike and extends with a trend change to NE-SW towards the Aegean Sea (Fig. 1). The graben is bounded by Menderes Massif to the north and south, while the basin is mainly covered by Quaternary sediments. A large number of faults of varying scales constitute the structure of the horst-graben system, of which six major segments extended along the north edge of the entire structure named Büyük Menderes Fault Zone. We have collected samples from the Kalafat, Yavansu and Priene-Sazlı faults to model their seismic history using fault scarp dating (Fig. 1).

3.2.1. Kalafat Fault

The 15 km long Kalafat Fault (Çakmakoğlu, 2006) is, in general, a WNW-trending normal fault with a minor component of right-lateral movement in the

northern side of a mountain of the same name, SE of Kuşadası City (Figs. 1). The fault juxtaposes the foot wall of Cycladic Massif against the hanging wall of Miocene volcano-sedimentary rocks overlaid by colluvium in front. There is no seismic record attributed to Kalafat Fault. Totally, 54 samples were taken out from ca. 4.6 m of the fault surface along two parallel strips.

3.2.2. Yavansu Fault

The Yavansu Fault is generally an E-W trending normal fault with a minor component of dextral movement, located in the southern slope of the Kalafat Mountain. Cycladic Massif constitutes its foot wall, against the Quaternary sediments in the hanging-wall. The fault is considered to be in the range between 2.5 to 50 km long (Hancock and Barka, 1987; Sümer et al., 2013). There are records of several earthquakes in Kuşadası in the time window of 1751-1893 AD (e.g., Soysal et al., 1981). The majority of the seismic events reported in the western extension of Yavansu Fault north of Samos Island, but none is directly assigned to the activity of Yavansu Fault. In total, 68 samples were collected from ca. 6.6 m along two sampling profiles.

3.2.3. Priene-Sazlı Fault

The Priene-Sazlı Fault is extended along the margin of the westernmost heights of the Büyük Menderes Graben (Figs. 1). Length of the fault estimated to be between the ranges of 30 to 40 km (Altunel et al., 2009; Sümer et al., 2013; Şaroğlu et al., 1992; Duman et al., 2011; Emre et al., 2013). Generally the Cycladic Massif constitutes the foot wall, whereas the hanging wall is made up of Quaternary sediments of the graben basin. The youngest mechanism of the fault is normal with a minor component of right-lateral movement. There are two major earthquakes recorded related to the Priene-Sazlı Fault. The historical earthquake occurred in 68 AD with an intensity of VII at the NE termination of the fault (Ergin et al., 1967). The instrumental earthquake of Söke-Balat on July 16, 1955 hit this region and caused heavy damages with magnitude of 6.8 (Öcal, 1958; Şengör 1987). In total, 117 samples were collected from ca. 12 m high fault scarp along four horizontally shifted profiles.

3.3. Gökova half-graben (Ören Fault)

The ENE-WSW-striking Gökova half-graben borders the Gulf of Gökova in the north with a height of more than 1000m, in the southeast part of Aegean Sea. The main part of the graben is offshore about 150 km long, which forms the Gulf of Gökova (Gürer and Yılmaz, 2002). The horst structure is characterized by E-W

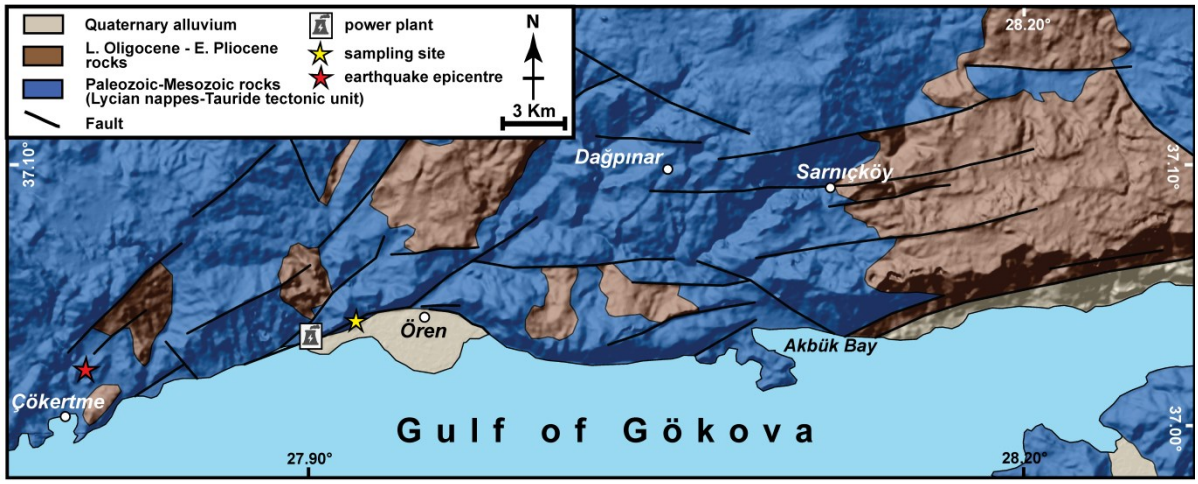

Fig. 4. Simplified geological map of Ören Fault around the sampling site (modified after Gürer and Yılmaz, 2002).

Fig. 5. Field view of the Ören Fault scarp with the sampling strip at the base of successive escarpment. The yellow arrows indicate base of the upper and older successive scarp levels.

trending listric normal faults, which intersect and displace the ENE-WSW trending oblique faults (Gürer and Yılmaz, 2002). Basically, Lycian Nappes constitutes the basement of this region. The Ören Fault extended along the half-graben was sampled in order to explore its seismic activity using fault scarp dating.

The approximately 100 km long E-W-trending Ören Fault is the main structure of the Gökova half-graben, which is strongly segmented along its strike (Figs. 1 and 4). In our sampling site, Lycian nappes and Tauride tectonic unit constitute the bedrock of the scarp against the low Quaternary alluvial (Fig. 4). On July 20, 2017 an earthquake with magnitude of 6.7 occurred in the west part of the Gökova half-graben, south of Bodrum City (Fig. 1). The closest earthquake to our sampling site hit the area on January 10, 2005 with magnitude of 5.5 with its epicenter about 15 km westward (USGS) (Fig. 4). The importance of study of the fault lies also in the installation of Kemerköy thermal power plant along the fault. We sampled 127 slabs from ca. 12 m high fault surface about 2 km apart from the power plant (Figs. 4 and 5). This number of samples is the maximum collected samples for fault scarp dating along a single fault probably worldwide.

4. Results

The results of fault scarp modeling using cosmogenic ^{36}Cl exposure dating for the Mugırtepe, Manastır, Kalafat, Yavansu and Priene-Sazlı faults have been discussed in detail in a series of previous research (Akçar et al., 2012; Tikhomirov, 2014; Mozafari et al., *submitted-a; submitted-b*). From seven sampling sites, cosmogenic ^{36}Cl measurements samples of Ören and Rahmiye faults are still due. The best fit results yielded in terms of number of seismic events, their ages, vertical component of slips and slip rates of the analyzed faults are summarized in Table 1. It should be noted that the number of reconstructed earthquakes are considered to be minimum, because the code is unable to extract the small earthquakes, but the ones that caused rupture and basically within 25% uncertainties for the age. In addition, the reconstructed amount of slips is the upper bound, since differentiation of slips within 15% of uncertainties is not always possible (Tikhomirov, 2014). Furthermore, potential magnitude of future earthquakes and probable magnitude of earthquakes in charge of modeled slips are provided (Table 1). We reconstructed at

least 12 major seismic events by analyzing cosmogenic ^{36}Cl over the last 15 ka in the western Anatolia. Each modeled seismic event represents a series of earthquakes clustered in a short time interval rather than a unique rupture (for further information see Mozafari et al., *submitted-a; submitted-b*).

Table. 1. Results for the data set of the examined fault scarps in western Anatolia

Fault	Number of events	Beginning of exposure (ka)	Age (ka)	Slip (m)	Slip rate (mm/yr)	Potential M of EQ	M of EQ based on modeled slip
Mugırtepe	1	27	6.0 ± 1.5	2.5 ± 0.4	> 0.1	5.5 - 5.9	6.9
Manastır	1	9	2.1 ± 0.8	7.0 ± 1.1	> 0.1	5.7 - 6.0	7.2
Kalafat	3	22	15.3 ± 3.8 8.4 ± 2.1 3.6 ± 0.9	0.7 ± 0.1 0.9 ± 0.1 3.1 ± 0.5	> 0.1 0.1 1.5	6.4 - 6.5	6.5 - 7.0
Yavansu	3	12	7.9 ± 2.0 3.4 ± 0.8 2.0 ± 0.5	0.6 ± 0.1 3.5 ± 0.5 2.6 ± 0.4	> 0.1 0.8 1.9	5.4 - 7.1	6.5 - 7.0
Priene-Sazlı	4	21	8.1 ± 2.0 6.0 ± 1.5 3.7 ± 0.9 2.2 ± 0.5	3.4 ± 0.5 1.5 ± 0.2 1.4 ± 0.2 1.5 ± 0.2	> 0.3 0.7 0.6 1.0	6.9	6.7 - 7.0

In Gediz Graben, the best fit result of the **Mugırtepe Fault** remarks that the fault broke at 6 ± 1.5 ka with a vertical slip amount of 2.5 ± 0.4 m (Tikhomirov, 2014). The vertical slip rate is calculated to be > 0.1 mm/yr. After this activity the fault was deactivated and a seismic event caused the exposure of 7.0 ± 1.1 m along the **Manastır Fault** at ca. 2.1 ± 0.8 ka (Tikhomirov, 2014). The yielded vertical slip rate for this seismic activity is estimated to be similar to that of Mugırtepe Fault. Most probably two historical earthquakes of 17 and 44 AD struck the Manisa region, caused displacement of the Manastır Fault scarp (Tikhomirov, 2014). In Büyük Menderes Graben, cosmogenic ^{36}Cl analysis of the **Kalafat Fault** indicates three earthquake events at ca. 15.3 ± 3.8 ka, 8.4 ± 2.1 ka, and 3.6 ± 0.9 ka with vertical

component of respective slips of 0.7 ± 0.1 m, 0.9 ± 0.1 m, and 3.1 ± 0.5 m (Mozafari et al., *submitted-b*). The average slip rates from the oldest to youngest modeled event were approximated to be > 0.1, 0.1, and 1.5 mm/yr, while the long-term slip rate is 0.6 mm/yr. The scenario of three seismic events, as the best fit for the **Yavansu Fault** remarks the ages of the seismic events are 7.9 ± 2.0 ka, 3.4 ± 0.8 ka, and 2.0 ± 0.5 ka with vertical component of associated slips of 0.6 ± 0.1 m, 3.5 ± 0.5 m, and 2.6 ± 0.4 m, respectively (Mozafari et al., *submitted-b*). The average values of vertical slip rates were estimated to be > 0.1, 0.8, and 1.9 mm/yr for the seismic events from the oldest to the youngest. The long-term slip rate is ca. 1 mm/yr. Our best fit result shows the **Priene-Sazlı Fault** experienced four major events at 8.1 ± 2.0 ka, 6.0 ± 1.5 ka, 3.7 ± 0.9 ka, and 2.2 ± 0.5 ka with the vertical components of related slip of 3.4 ± 0.5 m, 1.5 ± 0.2 m, 1.4 ± 0.2 m, and 1.5 ± 0.2 m, respectively (Mozafari et al., *submitted-a*). The modeled earthquake of ca. 2 ka is compatible with the historical earthquake of 68 AD. Mean values of slip rates of > 0.3, 0.7, 0.6, and 1.0 mm/yr are yielded from the oldest to the youngest reconstructed earthquakes. The long-term vertical slip rate of the fault is estimated to be 0.7 mm/yr.

5. Seismic activity in western Anatolia during the last 15 ka

The modeling of exhumation history of faults is a key step in evaluating seismic risks in order to minimize the potential damages of future earthquakes, particularly, in high populated regions for instance western Anatolia. All the investigated faults are considered as seismogenic faults (McCalpin, 2009) due to having capacity of producing earthquakes of larger than 5 in magnitudes, which emphasize the necessity of precise earthquake geochronology studies. In this study the paleoseismic behavior of Rahmiye Fault as well as Manastır and Mugırtepe faults in Gediz Graben (Akçar et al., 2012; Tikhomirov; 2014), Kalafat, Yavansu and Priene-Sazlı faults in Büyük Menderes Graben (Mozafari et al., *submitted-a; submitted-b*) and Ören Fault in Gökova half-graben were explored using cosmogenic ^{36}Cl during the last 15 ka in western Anatolia.

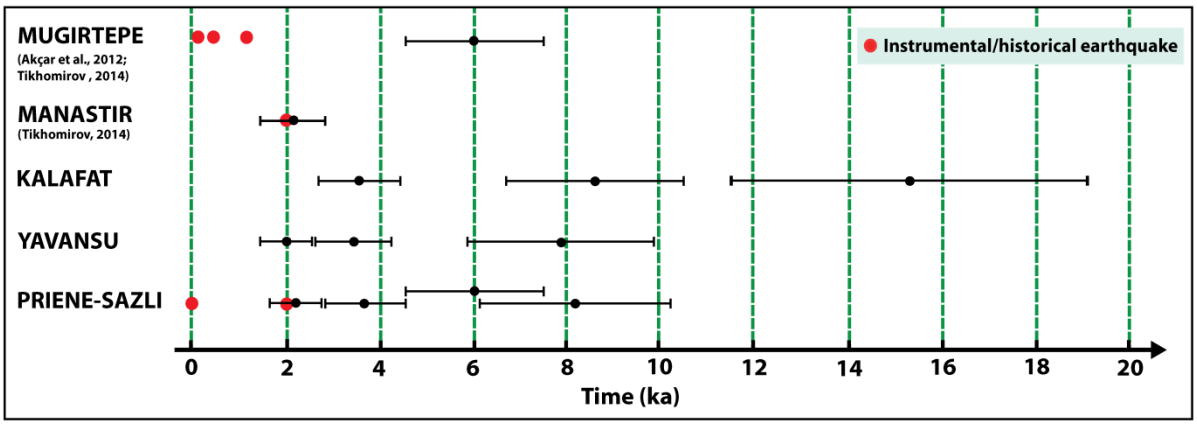

Fig. 6. Comparison of ages of modeled earthquakes using fault scarp dating in regional scale of western Anatolia; Black circles and lines show the age of modeled earthquakes with 25 % uncertainties. Red circles indicate timing of available historical and instrumental earthquakes.

With our modeling, we identified the oldest seismic activity period in western Anatolia related to Kalafat Fault in the Büyük Menderes Graben at ca. 15.3 ka (Fig. 6) with a vertical component of slip of minimum 0.7 m. In order to estimate potential magnitude of earthquakes and corresponding slip amounts and also to evaluate probable magnitude of past ruptures empirical relationships of Pavlides and Caputo (2004) and Wells and Coppersmith (1994) have been used (for detailed calculations see Mozafari et al., *submitted-a; submitted-b*). Slip amount of minimum 0.7 m of Kalafat Fault indicates an earthquake of 6.5 - 6.6 in magnitude. The Kalafat Fault, based on its 15 km length is capable of producing an earthquake with magnitude of 6.4 - 6.5 and accordingly slips of 0.5 - 0.6 m, at once. Therefore, the modeled slip is most likely made by two earthquakes occurred close in time. Kalafat Fault broke once again at ca. 8.4 ka (Fig. 6) with vertical component of slip of ca. 0.9 m. This amount of slip is expected to be produced by an earthquake with magnitude 6.6 - 6.8, which is larger than normal average expected earthquake and slip for this size fault. This event is also interpreted as a cluster of two earthquakes struck in a short time. Priene-Sazlı experienced a seismic event at ca. 8.1 ka (Fig. 6) with a minimum 3.4 m of vertical slip. The average 35 km long fault has potential of triggering an earthquake with magnitude of 6.8 - 7.0 and a consequence slip of 1.1 - 2.1 m. Therefore, the modeled slip was most likely produced by a couple of earthquakes clustered in close time. Yavansu Fault at ca. 7.9 ka ruptured (Fig. 6) with a vertical slip of minimum 0.6 m. About 50 km length of the fault, gives rise to produce an earthquake with magnitude of ca. 7.0 and slip of 1.7 - 2.6 m. The yielded event with 0.6 m of slip defines an earthquake with magnitude of 6.5, which exposed the fault

at once. The Priene-Sazlı Fault ruptured for the second time at ca. 6 ka (Fig. 6) with vertical slip of ca. 1.5 m, which possibly occurred as a single earthquake of 6.7 - 6.8 in magnitude. Further north in Gediz Graben, the Mugırtepe Fault broke at ca. 6 ka (Fig. 6) with vertical slip of ca. 2.5 m. Taking into account 3 km length of the fault, earthquake with magnitude of 5.5 - 5.9 is potential. However, slip amount of 2.5 m could be result of an earthquake with magnitude of 6.9, which is larger than the expected magnitude for Mugırtepe Fault. Therefore, it is interpreted to be occurred as a series of earthquakes that displaced the fault close in time. The Priene-Sazlı Fault experienced the third rupture at ca. 3.7 ka (Fig. 6) with vertical slip of ca. 1.4 m most likely as an individual earthquake with magnitude of 6.7 - 6.8. The Kalafat Fault broke simultaneously at ca. 3.6 ka (Fig. 6) with vertical slip of ca. 3.1 m, which requires an earthquake with magnitude of 7.0. Therefore, considering the length of the fault, several earthquakes were needed to expose the fault in this scale. Meanwhile, the Yavansu Fault experienced its second rupture at ca. 3.4 ka (Fig. 6) and a total vertical slip of ca. 3.5 m, which can be made by an earthquake of 7.0 in magnitude. This amount of slip likely is produced by several earthquakes. According to our modeling, the last rupture of the Priene-Sazlı Fault happened at ca. 2.2 ka, which is compatible with the historical earthquake of 68 AD (Fig. 6). A vertical slip of ca. 1.5 m exposed the fault, which probably was consequent of an earthquake with magnitude of 6.7 - 6.8. The Manastır Fault in Gediz Graben simultaneously broke at ca. 2.1 ka, correlated with the historical earthquakes of 17 and 44 AD in Manisa region (Fig. 6), with a large amount of slip of ca. 7 m. The 4.5 km length of the fault gives rise to earthquakes with magnitude of 5.7 - 6.0. The modeled slip of 7 m can be produced by an earthquake of 7.2 in magnitude, which is implausible for this fault. Therefore, we conclude this activity as a series of earthquakes close in time. The Yavansu Fault ruptured for the last time at ca. 2 ka (Fig. 6) with vertical slip of ca. 2.6, probably in a response to an earthquake of 6.9 in magnitude. The timing of the reconstructed seismic events of these faults reveals a high correlation of ages at ca. 2.0, 3.5, 6.0 and 8.0 ka, among which some correlate with historical data as well (Fig. 6). According to these synchronized activities, we introduce at least four periods of high seismic activity during Holocene time with recurrence interval of approximately 2000 years in a regional scale of western Anatolia. Considering this interval time span, our time is also considered as a period of high seismic activity

validated by the instrumental database, with the most recent major earthquake struck in south of Bodrum with magnitude of 6.7 on July 2017. We can also conclude that the next period of high seismic activity occurs in 2000 years.

Table 2. Recurrence interval of major earthquakes of a number of faults within the extensional region of Aegean Sea and Italy. The recurrence intervals similar to our results are bolded in the table.

Location	Fault	Recurrence Interval (yr)	Reference
Turkey	**Büyük Menderes Fault Zone**	**250 - 1900**	Altunel et al. (2009)
	North Anatolian Fault, southern branches **(Havran-Balıkesir Fault Zone)**	**1000 - 2000**	Sözbilir et al. (2016)
	North Anatolian Fault (different northern segments)	150 - 350	Ikeda et al. (1991) Rockwell et al. (2001; 2009) Hartleb et al. (2006) Kozacı et al. (2011) Özaksoy et al. (2010)
	North Anatolian Fault (Düzce Fault)	400 - 500 250 - 300	Sugai et al.(2001) Pantosti et al. (2008)
	East Anatolian Fault (Palu–Hazar Fault)	100 - 360	Çetin et al. (2003)
	North Anatolian Fault (Ladik Fault)	600 - 900	Yoshioka et al. (2000)
	North Anatolian Fault (Yenice Gönen Fault)	650	Kürçer et al. (2008)
	Dead Sea Fault Zone (Hacıpaşa fault), southern Turkey	650	Akyüz et al. (2006)
	Tuz Gölü Fault, Cental Turkey	10000	Kürçer & Gökten, 2014
Greece	Spili Fault (Crete)	4200	Mouslopoulou et al. (2014)
	the southern Lanada-Volvi Basin Margin Fault Zone	7000	Cheng et al. (1994)
	Sparta Fault	500 - 4500	Benedetti et al. (2002)
	Atalanti Fault	660 - 1120	Pantosti et al. (2004)
	Southern Mygdonia marginal Fault (Gerakarou segment)	7000	Pavlides (1996)
	Tyrnavos Fault (northern Thessaly)	**2000 - 2500**	Caputo et al. (2004)
	Kaparelli Fault (Gulf of Corinth)	**2500**	Kokkalas et al. (2007)
	Kaparelli Fault Mygdonia Fault Eliki Fault	**2300** 1000 400 - 900	Chatzipetros et al. (2005)
	Kaparelli Fault	3000 - 9000 4000 - 5000 10000 - 11000	Benedetti et al. (2003)
	A series of normal faults (Crete)	260 - 840	Caputo et al. (2006)
Italy	**Ovindoli–Pezza Fault**	**1000 - 3000**	Pantosti et al. (1996)
	Mognola Fault	**1000 - 3000**	Palumbo et al. (2004)
	Fucino Fault	**2000 - 3000**	Benedetti et al. (2013)
	Velino-Magnola Fault	1000 - 6000	Schlagenhauf et al. (2011)
Israel	Nahef East Fault	3000	Mitchell et al. (2001)

The recurrence interval of earthquakes on faults is strongly linked to the regional strain rate and fault size and in a second-order to the interactions of faults (e. g., Nicol et al., 1997; 2005; Walsh et al., 2001). A wide ranges of recurrence interval of earthquakes of many faults reported worldwide from hundreds to thousand years (e.g., California, Utah, Japan, China, Southern America and Alaska; Sieh, 1981). In several tectonic settings a regular pattern of the return period of earthquakes validates the concept of regional recurrence interval (e.g., Japan, southern Chile; Sieh, 1981). We provided recurrence interval of major earthquakes of a series of normal faults, along with strike-slip North and East Anatolian faults, within the extensional region of Aegean Sea, Israel and Italy (Table 2). Modeled return period in this study is relatively accordant with the upper limit of return period of large earthquakes in Büyük Menderes Fault Zone, which is in the range of 250 to 1900 years (Altunel et al., 2009). Furthermore, earthquake interval period in Havran-Balıkesir Fault Zone, southern part of North Anatolian is in the range of 1000 - 2000 years (Sözbilir et al., 2016). In general, North and East Anatolian faults indicated earthquake recurrence interval of 100 - 900 years (Ikeda et al., 1991; Rockwell et al., 2001; 2009; Hartleb et al., 2006; Kozacı et al., 2011; Özaksoy et al., 2010; Sugai et al., 2001; Pantosti et al., 2008; Çetin et al., 2003; Yoshioka et al., 2000; Kürçer et al., 2008; Akyüz et al., 2006). In central Turkey, Tuz Gölü Fault shows the earthquake recurrence interval of 10000 years (Kürçer and Gökten, 2014). In Greece, the earthquake recurrence intervals are ranged between 260 to 11000 years (Mouslopoulou et al., 2014; Cheng et al., 1994; Benedetti et al., 2002; Pantosti et al., 2004; Pavlides, 1996; Chatzipetros et al., 2005; Benedetti et al., 2003; Caputo et al., 2006). Kaparelli Fault with 2300 – 2500 years (Kokkalas et al., 2007; Chatzipetros et al., 2005) and Tyrnavos Fault with 2000 – 2500 years (Caputo et al., 2004) of earthquake interval periods are compatible with our results. On Nahef East Fault in Israel, the return period is estimated to be about 3000 years (Mitchell et al., 2001). In Italy the recurrence interval of large earthquakes are between 1000 to 6000 years (e.g. Schlagenhauf et al., 2011), with a range of 1000 – 3000 years on Ovindoli-Pezza and Mognola faults (Pantosti et al., 1996; Palumbo et al., 2004) and 2000 – 3000 years on Fucino Fault (Benedetti et al., 2013). Taking into account the Aegean extensional region as well as Italy, which are strongly controlled by normal faults with the approximate length of 40 - 50 km, the

recurrence interval of major earthquakes on several faults are approximately 2.5 ka in average (Table 2).

Putting our results into extent of regional tectonic regime, we present a broader overview for the understanding of Holocene deformation pattern in western Anatolia and how it is linked to the convergence of African plate. African plate is being subducted beneath the Aegean plate, which in the first plate the shortening parallel to the Hellenic arc resulted in thrust and strike-slip fault evolutions, while on the latter extension is mostly evident by normal faulting explicitly in western Anatolia and Greece. The exact rate of this convergent is still under debates and rate of 10 mm/yr (Oral et al. 1995) up to 40 mm/yr (Shaw and Jackson, 2010) were reported for this northward motion. This large-scale movement constrains a huge amount of strain into the Aegean plate, which accommodates partially on the faults, particularly the ones with the parallel/sub-parallel orientation to the subduction trends. Shaw and Jackson (2010), state that maximum 20 % of this motion is seismically accommodated, but most part of this high amount of energy is aseismically consumed. The total strain, however, will be partially loaded on the faults of Anatolian plate inland and the majority of this amount is basically assumed to be transmitted on the largest faults (Cowie et al., 2007). The average long-term vertical slip rates of the studied faults estimated to be in a range of 0.1 to 1.9 mm/yr, which involves a small portion of the above said northward rapid movement. The partial strain accumulation on every discrete fault is not provided to be determined using fault scarp dating method. However, short-term vertical slip rates of the faults show general acceleration of fault activity through time (Table 1), which can indicate that western Anatolia in the recent time is experiencing the highest amount of releasing of accumulated strain during Holocene. Accordingly, we can expect more frequent occurrences of earthquake in a near future. Nevertheless, fault seismic activity is not merely connected to the localization of strain in a regional scale, but is also affected by a variety of factors namely local pattern of nearby fault network, heterogeneity of bedrock, fault zone degree of strength and viscosity or viscoelasticity condition of lower crust (e.g., Cowie et al., 2007). All in all, our findings together with the existing seismic data in western Anatolia highlights the necessity of a more comprehensive

earthquake hazard plan in order to reduce the potential damages following future earthquakes.

6. Conclusions

We have explored several normal fault scarps in western Anatolia based on the fault scarp dating using cosmogenic ^{36}Cl in order to model the history of paleoearthquakes. At least 12 major seismic events mostly occurred as clustered earthquakes close in time with a magnitude of 5.4 - 7.1 were modeled. Four synchronous ages of seismic events at ca. 2.0, 3.5, 6.0 and 8.0 ka, lead us to introduce the return period of ca. 2000 high seismic activity in a regional scale of western Anatolia. Considering this time interval, our time with record of a large number of large earthquakes is a high seismic period, and the subsequent one happens in 2000 years. This return period is compatible with return period of several normal faults within the extensional region of Aegean Sea and Italy. The acceleration of vertical slip rates through time manifest that western Anatolia is generally in its most active period through the entire Holocene time. The high potential of fault scarp dating tool to model seismic behavior of faults and in a larger scale in a tectonic setting is shown by this study. Our findings provides informative documents in order to better understand the complex deformation of western Anatolia and to supply helpful documents to minimize the seismic risks of future earthquakes of this seismic-prone region.

Acknowledgments

This project is funded by a grant from the Dokuz Eylül University (Research Project No. 2006.KB.FEN.008), the Surface Exposure Dating Laboratory at the University of Bern, the Bern University Research Foundation and Swiss National Science Foundation (Project No. 200021-147065). We would like to thank Dr. Hans-Arno Synal and the staffs of Laboratory of Ion Beam Physics, ETH Zurich for their help and support of AMS measurements of a large number of samples. We also wish to thank the students and technicians of Dokuz Eylül University, who accompanied and supported us during our fieldwork and sampling.

References

- Akçar, N., Tikhomirov, D., Özkaymak, Ç., Ivy-Ochs, S., Alfimov, V., Sözbilir, H., Uzel, B., Schlüchter, Ch., 2012. ^{36}Cl Exposure Dating of Paleoearthquakes in the Eastern Mediterranean: First Results from Western Anatolian Extensional Province, Turkey. GSA Bulletin 124, no. 11/12, 1724-1735.
- Akyüz, H., Altunel, E., Karabacak, V., Yalçiner, Ç., 2006. Historical earthquake activity of the northern part of the Dead Sea fault zone, southern Turkey. Tectonophysics, 426, 281-293.
- Altunel, E., 1998. Evidence for damaging historical earthquakes at Priene, Western Turkey. Turkish Journal of Earth Sciences 7, 25-35.
- Altunel, E., Akyüz, S., Meghraoui, M., Kiyak, N.G., Karabacak, V., Yalçiner, Ç., 2009. Büyük Menderes Fay Zonunun Arkeosismolojisi ve Paleosismolojisi.
- Ambraseys, N.N. 1988. Engineering seismology. Earthquake Engineering and Structural Dynamics 17, 1-105.
- Ambraseys, N., 2009. Earthquakes in the Mediterranean and Middle East: a multidisciplinary study of seismicity up to 1900. Cambridge University Press, 947 p.
- Ambraseys, N.N., Jackson, J.A., 1998. Faulting associated with historical and recent earthquakes in the Eastern Mediterranean region, Geophysical Journal International 133, no. 2, 390-406.
- Barka, A.A., Sakınç, M., Görür, N., Yılmaz, Y., Şengör, A.M.C., Ediger, V.Ş., 1994. Is Aegean extension a consequence of the westerly escape of Turkey? EOS Transactions of the American Geophysical Union 75, 116-117.
- Benedetti, L., Finkel, R., King, G., Armijo, R., Papanastassiou, D., Ryerson, F.J., Flerit, F., Farber, D., Stavrakakis, G., 2003. Motion on the Kaparelli fault (Greece) prior to the 1981 earthquake sequence determined from Cl-36 cosmogenic dating, Terra Nova, v. 15, no. 2, p. 118-124.
- Benedetti, L., Finkel, R., Papanastassiou, D., King, G., Armijo, R., Ryerson, F., Farber, D., Flerit, F., 2002. Post-glacial slip history of the Sparta fault (Greece) determined by Cl-36 cosmogenic dating: Evidence for non-periodic earthquakes, Geophysical Research Letters, 29, no. 8, 1246, doi: 10.1029/2001GL014510.
- Benedetti, L., Manighetti, I., Gaudemer, Y., Finkel, R., Malavieille, Y., Pou, Kh., Arnold, M., Aumaître, G., Bourlès, D., Keddadouche, K., 2013. Earthquake synchrony and clustering on Fucino faults (Central Italy) as revealed from in situ ^{36}Cl exposure dating. Journal of Geophysical Reasearch, Solid Earth 118, 4948-4974.
- Boğaziçi University Kandilli Observatory and Earthquake Research Institute (KOERI). Retreived from (www.koeri.boun.edu.tr/scripts/lst4.asp)
- Çakmakoğlu, A., 2006. Dilek yarımadası-söke ve selçuk çevresinin Jeolojisi.
- Caputo, R., Helly, B., Pavlides, S., Papadopoulos, G., 2004, Palaeoseismological investigation of the Tyrnavos Fault (Thessaly, Central Greece), Tectonophysics, 394, 1-20, doi:10.1016/j.tecto.2004.07.047.
- Caputo, R., Monaco, C., Tortorici, L., 2006. Multiseismic cycle deformation rates from Holocene normal fault scarps on Crete (Greece), Terra Nova, 18(3), 181-190.
- Çetin, H., H. Güneyli, Mayer, L., 2003. Paleoseismology of the Palu-Lake Hazar segment of the East Anatolian Fault Zone, Turkey, Tectonophysics, 374, 163-197, doi:10.1016/j.tecto.2003.08.003.
- Chatzipetros, A., Kokkalas, S., Pavlides, S., Koukouvelas, I., 2005, Palaeo-seismic data and their implications for active deformation in Greece, Journal of Geodynamics, v. 40, nos. 2–3, p. 170–188.
- Cheng, S., Fang., Z., Pavlides, S., Chatzipetros, A., 1994. Preliminary study of Paleoseismicity of the Southern Lanada Volvi Basin margin fault zone, Thessaloniki, Greece, Bulletin of the Geological Society of Greece, Vol. XXX/1, 401-407.
- Çiftçi, N.B., Bozkurt, E., 2009, Evolution of the Miocene sedimentary fi ll of the Gediz graben, SW Turkey: Sedimentary Geology, v. 216, no. 3-4, p. 49-79.
- Cluff, L.S., Cluff, J.L., 1984. Importance of assessing degrees of fault activity for engineering decisions, Proceeding 8th World Conference on Earthquake Engineering, vol. 2, 629-636.
- Cowie, P.A., Phillips, R.J., Roberts, G.P., McCaffrey, K., Zijerveld, L.J.J., Gregory, L.C., Faure Walker, J., Wedmore, L.N.J., Dunai, T.J., Binnie, S.A., Freeman, S.P.H.T. , Wilcken,

K., Shanks, R.P., Huismans, R.S., Papanikolaou, I., Michetti, A.M., Wilkinson, M., 2017. Orogen-scale uplift in the central Italian Apennines drives episodic behaviour of earthquake faults, Scientific Reports 7, Article number 44858.

- Cowie, P.A., Roberts, G.P., Mortimer, E., 2007. Strain localization within fault arrays over timescales of 10^0-10^7 years (Observations, explanations, and debates). *In* Tectonic faults: agents of change on a dynamic earth. Edited by M.R. Handy, G. Hirth, N. Hovius. MIT Press, Cambridge, Mass., 47-78.
- Dewey, J.F., Şengör, A.M.C., 1979. Aegean and surrounding region: complex multiplate and continuum tectonics in a convergent zone. Geological Society of America Bulletin 90, 84–92.
- Duman, T.Y., Emre, Ö., Özalp, S., Elması, H., 2011. Active fault map series of Turkey (scale 1:250,000), General Direct. Mineral Res. Explor., Aydın (NJ 35-11).
- Emre, Ö., Duman, T.Y., Özalp, S., Elması, H., Olgun, Ş., Şaroğlu, F., 2013. Active fault map of Turkey (scale 1:250,000), General Direct. Mineral Res. Explor., Special Publication Series - 30.
- Ergin, K., Güçlü, U., Uz, Z., 1967. A Catalogue of Earthquakes for Turkey and Surrounding Area (11 A.D.–1964). Technical University of İstanbul, Publications, no. 24 (in Turkish).
- Eyidoğan, H., 1988. Rates of crustal deformation in western Turkey as deduced from major earthquakes. Tectonophysics, 148, 83-92.
- Görür, N., Sengör, A.M.C., Sakinü, M., Akkök, R., Yiğitbaş, E., Oktay, F.Y., Barka, A., Sarica, N., Ecevitoğlu, B., Demirbağ, E., Ersoy, Ş., Algan, O., Güneysu, C., Aykol, A., 1995. Rift formation in the Gökova region, southwest Anatolia: implications for the opening of the Aegean Sea, Geological Magazine 132, 637-650.
- Guidoboni, E., Comastri, A., Traina, G., 1994. Catalogue of Ancient Earthquakes in the Mediterranean Area up to the10th Century. Istituto Nazionale di Geofi sica, ISBN: 88-85213-06-5.
- Gürer, Ö.F., Yılmaz, Y., 2002. Geology of the Ören and surrounding areas, SW Anatolia, Turkish Journal of Earth Sciences, Vol. 11, 1-13.
- Hancock, P.L., Barka, A.A., 1987. Kinematic indicators on active faults in western Turkey, Journal of Structural Geology 9, No. 5/6, 573-584.
- Hartleb, R.D., Dolan, J.F., Kozaci, Ö., Akyüz, H.S., Seitz, G.G, 2006. A 2500-yr-long paleoseismologic record of large, infrequent earthquakes on the North Anatolian fault at Çukurçimen, Turkey, GSA Bulletin 118 (7-8), 823-840.
- Ikeda, Y., Suzuki, Y., Herece, E., Şaroğlu, F., Isikara, A.M., Honkura, Y., 1991. Geological evidence for the last two faulting events on the north Anatolian Fault zone in the Mudurnu Valley, western Turkey, Tectonophysics, 193, Issue 4, 335-345.
- Jackson, J. A., McKenzie, D., 1988. Rates of active deformation in the Aegean Sea and surrounding areas, Basin Res., 1, 121-128.
- Kissel, C., Laj, C., 1988. The tertiary geodynamical evolution of the Aegean arc: a palaeomagnetic reconstruction. Tectonophysics, 146, 183-201.
- Koçyiğit, A., Yusufoğlu, H., Bozkurt, E., 1999. Evidence from the Gediz Graben for episodic two-stage extension in western Turkey. Journal of the Geological Society of London 156, 605-616.
- Kokkalas, S., Pavlides, S., Koukouvelas, I., Ganas, A., Stamatopoulos, L. 2007. Paleoseismicity of the Kaparelli fault (eastern Corinth Gulf): Evidence for earthquake recurrence and fault behaviour, Bollettino della Societa Geologica Italiana, 126 (2), 387-395.
- Kozacı, Ö., Dolan, J.F., Yönlü, Ö., R.D., Hartleb, 2011. Paleoseismologic evidence for the relatively regular recurrence of infrequent, large-magnitude earthquakes on the eastern North Anatolian fault at Yaylabeli, Turkey, Litosphere, v. 3; no. 1; 37–54.
- Kürçer, A., Chatzipetros, A., Tutkun, S.Z., Pavlides, S., Ateş, Ö., Valkaniotis, S., 2008. The Yenice–Gönen active fault (NW Turkey): Active tectonics and palaeoseismology, Tectonophysics 453, 263 -275.
- Kürçer, A., Gökten, Y.E., 2014. Neotectonic-period characteristics, seismicity, geometry and segmentation of the Tuz Gölü Fault Zone, Maden Tetkik ve Arama Dergisi, 149, 19-69 (In Turkish)
- Le Pichon, X., Angelier, J., 1979. The Aegean arc and trench system: a key to the neotectonic evolution of the eastern Mediterranean area. Tectonophysics, 60, 1–42.
- Le Pichon X, Angelier J. 1981. The Aegean Sea. Philosophical Transactions of the Royal Society of London A300, 357-372.

- Le Pichon X., Chamot-Rooke C., Lallemant S., Noomen R., Veis G., 1995. Geodetic determination of the kinematics of Central Greece with respect to Europe: implications for Eastern Mediterranean tectonics, J. Geophys. Res. 100, 12675–12690.
- McCalpin, J.P., ed, 2009, Paleoseismology, London, Academic, 629 p.
- McKenzie, D., 1978. Active tectonics of the Alpine-Himalayan belt: the Aegean Sea and surrounding regions, Geophysical Journal international 55*,* 217-254.

- Meulenkamp, J.E., Wortel, W.J.R., Van Wamel, W.A., Spakman, W., Hoogerduyn Strating, E., 1988. On the Hellenic subduction zone and geodynamic evolution of Crete in the late middle Miocene. Tectonophysics, 146, 203–215.
- Mitchell, S.G., Matmon, A., Bierman, P.R., Enzel, Y., Caffee, M., Rizzo, D., 2001. Displacement history of a limtesone normal fault scarp, northern Israel, from cosmogenic ^{36}Cl, J. geophys. Res., 106 (B3), 4247-4264.
- Mouslopoulou, V., Moraetis, D., Benedetti, L., Guillou, V., Bellier, O., Hristopulos, D., 2014. Normal faulting in the forearc of the Hellenic subduction margin: Paleoearthquake history and kinematics of the Spili Fault, Crete, Greece. - Journal of Structural Geology 66, 298-308.
- Mozafari, N., Sümer, Ö., Tikhomirov, D., Ivy-Ochs, S., Alfimov, V., Vockenhuber, Ch., İnci, U., Sözbilir, H., Akçar, N., *submitted (a).* Holocene seismic activity of the Priene-Sazlı Fault revealed by cosmogenic ^{36}Cl, western Anatolia, Turkey.
- Mozafari, N., Tikhomirov, D., Sümer, Ö., Özkaymak, Ç., Uzel, B., Yesilyurt, S., Ivy-Ochs, S., Vockenhuber, Ch., Sözbilir, H., Akçar, N., *submitted (b),* Seismic activity of the Büyük Menderes Graben (western Turkey) during the last 20 ka: Insights from cosmogenic ^{36}Cl analysis.
- Nicol, A., Walsh, J.J., Manzocchi., T., Morewood, N., 2005. Displacement rates and average earthquake recurrence intervals on normal faults, Journal of Structural Geology 27, 541–551.
- Nicol, A., Walsh, J.J., Watterson, J., Underhill, J.R., 1997. Displacement rates of normal faults. Nature 390, 157–159.
- Öcal, N., 1958. Söke-Balat zelzelesi (Söke-Balat earthquake), Ist. Kandili Rasathanesi Sismoloji Yay., 2.
- Oner, Z., Dilek, Y., 2011. Supradetachment basin evolution during continental extension: The Aegean province of western Anatolia, Turkey, Geological Society of America Bulletin 123, no. 11-12;2115-2141
- Oral*,* M.B., Reilinger, R.E., Toksoz, M.N., Kong. R.W., Barka, A.A., Kinik, I., Lenk, O., 1995. Global Positioning System offers evidence of plate motions in eastern Mediterranean, EOS, Vol. 76, No. 2.
- Özaksoy, V., Emre, Ö., Yıldırım, C., Doğan, A., Özalp, S., Tokay, F., 2010. Sedimentary record of late Holocene seismicity and uplift of Hersek restraining bend along the North Anatolian Fault in the Gulf of Izmit, Tectonophysics 487, 33-45.
- Özkaymak, Ç., Sozbilir, H., Uzel, B., Akyuz, H.S., 2011. Geological and palaeoseismological evidence for late Pleistocene–Holocene activity on the Manisa Fault Zone, western Anatolia. Turkish Journal of Earth Sciences 20 (4), 449–474.
- Palumbo, L., Benedetti, L., Bourles, D., Cinque, A., Finkel, R., 2004. Slip history of the Magnola fault (Apennines, Central Italy) from ^{36}Cl surface exposure dating: evidence for strong earthquake over the Holocene, Earth planet. Sci. Lett., 225, 163-176.
- Pantosti, D., Collier, R., D'Addezio, G., Masana, E., and Sakellariou, D., 1996. Direct geological evidence for prior earthquakes on the 1981 Corinth fault (central Greece), Geophysical Research Letters, v. 23, no. 25, p. 3795–3798, doi: 10.1029/96GL03647.
- Pantosti, D., De Martini, P.M., Papanastassiou, D., Lemeille, F., Palyvos, C., Stavrakakis, G., 2004. Paleoseismological trenching across the Atalanti Fault (Central Greece): evidence for the ancestors of the 1894 earthquake during the Middle Ages and Roman times. Bull. Seismol. Soc. Am., 94, 531–549.
- Pantosti, D., Pucci, S., Palyvos, N., De Martini, P.M., D'Addezio, G., Collins, P.E.F., Zabci, C., 2008. Paleoearthquakes of the Duzce fault (North Anatolian Fault Zone): Insights for large surface faulting earthquake recurrence, Journal of Geophysical Research, Vol. 113, B01309.
- Pavlides, S., 1996. First palaeoseismological results from Greece: Annali di Geofisica, v. 39, p. 545–555.

- Pavlides, S., Caputo, R., 2004. Magnitude versus faults' surface parameters: Quantitative relationships from the Aegean Region. Tectonophysics, 380, 159-188.
- Rockwell, T., Barka, A., Dawson, T., Thorup, K., Akyuz, S., 2001. Paleoseismology of the Gazikoy-Saros segment of the North Anatolia fault, northwestern Turkey: Comparison of the historical and paleoseismic records, implications of regional seismic hazard, and models of earthquake recurrence, Journal of Seismology, 5(3), 433-448.
- Rockwell , T.K. , Ragona, D. , Akbalic, B. , Aksou, M.E. , Barka, A.A. , Ferry, M. , Klinger, Y., Langridge, R. , Meghraoui, M., Meltzner, A.J., Satir, D., Seitz, G., Ucarkus, G., 2009. Palaeoseismology of the North Anatolian Fault near the Marmara Sea: implications for fault segmentation and seismic hazard, *In* Palaeoseismology: Historical and Prehistorical Records of Earthquake Ground Effects for Seismic Hazard Assessment. Edited by K. Reicherter, A.M. Michetti, P. G. Silva, The Geological Society, London, Special Publications, 316 p (31-54).
- Şaroğlu, F., Emre, Ö., Kuşçu, I., 1992. Active Fault Map of Turkey (scale 1:1,000,000). General Direct. Mineral Res. Explor. (MTA), Ankara, Turkey.
- Schlagenhauf, A., Gaudemer, Y., Benedetti, L., Manighetti,I., Palumbo, L., Schimmelpfennig, I., Finkel, R., Pou, K., 2010. Using in situ chlorine-36 cosmonuclide to recover past earthquake histories on limestone normal fault scarps: A reappraisal of methodology and interpretations, Geophysical Journal International, v. 182, no. 1, p. 36-72.
- Schlagenhauf, A., Manighetti, I., Benedetti, L., Gaudemer, Y., Finkel, R., Malavieille, J., Pou, K., 2011. Earthquake supercycles in Central Italy, inferred from ^{36}Cl exposure dating. Earth and Planetary Science Letters, 307 (3-4), 487–500.
- Şengör, A.M.C., 1987. Cross-faults and differential stretching of hanging walls in regions of low-angle normal faulting: examples from western Turkey. *In* Coward, M.P., Dewey, J.F., Hancock, P.L. (Eds.), Continental Extensional Tectonics. Geological Society of London, Special Publication 28, 575-589.
- Şengör, A.M.C., Görür, N., Şarğlu, F., 1985. Strike-slip faulting and related basin formation in zones of tectonic escape: Turkey as a case study. In: Biddle, K., Christie-Blick, N. (Eds.), Strike-Slip Deformation, Basin Formation and Sedimentation. Society of Economic Paleontologists and Mineralogists, Special Publications 37, 227-264.
- Seytoğlu, G., Scott, B., 1991. Late Cenozoic crustal extension and basin formation in west Turkey. Geological Magazine 128, 155–166.
- Seytoğlu, G., Scott, B., 1992. The age of the Buyuk Menderes Graben (western Turkey) and its tectonic implications. Geological Magazine 129, 239–242.
- Seytoğlu, G., Scott, B.C., 1996. The age of Alaşehir graben (west Turkey) and its tectonic implications. Geological Journal 31, 1–11.
- Seytoğlu, G., Scott B, Rundle CC. 1992. Timing of Cenozoic extensional tectonics in West Turkey. Journal of the Geological Society, London 149, 533-538.
- Shaw, B., Jackson, J., 2010. Earthquake mechanisms and active tectonics of the Hellenic subduction zone. Geophysical Journal International 181, 966-984.
- Shebalin, N.V., Karnik, V., Hadzievski, D. (eds.), 1974. Catalogue of earthquakes of the Balkan region. I, UNDP- UNESCO Survey of the seismicity of the Balkan region. Skopje, 600 p.
- Sieh, K.E., 1981. A review of geological evidence for recurrence times of large earthquakes, *In* Earthquake Prediction: An international Review (Simpson, D.W. & Richards, P.G., Eds.), American Geophysical Union, Maurice Ewing Series, vol. 4, 181-207.
- Soysal, H., Sipahioğlu, S., Kolçak, D., Altınok, Y., 1981. Historical earthquake catalogue of Turkey and surrounding area (2100 B.C.-1900 A.D.). Technical Report, TUBİTAK, No: TBAG-341.
- Sözbilir, H., Özkaymak, Ç., Uzel, B., Sümer, Ö., Eski, S., Tepe, Ç., 2016. Palaeoseismology of the Havran-Balıkesir Fault Zone: evidence for past earthquakes in the strike-slip-dominated contractional deformation along the southern branches of the North Anatolian fault in northwest Turkey, Geodinamica Acta, 28: 4, 254-272.
- Sümer, Ö., Inci, U., Sözbilir, H., 2013. Tectonic evolution of the Söke Basin: Extension-dominated transtensional basin formation in western part of the Büyük Menderes Graben, Western Anatolia, Turkey. Journal of Geodynamics 65, 148-175.
- Taymaz, T., Jackson, J., McKenzie, D., 1991. Active tectonics of the north and central Aegean Sea, Geophysical J. Int., 106, 433-490

- Tikhomirov, D., 2014. PhD thesis, University of Bern, An advanced model for fault scarp dating and paleoearthquake reconstruction, with a case study of the Gediz Graben formation (Turkey).
- United States Geological Survey National Earthquake Information Center (USGS-NEIC) (earthquake.usgs.gov/contactus/golden/neic.php).
- Walsh, J.J., Childs, C., Manzocchi, T., Imber, J., Nicol, A., Meyer, V., Tuckwell, G., Bailey, W.R., Bonson, C.G., Watterson, J., Nell, P.A.R., Strand, J., 2001. Geometrical controls on the evolution of normal fault systems, in: Holdsworth, R.E. (Ed.), The Nature of the Tectonic Significance of Fault Zone Weakening Geological Society of London Special Publication, 186, pp. 157–170.
- Wells, D.L., Coppersmith, J.K., 1994. New empirical relationships among magnitude, rupture length, rupture width, rupture area, and surface displacement. Bulletin of the Seismological Society of America 84, 974-1002.
- Yönlü, Ö., Altunel, E., Karabacak, V., Akyüz, S., Yalçıner, Ç., 2010. Offset archaeological relics in the western part of the Büyük Menderes Graben, (western Turkey) and their tectonic implications. The Geological Society of America 471, 269-279 (Special Publications).
- Yoshioka, T., Okumura, K., Kuscu, I., Emre, Ö., 2000. Recent surface faulting of the North Anatolian fault along the 1943 Ladik earthquake ruptures, Bulliten of Geological Survey of Japan, Vol. 51 (1), 29 – 35.
- Zreda, M., Noller, J., 1998. Ages of prehistoric earthquakes revealed by cosmogenic chlorine-36 in a bedrock fault scarp at Hebgen Lake. Science, 282, 1097-1099.

Chapter 5

Conclusions and outlook

1. Conclusions

In this thesis, we applied fault scarp dating using cosmogenic ^{36}Cl on several fault scarps in western Anatolia, one of the most seismically active regions in the world. There, a roughly N-S extensional tectonic regime, since early Miocene caused the formation of large-scale horst-graben systems namely Büyük Menderes Graben, Küçük Menderes Graben, Gediz Graben and Gökova half-graben bounded by a large number of normal faults, locally built in carbonates. The high populated western Anatolia is subjected to many major earthquakes recorded historically and instrumentally, which highlights the necessity of seismic studies in order to minimize potential seismic-related damages. However, the instrumental record of earthquakes started since 1900 and the historical earthquakes in the Eastern Mediterranean and Middle East were recorded only since 2100 B.C. (Shebalin et al., 1974; Soysal et al., 1981; Ambraseys, 2009). In order to model a long-term seismic behavior of faults and assessment of destructive earthquakes, more data in addition to the available database within this short time span is required. The existence of well-preserved normal faults in carbonate bedrock makes western Anatolia a natural laboratory to investigate paleoseismic history using cosmogenic ^{36}Cl exposure dating.

In order to provide a long-term modeling of seismic behavior in western Anatolia, we studied several fault scarps within the Büyük Menderes Graben (Kalafat, Yavansu and Priene-Sazlı, faults), Gediz Graben (Rahmiye Fault), Gökova half-graben (Ören Fault) by collecting 453 samples along well-preserved fault scarp surfaces. Then, a comparison was done with the results of analyzed samples of fault scarp dating of Manastır and Mugırtepe faults within Gediz Graben (Akçar et al., 2012; Tikhomirov, 2014). In Gediz Graben, the **Mugırtepe Fault** experienced one seismic event at 6 ± 1.5 ka with a vertical slip value of 2.5 ± 0.4 m. The vertical slip rate for this seismic event is yielded > 0.1 mm/yr. Then the Mugırtepe Fault remained inactive and the **Manastır Fault** broke at 2.1 ± 0.8 ka with ca. 7.0 ± 1.1 m of vertical slip. The calculated vertical slip rate is similar to the Mugırtepe Fault. Most possibly two historical events of 17 AD (Ambraseys, 1988) and 44 AD (Ergin et al. 1967; Soysal et al., 1981) in Manisa region caused displacement of the Manastır

Fault scarp (Tikhomirov, 2014). The data analysis of the **Kalafat Fault** shows that three earthquakes caused fault displacement at ca. 15.3 ± 3.8 ka, 8.4 ± 2.1 ka, and 3.6 ± 0.9 ka with vertical component of related slips of 0.7 ± 0.1 m, 0.9 ± 0.1 m, and 3.1 ± 0.5 m. The average slip rates from the oldest to youngest modeled event were estimated > 0.1, 0.1, and 1.5 mm/yr, whereas the cumulative slip rate is 0.6 mm/yr. The **Yavansu Fault** experienced the similar number of events at 7.9 ± 2.0 ka, 3.4 ± 0.8 ka, and 2.0 ± 0.5 ka with vertical component of slips of 0.6 ± 0.1 m, 3.5 ± 0.5 m, and 2.6 ± 0.4 m, respectively. The mean values of vertical slip rates were approximated to be > 0.1, 0.8, and 1.9 mm/yr for the earthquakes from the oldest to the youngest. The long-term slip rate is estimated to be ca. 1 mm/yr. Our results indicates that the **Priene-Sazlı Fault** experienced four destructive seismic events at 8.1 ± 2.0 ka, 6.0 ± 1.5 ka, 3.7 ± 0.9 ka, and 2.2 ± 0.5 ka with the vertical component of slips of 3.4 ± 0.5 m, 1.5 ± 0.2 m, 1.4 ± 0.2 m, and 1.5 ± 0.2 m, respectively. The reconstructed earthquake of ca. 2 ka correlates well with the historical earthquake of 68 AD. Average values of slip rates from the oldest to the youngest modeled earthquake of > 0.3, 0.7, 0.6, and 1.0 mm/yr were yielded. The long-term vertical slip rate of the fault is approximated to be 0.7 mm/yr. The investigated faults are considered as seismogenic faults due to having potential of triggering earthquakes of larger than 5 in magnitudes. The explored earthquake at ca. 15 ka related to Kalafat Fault is the oldest seismic event modeled by fault scarp dating analysis of western Anatolia. Consideration of all the results from of the Priene-Sazlı, Kalafat, Yavansu, Mugırtepe and Manastır faults, reveals that western Anatolia experienced at least four periods of high seismic activity during Holocene at ca. 2.0, 3.5, 6.0 and 8.0 ka. According, the regional return period of approximately 2000 years is yielded, which is consistent with the return period of earthquakes on several faults in the extensional tectonic setting of Aegean Sea as well as Italy. Taking into account the return period of modeled seismic events together with the number of destructive earthquakes occurred during the last century, this region is in another high seismically active period. Consequently, the occurrence of the next large seismic period in 2000 years is not beyond rational expectation. According to the increase in values of vertical slip rates of the investigated faults through time, it can be claimed that western Anatolia accumulated the highest amount of strain during the last 2000 years in comparison with the entire Holocene time. This huge amount of energy is

being released by the major earthquakes, which were instrumentally recorded through the last decades.

2. Outlook

During the last two decades the plausibility of fault scarp dating using cosmogenic ^{36}Cl have been proven by a series of studies on normal faults worldwide. Our study also showed high potential of this tool in order to long-term seismic modeling of a specific fault and in a wider extent, of a regional tectonic framework. Where seismic data are missing or are incomplete, fault scarp dating is not only able to determine the age of past earthquakes, but the vertical component of slips responsible for the seismic events prior and within the short time span of available seismic archives. Even though the technique is expensive and preparation of a large number of samples for every given fault is very time consuming, but at the moment it provides one of the most precise methods to explore geochronology of paleoearthquakes lost in the history of human beings life. We will provide more information and expand our dataset following the measurements of cosmogenic ^{36}Cl of samples of Ören and Rahmiye faults. The most recent major earthquake in western Anatolia with magnitude of 6.7 occurred on July 20, 2017 in south of Bodrum City in the western extension of Ören Fault. This disaster caused death of two and injury of hundreds of people. There are still numerous active faults in western Anatolia, whose seismic activity history is entirely unknown or poorly understood. One of those is Efes Fault in Küçük Menderes Graben, close to the Izmir City, that is recommended to be studied using fault scarp dating. The occurrence of damaging earthquake is a warning that active faults should be respected more seriously. Our study can be a big step to contribute earthquake hazard assessment of the seismic-prone and highly populated region of western Anatolia jointly with the available earthquake database.

References

- Akçar, N., Tikhomirov, D., Özkaymak, Ç., Ivy-Ochs, S., Alfimov, V., Sözbilir, H., Uzel, B., Schlüchter, Ch., 2012. ^{36}Cl Exposure Dating of Paleoearthquakes in the Eastern Mediterranean: First Results from Western Anatolian Extensional Province, Turkey. GSA Bulletin 124, no. 11/12, 1724-1735.

- Ambraseys, N., 2009. Earthquakes in the Mediterranean and Middle East: a multidisciplinary study of seismicity up to 1900. Cambridge University Press, 947 p.
- Ambraseys, N.N., Jackson, J.A., 1998. Faulting associated with historical and recent earthquakes in the Eastern Mediterranean region: Geophysical Journal International 133, no. 2, 390-406.
- Ergin, K., Güçlü, U., Uz, Z., 1967. A Catalogue of Earthquakes for Turkey and Surrounding Area (11 A.D.–1964). Technical University of İstanbul, Publications, no. 24 (in Turkish).
- Shebalin, N.V., Karnik, V., Hadzievski, D. (eds.), 1974. Catalogue of earthquakes of the Balkan region. I, UNDP- UNESCO Survey of the seismicity of the Balkan region. Skopje, 600 p.
- Soysal, H., Sipahioğlu, S., Kolçak, D., & Altınok, Y., 1981. Historical earthquake catalogue of Turkey and surrounding area (2100 B.C.-1900 A.D.). Technical Report, TUBİTAK, No: TBAG-341.
- Tikhomirov, D., 2014. PhD thesis, University of Bern, An advanced model for fault scarp dating and paleoearthquake reconstruction, with a case study of the Gediz Graben formation (Turkey).

Declaration of consent

on the basis of Article 28 para. 2 of the RSL05 phil.-nat.

Name/First Name: Mozafari Amiri/Nasim

Matriculation Number: 13-123-294

Study program: Exogene Geology

Bachelor ☐ Master ☐ Dissertation ☑

Title of the thesis: Using cosmogenic 36Cl to determine periods of enhanced seismicity in western Anatolia, Turkey

Supervisor: PD Dr. Naki Akçar

I declare herewith that this thesis is my own work and that I have not used any sources other than those stated. I have indicated the adoption of quotations as well as thoughts taken from other authors as such in the thesis. I am aware that the Senate pursuant to Article 36 para. 1 lit. r of the University Act of 5 September, 1996 is authorised to revoke the title awarded on the basis of this thesis. I allow herewith inspection in this thesis.

Bern/22.08.2017

Place/Date

Signature

Curriculum vitae

Nasim Mozafari Amiri

Personal Information

Nationality: Iranian

Birthday: 23-08-1979

Place of birth: Babol, Iran

Education

Oct. 2013 - Sep. 2017	PhD in Exogene Geology, Bern University, Bern, Switzerland.
Sep. 2010 - May. 2013	M.Sc. in Bedrock Geology, Lund University, Lund, Sweden.
Sep. 2004 - Sep. 2007	M.Sc. in Tectonics, Shahid Beheshti University, Tehran, Iran.
Sep. 1998 - Jul. 2002	B.Sc. in Geology, Agricultural and natural resources University of Gorgan, Gorgan, Iran.